University of North Dakota
UND Scholarly Commons

Theses and Dissertations | Theses, Dissertations, and Senior Projects

January 2015

Influence Of High-Intensity Turbulence On Laminar Boundary Layer Development On A Cylindrical Leading Edge: Enhancement To Eddy Diffusivity

Juli Pearson

Follow this and additional works at: https://commons.und.edu/theses

Recommended Citation
Pearson, Juli, "Influence Of High-Intensity Turbulence On Laminar Boundary Layer Development On A Cylindrical Leading Edge: Enhancement To Eddy Diffusivity" (2015). *Theses and Dissertations*. 1823.
https://commons.und.edu/theses/1823

This Thesis is brought to you for free and open access by the Theses, Dissertations, and Senior Projects at UND Scholarly Commons. It has been accepted for inclusion in Theses and Dissertations by an authorized administrator of UND Scholarly Commons. For more information, please contact zeineb.yousif@library.und.edu.

INFLUENCE OF HIGH-INTENSITY TURBULENCE ON LAMINAR BOUNDARY LAYER DEVELOPMENT ON A CYLINDRICAL LEADING EDGE: ENHANCEMENT TO EDDY DIFFUSIVITY

by

Juli K. Pearson
Bachelor of Science, University of Minnesota, 2009

A Thesis

Submitted to the Graduate Faculty

of the

University of North Dakota

in partial fulfillment of the requirements

for the degree of

Master of Science

Grand Forks, North Dakota
August
2015

Copyright 2015 Juli K Pearson

This thesis, submitted by Juli K. Pearson in partial fulfillment of the requirements for the Degree of Master of Science from the University of North Dakota, has been read by the Faculty Advisory Committee under whom the work has been done and is hereby approved.

_____
Forrest Ames Chairperson

_____
Nanak Grewal

_____
Gautham Krishnamoorthy

This thesis is being submitted by the appointed advisory committee as having met all of the requirements of the School of Graduate Studies of the University of North Dakota and is hereby approved.

_____
Wayne Swisher
Dean of the School of Graduate Studies

_____
Date

PERMISSION

Title	Influence of High-Intensity Turbulence on Laminar Boundary Layer Development on a Cylindrical Leading Edge: Enhancement to Eddy Diffusivity
Department	Mechanical Engineering
Degree	Master of Science

In presenting this thesis in partial fulfillment of the requirements for a graduate degree from the University of North Dakota, I agree that the library of this University shall make it freely available for inspection. I further agree that permission for extensive copying for scholarly purposes may be granted by the professor who supervised my thesis work, in his absence, by the Chairperson of the department or the dean of the School of Graduate Studies. It is understood that any copying or publication use shall not be allowed without my written permission. It is also understood that due recognition shall be given to me and to the University of North Dakota in any scholarly use which may be made of any material in my thesis.

Juli K. Pearson
July 6, 2015

TABLE OF CONTENTS

LIST OF FIGURES

Figure

LIST OF TABLES

Table

NOMENCLATURE

A^+	Van Driest constant
a	Speed of Sound
ABS	Acrylonitrile-Butadiene-Styrene
ATM	Algebraic Turbulence Model
C_D	Drag coefficient
Cf/2	Skin friction coefficient $\boldsymbol{Cf/2 = \tau_o/(\rho U_\infty{}^2)}$
C_P	Specific heat at constant pressure
C	Specific Heat
C_μ	A constant from the K-ε model
D	Diameter of cylindrical leading edge
D_v	This is the near wall dampening function
D*iff*	The diffusivity
DNS	Direct Numerical Simulation
FSTI	Free Stream Turbulence Intensity
h	Enthalpy
k	Thermal conductivity
k	Instantaneous value for the turbulent kinetic energy
$\bar{k}$	Time mean value for turbulent kinetic energy
k'	The fluctuating component of the turbulent kinetic energy
L	Length Dimensionless
l	Length
ℓ	Mixing length

Lu	The energy length scale
M	Mach number
m	Mass
Nu	Nusselt number
P	Pressure
Pr	Prandtl number
q	Heat energy caused by a temperature gradient, J
r	Radius
R_{air}	Universal gas constant
R	Result data
Re_D	Reynolds number diameter
Re_x	The Reynolds number using the x-direction length
St	Stanton number
T	Temperature of free stream
t	Temperature at a location
TRL	Turbulence, Reynolds number, and length scale parameter
Tu	Turbulence
u	Streamwise x-direction velocity
$\bar{u}$	The averaged x-direction velocity
u’	RMS normal fluctuation of x-direction velocity
U^+	Dimensionless velocity
U	Dimensionless Velocity
u_τ	The shear velocity

V	Total mean velocity
v’	y component velocity
$\bar{v}$	Averaged y component velocity
v	Y direction velocity variant
x	Streamwise distance across the surface of stagnation region
y	Normal distance from the surface
y	Length in the “y” direction
Y^+	Dimensionless boundary layer height

Greek symbols

γ	Fraction of flow in transition
Δ	Difference or change
δ	Thickness of the momentum boundary layer
δ1	Displacement Thickness
δ2	Momentum thickness
Ɛ	Turbulent dissipation rate
ε_M	Eddy diffusivity for momentum
ε_H	Eddy diffusivity for heat transfer
η	Similarity parameter
κ	Mixing length constant
λ	Mixing length constant
μ	Dynamic viscosity
ν	Kinimatic viscosity
$\nu_{M,o}$	The eddy diffusivity as defined by Ames et al.

ξ	Dimensionless expression
υ_m	The eddy viscosity
ρ	Density
τ	Shear
φ	Dimensionless parameter
ϵ	Eddy diffusivity used by other sources

Subscripts

∞	Infinity or free stream value
d	Diameter
h	hydraulic diameter or diameter
i	Inner
m	Momentum component
o	Outer
s	Located at the surface
t	Turbulent component
w	Wall location
x	Distance
xt	This is th distance where the transition begins from laminar to turbulent flow

ACKNOWLEDGEMENTS

I would like first to thank Forest Ames for his expertise, guidance, patience and instruction in the field of Mechanical Engineering and for taken me on as his graduate student in his busy schedule. I am grateful to the University of North Dakota for providing me this excellent opportunity for higher education. I would like to express my sincere gratitude to the staff and faculty of this university that taught me new skills and helping me build up my strengths. I especially want to thank Jay Evenstad and Gary Dubuque for helping me design many of the setups for experimentation. I also would like to thank DOE and Rolls-Royce for the funding that provided me financial support during graduate school.

I also want to thank my family, in particular, my parents, who have supported me in my decision to attend grad school. I also would like to thank my friends who have been a great help to me while I was away at Grand Forks. I want to single particularly out my dear friend Bonnie who balanced her schooling as well as being my best friend. Finally, I would like to thank Eph Sparrow, who encouraged me to get an additional education after completing my bachelor in science so that I could be a more rounded and knowledgeable person.

ABSTRACT

The growing demand for increased efficiency in turbine engine designs has sparked a growing interest for research of air flow around curved surfaces. The turbine's operating conditions result in material property constraints, especially in the first stage turbine vanes and blades. These turbine vane components experience extreme loading conditions of both high temperature and high turbulence intensities exiting the combustor. The surface of the turbine blades has cylindrical leading edges that promote stabilizing flow accelerations. These convex surfaces can cause a reduced eddy diffusivity across the boundary layer.

This thesis reviews measurements of velocity and turbulence intensities taken just shy of the thirty degrees offset from the stagnation line of a two-dimensional cylindrical leading edge under a wide range of turbulence and flow conditions flow conditions. Flow conditions and velocity measurements were gathered with respect to the distance to the surface. The length of the measurements extended from the surface to beyond the boundary layer's edge. The instrumentation used to collect data was a single wire driven by a constant temperature anemometer bridge. The hot wire is specially modified to measure data near the cylindrical leading edges curved surface. The traversing system allowed the acquisition of high-resolution boundary layer data. The traversing system was installed internally to the cylindrical leading edge to reduce probe blockage.

The test model's design had a 40.64 cm diameter cylindrical leading edge. A cylindrical leading edge is a convex surface that has a constant radial distance from the center, until 30 degrees from the stagnation line. At this point, the radius gradually increases transversely to promote high acceleration across the test vane surface. This design of the remaining test surface curvature results in smoothly varying but reduced acceleration by gently increasing the radius located between the surface and the cylindrical leading edge's center. This cylindrical leading edge test surface is designed to represent a two-dimensional turbine vane surface. The test apparatus's design included easy access to the internal testing apparatuses that could be either measure flows along the stagnation point or 27 degrees offset from the stagnation point. The test apparatus's design allowed room for the test equipment by using solid modeling software to ensure the necessary space was available.

Velocity profiles were collected and analyzed to determine the near wall eddy diffusivity distribution that determined the near wall eddy diffusivity distribution that was compared to the Algebraic Turbulence Model (ATM). This model estimates the local eddy diffusivity based on local turbulence conditions and the distance from the wall. The boundary layer data were collected and compared against the ATM model. The analyzes used a dimensionless shear stress distribution that was estimated using both a program named "STAN 7" and an algebraic shear stress distribution from White (White, 1974, p. 446). The results showed how much of the boundary layer is affected by the turbulence intensity, the Reynolds number, and the free stream flow's conditions.

CHAPTER I

INTRODUCTION

The rising costs of fossil fuels and labor have driven industries like power and aviation to increase the efficiencies and life of turbine engines. The turbine vane can experience gas temperatures well above the melting point of the material: potentially resulting in distress on the parts. Increasing the lifespan of components increases the revenue service and reduces the life cycle costs. Understanding the effects of how the eddies straining along the surface influences heat transfer on the surfaces allows better turbine vane and blade designs that incorporate the advantages of delayed transition due to acceleration. These better designs have better efficiencies and longer material life.

The high heat load on first stage gas turbine vanes creates design challenges when maintaining turbine component temperatures below material limits. The high temperature, highly turbulent gasses that exit from the engine's combustor results in a high heat load on these turbine vane surfaces. Heat transfer on turbine engine surfaces is strongly affected by the boundary layer and where the transition occurs along the surface. High free stream turbulence also influences surface drag that that affects machine efficiencies.

The leading edge of the turbine vane first experiences the free-stream flow exiting the combustor. These flows that exit the combustor produce very high heat loads and turbulence intensities. These flow characteristics also influence boundary layer

development further downstream. In this thesis, the observation of the laminar boundary layer, about twenty-six point nine degrees offset from the stagnation line will occur under several controlled free-stream flow conditions. Results of the momentum boundary layer structure will reveal eddy straining effects on boundary layer development. The measurements taken will include the system temperatures, the system pressures, averaged and variant velocities along the boundary layer and the respective distance from the surface, in addition to an eight to one variation of the Reynolds number.

The high-intensity turbulence in the free stream and acceleration around the cylindrical leading edge influences the boundary layer development that occurs near the cylindrical stagnation line. The intent of this research is to improve our understanding of the development and structure of the laminar boundary layer under these conditions. The comparison made between the experimental measurements acquired on the laminar boundary of 40.64 cm diameter cylindrical leading edge model, and earlier work on the stagnation line fluid dynamics will show the behavior of the momentum boundary layer. These conditions will be systematically changed using a larger grid and a smaller one at two locations and a simulated aero-combustor at two conditions.

These results can be used for predictive modeling in the turbine industry, as turbine vane diameters are increasing in size. Understanding how these variables in the flow conditions affect boundary layer development away from the leading edge of the vane. This work coincides with another student's thesis who is taking turbulence data along the stagnation streamline.

The goal is to establish the relationship the turbulence influenced by eddy straining has on both the momentum boundary layer and the thermal boundary layer.

Understanding this relationship opens up the methodology for future testing and design of turbine blades. A comparison of earlier work, Preethi Gandavarapu, on heat transfer for the same shape profile should reveal the relationship between the heat transfer and the fluid dynamics for large, traversing diameter, cylindrical leading edge Preethi Gandavarapu's heat transfer augmentation results will be used to compare with the local measurement of eddy diffusivity (Gandavarapu, 2011).

CHAPTER II

LITERATURE REVIEW

The study of turbulent flow encountering curved surfaces has spanned over several decades. In some ways, the flow over a curvature can be compared to a flat plate. However, there are differences in the boundary layers. The analysis of this widely discussed subject has resulted in a significant amount of research for many decades. Many engineering fields, particularly turbine engine vanes and blades, look to improving their products by examining the fluid dynamics. Curved surfaces can have a convex or concave curvature to model different surfaces of the turbine blades. Understanding how the exterior design affects heat transfer will influences how interior cooling is designed.

In the last ten years advances in turbulence generation have allowed researchers to achieve Turbulence (Tu) levels of ten to twenty percent within the free stream, which is closer to what a turbine vane can experience. Equation [1] defines the turbulence as the RMS fluctuation of velocity divided by the free stream velocity (Radomsky & Thole, 1999).

$$Tu = \frac{u'}{u_\infty} \qquad [1]$$

Gas turbine engines experience flows that have high Free Steam Turbulence Intensity (FSTI) that influence heat transfer rates and drag on both turbine blades and vanes. The transition is influenced by flow accelerating along the surfaces of the turbine blades and vanes. These conditions can also lead to the flow experiencing bypass

transition. However, acceleration acts as a stabilizing effect on surfaces that can offset curvature effects and delay transition. Acceleration on a cylindrical leading edge can result in a laminar boundary layer, with augmented heat transfer.

In 1970, Willmarth and Yang talked about the relationship between eddies and the pressure measurements they collected. Their experiment observed the turbulent boundary layer on both a flat plate and a traversing curvature. The surface was designed to be just flexible enough to be disturbed by pressure fluctuations. The results indicated that convection speeds were equal in both the planar and the traverse curvature. However, the velocity profile in the traversing curvature appeared more "full" than that of the flat plate. Further, the decay of eddies near the wall occurred faster with the traversing curvature (Willmarth, 1970).

The author's hypotheses that are traversing curvatures created more shearing against the eddies by the surface so that smaller eddies formed near to the surface. These smaller eddies were able to be closer to the wall but dissipated at a faster rate. The larger eddies further from the surface experience shear from the curve on the surface. The authors suggested shear from the convex surface increases the velocity (Willmarth, 1970). So one could imagine the eddy with angular momentum reducing its radius and as a result increasing its angular velocity.

Britter, Hunt, and Mumford wrote an article in 1979 concerning the distortion of turbulence by a circular cylinder. They found that large length scales would cause the flow to see an increase in u' and w' near the cylinder, whiles small length scales will see a dampening of these fluctuations. They also found that the turbulence intensity affects

the magnitude of mixing at the stagnation and broadness its influence (Britter, Hunt, & Mumford, 1979).

Blair also wrote the "Influence of Free-Stream Turbulence in Favorable Pressure Gradients" in 1982. This article discussed how favorable pressure gradients affect the transition to turbulent flow. The data measured from flow across a flat plate experiencing reduced the cross-sectional area. It is important to note that for this case there's no shear from the angle on the surface and the free stream velocity is parallel to the plate with the measurements. The author indicated for his case that acceleration did not affect the transitional Reynolds number, and the results agreed with Van Driest and Blumer's correlation for transitional onset (Blair, 1982).

Another interesting point in this 1982 article by Blair showed the thermal boundary layer development trailed the momentum boundary layer. The author also mentioned that the temperature profile was larger than the momentum boundary layer. The author pointed out that this is because the thermal boundary layer was not as strongly dependent on this acceleration. The author believed this was because of the relationship the pressure gradient had on the turbulent transfer of heat (Blair, Influence of Free-Stream Turbulence on Boundary Layer Transition in Favorable Pressure Gradients, 1982).

Blair conducted an experiment where a zero pressure gradient existed along the test surface. The experimentation modeled the free-stream flowing across a flat plate. The author concluded that upon a plate under these conditions that the free stream turbulence had a strong influence on skin friction and heat transfer (Blair, 1983). Further analysis of

the data revealed that increasing free stream turbulence dampened the wake region of the velocity profile.

Further Blair showed that the data's skin friction would increase as the free stream turbulence is increased. The interesting part of this data implies lower Reynolds numbers are not as influenced by free stream turbulence as the higher Reynolds numbers, for a flat plate. This occurrence also appeared for all of the different trials done on a flat plate discussed above (Blair, 1983).

Sparrow and Miyazaki in 1977 developed a method of prediction of heat transfer rates documented in "Analysis of Effects of Free-Stream Turbulence on Heat Transfer and Skin Friction" by including free stream vortices effects. They proposed a prediction of the momentum diffusivity as a function of free stream vortices and expressed the relationship as a dimensionless expression. They used previous studies on turbulent flow to set constants. The prediction mentioned above prediction works in regions where the fluctuations of the velocity are strong and not limited by the wall. (Miyazaki & Sparrow, 1977).

In "An Algebraic Model for High Intensity Large Scale Turbulence," an accurate correlation predicted both the eddy diffusivity and the velocity on a pressure surface. This model, which is called the Algebraic Turbulence Model (ATM), used the free stream turbulence conditions and the normal distance from the surface to predict the eddy viscosity for momentum. Additionally the near wall dampening effects were captured. A comparison between data from a cascade vane set up and the ATM model above. The results from the model agreed well with the prediction (Ames, Kwon, & Moffat, 1999)

The authors indicated that in the stagnation region of the flow, the ATM model predicted lower values of heat transfer than the data. The authors suggested that this was from the influence of the stagnation region and the free stream turbulence which "strains" the flow and encouraged mixing. This strain field results in an intensification of the smaller eddies near the wall as indicated by the normal velocity varying component "v'" measurements (Ames, Kwon, & Moffat, 1999).

In the article "Flow Field Measurements for a Highly Turbulent Flow in a Stator Vane Passage" by Radomsky and Thole, reviewed how flows with FSTI close to twenty percent. They were also able to measure all three directions of the flow velocities. The authors indicated that the turbulence "remained high" in the passageways of the turbine vanes. The authors believed this might explain the "production of shear stress" when combined with the curvature of the streamlines. The results showed the higher FSTI resulted in transition occurring further downstream. The authors also indicated that augmented of heat transfer occurred on the "pressure side" of the vane (Radomsky & Thole, Flowfield Measurements for a Highly Turbulent Flow in a Stator Vane Passage, 1999).

Randomsky and Thole studied the free turbulence effects on turbine stator vanes for very high turbulence intensities of 19.5% and very low intensities of 0.6%. They measured surface temperature and velocity profiles of the stator vanes. They found that the locations of lowest augmentation between the low turbulence case and the high turbulence case occurred in the same place vortices occurred (Radomsky & Thole, 2000).

Randomsky and Thole believed that the flow of the vortices had greater influence in these areas. Lower freestream turbulence cases had peak heat transfer augmentation

located in the stagnation region and fell off once the flow exited this region. General flow behavior rules out other possibilities (Radomsky & Thole, 2000).

In 2000, Bae, Lele, and Sung completed a numerical simulation of stagnation region heat transfer. Here the authors reviewed the flow hitting a flat plate. From these results, the authors concluded that the counter rotating vortices have a greater influence on heat transfer (Bae, Lele, & Sung, 2000).

Erickson and Ames wrote a paper called, "Effects of a Realistically Rough Surface on a Vane Heat Transfer Including the Influence of Turbulence Condition and Reynolds number." This paper showed that turbine vanes at high Reynolds number and high FSTI. The results showed how FSTI effect the heat transfer along the vane's surface. The Augmentation of the heat transfer appeared to affect the distribution of heat transfer across the surface. The results showed Stanton number peaks higher downstream than that of the stagnation region. In the experiments, the authors reviewed the effects of roughness on a vane affected heat transfer (Erickson, Ames, & Bons, 2012).

Both the cylindrical leading edge and the vane have a convex curvature in the stagnation region. When looking at the data on the smooth surfaces, it appeared that the higher FSTI had augmented the flow far downstream of the stagnation region when compared to the Low FSTI. Also, higher FSTI had surface Nusselt numbers that appeared to be higher and steeper (Erickson, Ames, & Bons, 2012). Equation [2] defines the Stanton number as the Nusselt number divided by the product of the Prandtl and Reynolds number (William Kays, 2005).

$$St = \frac{h}{\rho u_\infty c} = \frac{Nu_D}{Pr \times Re} \quad [2]$$

Mayle had worked on the transition in his 1991 paper concluded that experimental conditions may reach a point where the onset of transition occurs. In this paper, the author expressed that a boundary layer under transition has both laminar and turbulent conditions. The driving forces behind this onset (besides Reynolds number), is free stream turbulence and unsteadiness in the flow. Therefore the path of boundary layer transition is related to the local Rex, the Rex at transition onset and the local spot production rate and predictions should use the following correlation made by Mayle described in Equation 3 (Mayle R. E., 1991).

$$\gamma = 1 - exp[-\bar{n}\sigma(Re_x - Re_{xt})^2] \quad [3]$$

The expression above is used for flow in transition since the flow will show both laminar and turbulent flow. The symbol γ designates the proportion of turbulence in transitional flow. Mayle had said that a rule of thumb Reynolds number for distance was about 350,000 as described in Equation 4 (Mayle R. E., 1991).

$$F(x) = (1-\gamma)f(x)_{Laminer} - \gamma f(x)_{Turbulant} \quad [4]$$

The big driving forces behind the onset of transition, besides Reynolds number is free stream turbulence and unsteadiness in the flow. Therefore to find the boundary layer thickness during under transition. Therefore he used the symbol "γ" as the proportion of turbulent flow in the transitional flow (Mayle R. E., 1991). Therefore, the boundary layer in transition may be predicted and analyzed. This paper implies that transition has turbulent characteristics of higher mixing.

In 1997, Volino and Simon reviewed the boundary layer under conditions of high free stream turbulence and strong acceleration conditions. In their paper, "Boundary Layer Transition under High Free Stream Turbulence and Strong Acceleration

Conditions: Part 1- Mean Flow Results," the flow accelerated across a concave surface as compared to a convex surface. The goal was to see how this curvature and the free stream turbulence would affect the transition in the boundary layer. Transition in a boundary layer increases the heat transfer and drag. The author felt that understanding, where the transition occurs on a surface, was critical to airfoil design (Volino & Simon, 1997, A).

In "Boundary Layer Transition under High Free-Stream Turbulence and Strong Acceleration Conditions: Part 1 – Mean Flow Results," R.J. Volino and T.W. Simon studied the effects of strongly accelerated flow under high FSTI conditions have when measurements are collected at various points along the accelerating surface. The FSTI investigated was about eight percent free-stream turbulence with length scales of two and four centimeters (Volino & Simon, 1997, A).

They found that the turbulence decayed across the surface which the authors expressed this occurred in reality. They found that when comparing the effects of acceleration on flow, greater suppression of boundary layer growth was experienced. The authors believed that the acceleration for their concave curvature reduced the impact of the curvature. However, the authors also expressed that this observance most likely does not explain the relationship between curvature and acceleration. The author wanted to see results with objects of stronger curvatures (Volino & Simon, 1997, A).

In 1997, Volino and Simon published the article, "Boundary Layer Transition under High Free Stream Turbulence and Strong Acceleration Conditions: Part 2- Turbulent Transport results." These authors expressed that acceleration across the surface suppressed the eddy viscosity as compared with an unaccelerated flow on the strong concave surface. They also found in some areas of the flow the thermal boundary layer

was thicker than the momentum boundary layer. The authors believed the flow was experiencing transition because of the way that the boundary layer profile of u'increases and the peak moves toward the surface. The boundary layer only became fully turbulent flow further downstream when the acceleration rate was lowered and the Reynold's number was increased. (Volino & Simon, 1997, B)

The authors indicated that the Reynolds analogy is valid for both accelerated and unaccelerated flows under their design conditions since the ratio of the momentum eddy diffusivity to the eddy diffusivity of heat transfer were nearly equal. Also, the turbulent Prandtl number was equal to unity. (Volino & Simon, 1997, B) See the appendix for the derivation of the Equation 5.

$$1/Pr_t = \frac{\overline{v't'}}{\left(\frac{\dot{q}''}{\rho C}\right)} = 1 \ (for\ Reynolds\ Analogy) \ [5]$$

In a Paper written in 2005 by A.C. Nix and T.E. Diller in the 2005 Turbo Expo, the authors reviewed how augmented heat transfer in the stagnation region relates to the influence of Free Stream Turbulence. The collection of measurements occurred taken along the cylindrical leading edge vane apparatus in the stagnation region of the flow. The heat transfer measurements occurred at the stagnation region reaching away from the surface. Some of their results were interesting. The highest coherence for one of the locations was the closest location to the surface (Nix & Diller, 2005).

The Nix and Diller concluded from their results on the fluid dynamics and heat flux data that several patterns occur when the flow changes. When there was a drop in the integral length scale the author said that it was "indicative of vortex shedding" (Nix & Diller, 2005, p. 7). Further, the authors expressed interest in the results from the small

region affected by FSTI. They said, "for which the free stream velocity fluctuations affect surface heat transfer roughly centered on the frequency related to the integral length scale" (Nix & Diller, 2005, p. 7). The authors suggested that this indicated that large-scale turbulent eddies could augment flow (Nix & Diller, 2005).

In the article "Reynolds Stress Calculations for Pre-Transition Boundary Layers with Turbulent Free Streams" written by Mayle, Schultz, and H.J. Baur, the authors examined flow in pre-transition flows. One of the interesting findings in this article was that the $-\overline{u'v'}$ terms maximum occurs in the near transitional boundary layer about 1/3 as high as a turbulent boundary layer. (Mayle, Schultz, & H.J., 2008) Where $-\overline{u'v'}$ is defined in Equation 6 as the product of the eddy diffusivity and the velocity gradient (William Kays, 2005, p. 182).

$$\varepsilon_m \times \frac{du}{dy} = -\overline{u'v'} \quad [6]$$

The authors also indicated that the flow has essential behaviors for certain events. The authors implied that in some cases when the flow approaches separation the $-\overline{u'u'}$ max sharply increases. The authors speculated that separation can be avoided when the flow begins to go in transition as seen when $-\overline{u'v'}$ rises. The results showed that the boundary layer had higher $-\overline{u'v'}$ than predicted when the flow heads near transition. Also it is clear that amplification was not related to just the FSTI as the authors also believed that the effect on the FSTI has on the flow is "accumulative" which means that distance along the surface plays a major part (Mayle, Schultz, & H.J., 2008).

In 2011, a paper written by J. G. Wissink and W. Rodi, reviews the Direct Numerical Simulation "DNS" of freestream wake interacting with the stagnation region

of a cylinder. He set up his simulation to impinge vortices on the surface of the cylinder. There were three test conditions: no wake and no turbulence, wake no turbulence, and turbulence and wake. The authors designed a disturbance to produce a wake with small vortices that will disturb the cylinders surface (Wissinck & Wolfgang, 2011).

J. G. Wissink and W. Rodi highlighted three conditions, known from the literature that affect the stagnation heat transfer influenced by FSTI. For these laminar boundary layers, three observances tend to occur for augmentation due to the FSTI in a laminar boundary layer. First the acceleration, which is also needed to keep the flow laminar, must be present. Secondly, the free stream characteristics higher Reynolds numbers, higher FTSI, and lower length scales result in higher heat transfer levels at the stagnation region. Finally, the wake frequency within the free stream has strong enough effects on lower Reynolds numbers to amplify heat transfer (Wissinck & Wolfgang, 2011).

J. G. Wissink and W. Rodi's DNS results showed that the approaching free stream flows slowed the most when there were awake and no turbulence, then with the high FSTI. The case without the wake slowed the least of the different tests. The flows without FSTI transitioned sooner than the flow with it. The authors Designed a DNS of an eddy injected into the flow passing a cylinder. The results showed the eddy was already being "dispersed by the strongly accelerating mean flow before it can reach the immediate vicinity of the cylinder," thus the average flow can influence these free stream vorticies. This dispersion indicates that DNS showed a delay in transition due to FSTI. Once the free stream vorticity reaches, the cylinder and the "the vertical structures from the wake were found to be significantly stretched by the strongly accelerating wall-parallel

(circumferential) flow into elongated vortex tubes that became increasingly aligned with the direction of the flow" (Wissinck & Wolfgang, 2011).

In Preethi Gandavarpu's Master's Thesis, the Nu_D measured along the surfaces of two cylindrical leading edges of four and sixteen inches showed interesting results which agreed with previous discussed studies that high velocity and high turbulence flows experience heat transfer augmentation and low Reynolds number flows had peaks of Nu_D at the stagnation region. The data also expanded the TRL parameter range. Also the validity of the correlation amplification was reviewed, data beyond a TRL of 10 had a lower TRL than the curve. The TRL shown in Figure 1, compilation shows the data of Gandavarapu. Equations 7 and 8 show how TRL is calculated and how the Nusselt number was dependent on the TRL (Gandavarapu, 2011).

$$TRL = Tu \times {Re_D}^{\frac{5}{12}} \times \left(\frac{D}{Lu}\right)^{\frac{1}{3}} \quad [7]$$

$$\frac{Nu}{Nu_o} = 0.004 * TRL \quad [8]$$

This TRL relationship was particularly true of low velocity flows on the smaller cylindrical leading edge. Also, the smaller cylinder's Nusselt number would consistently peak in the stagnation region. This pattern would indicate that convection of the fluids heat would be strongest in the stagnation region (Gandavarapu, 2011). Below please find the definition of the Nusselt number presented by Kays in Equation 9 (William Kays, 2005).

$$Nu_D = \frac{hD}{K} = \frac{Convective\ Heat\ Transfer\ of\ Fluid}{Conductive\ Heat\ Transfer\ of\ Fluid} \quad [9]$$

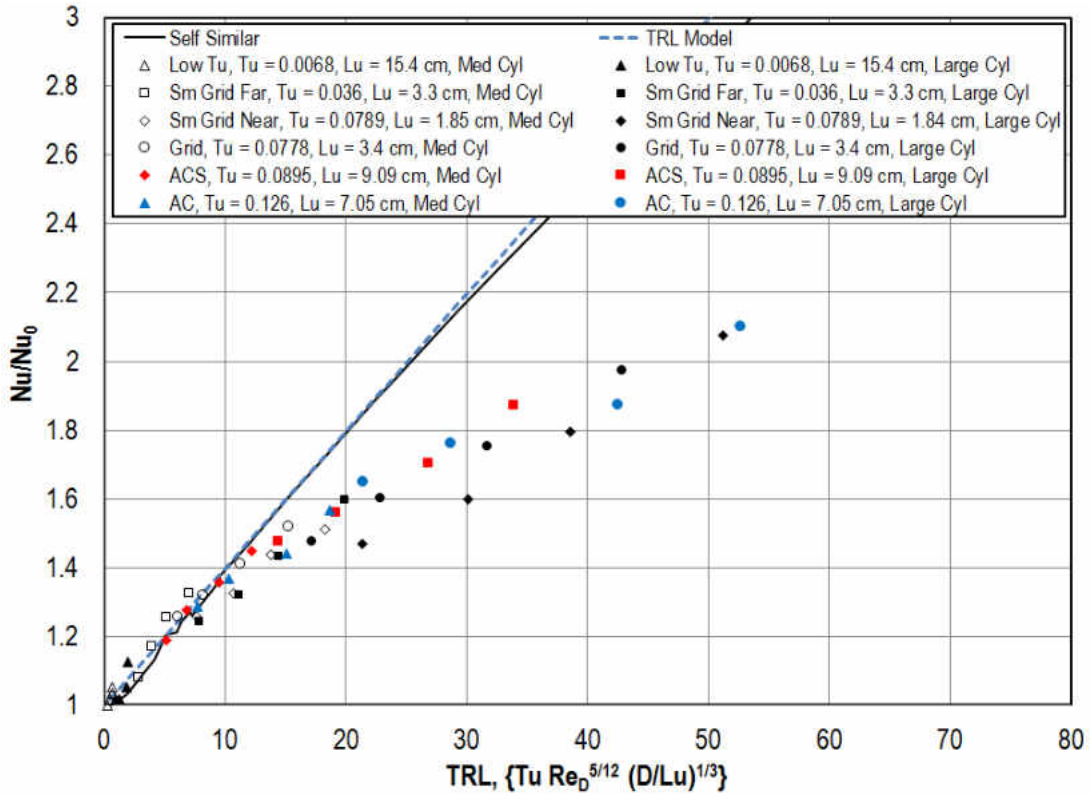

Figure 1. TRL results with added data (Gandavarapu, 2011).

However, the larger cylindrical leading edge saw the Nu_D peak for Re_d of 250,000 case for the Derivative Aero Combustor with the spool. As the Reynolds number increased to 500,000, a far downstream location of peaking occurred for the flow conditions with "Tu" greater than 0.08 (Gandavarapu, 2011).

For the large diameter cylindrical leading edge of 0.4064 meter results had different results. The cylindrical leading edge for Reynolds number of 62,500 and 125,000 cases the peak occurred at the stagnation line. However, but the span of the peak is more spread out over a further distance the stagnation region (Gandavarapu, 2011).

The data showed the larger sixteen inches Cylindrical Leading Edge Surface had greater augmentation then, the smaller four-inch Cylinder, but less "absolute heat transfer." Further there appeared to be an augmentation in the Nusselt number occurring

in the near stagnation region in the vicinity of the larger diameter cylinder. For the Reynolds number of 250,000 cases, the far downstream location results showed the stagnation region to have a broad Nusselt number profile along the surface, compared to the peaks experienced in the higher number turbulence numbers. The author expressed that the intensification of heat transfer was shorter weaker for the higher FSTI flows (Gandavarapu & Ames, 2013).

The work was done by N. Chowdhury at the stagnation region of this same large cylindrical leading edge apparatus in his thesis. Data collected from the stagnation line under the same range of Reynolds numbers and FSTI conditions. One of the first results showed that the velocity ratio of the free stream had demonstrated that near the stagnation region that velocity appeared faster than what the prediction from the CFD modeling showed. For some of the conditions, the velocity decay seems to decrease near the stagnation point due to high-intensity lateral velocity fluctuations. Also, the smaller Reynolds numbers have slightly higher ratios than the other numbers and the predictions presented in the paper. The lower values dip below the CFD prediction and then over shoot it (Chowdhury N. H., 2012). Unfortunately lower velocity measurements taken near the surface also have higher uncertainties. Therefore, slight differences in results may not mean much.

He found the fluctuating velocity become larger than the free stream before the surface for larger length scale values. The point closest to the surface shows then dropping just below the free stream values, but still relatively higher ratios than the other conditions. This increase in the velocity variance shows amplification of disturbances for

these two larger length scales conditions (Chowdhury N. H., 2012). These results match earlier work from Britter, Hunt, and Mumford (Britter, Hunt, & Mumford, 1979).

The results showed both the conditions (ACS and GS2), where the added distance to the flow had a larger value of the energy length scale "Lu." The "AC1" and the "ACS" had a greater magnitude of Lu then GS1 and GS2. The integral length scale results also showed this. These conditions without the decay spool had higher dissipation than those that occurred for the ACS and the GS2 for the Reynolds number of 250,000 cases near the surface or stagnation.

Additionally the dissipation data revealed for the Reynolds number of 62,500 case results had less dissipation than without the cylinder. The GS2 and ACS cases with a Reynolds number of 250,000 either equaled or surpassed the dissipation experienced (Chowdhury N. H., 2012).

CHAPTER III

EXPERIMENTAL APPROACH

The experiment was designed to observe the effect of free-stream turbulence, influenced by the stagnation strain field, on the boundary layer developing directly downstream of the stagnation region. The objective required measurements of the velocity taken within the fluid-dynamic boundary layer. These measurements include the velocity fluctuations, the total pressure, and the atmospheric conditions. Because the boundary layer of turbine vane is small, the design of the vane required a dimensional increase the scale. The measurement equipment had been concealed by the test apparatus or the cylindrical leading edge to avoid disrupting the sensitive boundary layer.

The design of experiment focused on the collection of data thirty degrees downstream from the stagnation region of the apparatus. This location produced a sufficient local velocity to allow accurate measurements but close enough to experience the influence of the stagnation strain field. Changes to the setup created access to equipment without interfering with the fluid dynamics. Further design features allowed ease of access to the equipment inside the cylindrical leading edge tip. To compensate for the height of the boundary layer, a new traversing device, and a modified 55P14 hot wire allowed measurement closer to the surface.

Measurements and calibrations were collected at the University of North Dakota's Large Scale Low Wind Speed Tunnel and the Cascade Facility in Grand Forks North

Dakota. The wind tunnel design produced different flow conditions by adding different test sections and grids to achieve the desired turbulence intensities. The wind tunnel can create conditions ranging from very low Reynolds number, and low turbulence intensity flows with high turbulent intensity flows that reach up to 13 percent or more.

The wind tunnel different sections help produce the desired inlet turbulence conditions. Air enters the filter box from the surrounding area to the blower. The filter protects the sensitive, hot wire anemometer, from damaging debris. After the air exits the filter, the air passes through the centrifugal blower. The flow then enters the multi-vane diffusers where the air recovers the static pressure by slowing the air flow and evenly distributing the velocity profile. An even distribution improves heat transfer through the heat exchanger as shown in Figure 2, which shows the wind tunnel set up (Gandavarapu, 2011).

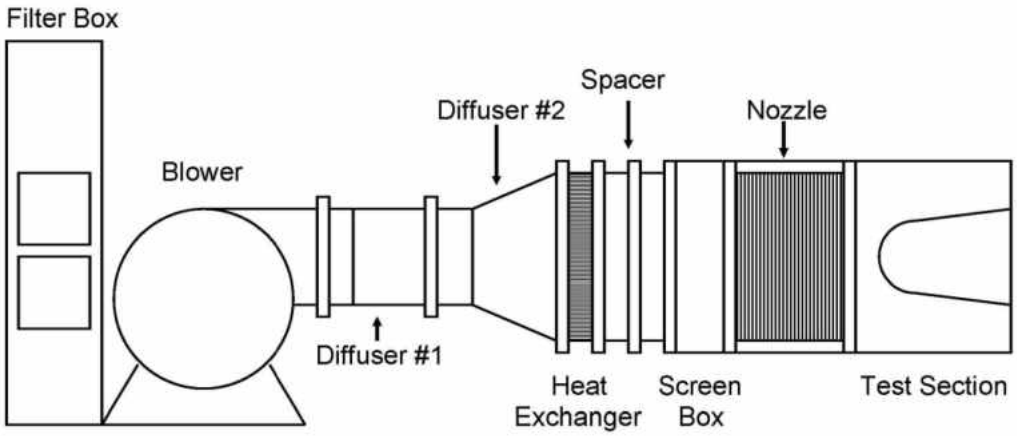

Figure 2 Wind tunnel set up.

The heat exchanger is air to water heat exchanger; it regulates the air temperature. The heat exchanger uses water which passes through its finned tubes to cool the air flow: allowing constant air temperature. A hundred-gallon recirculation tank supplies water.

The temperature of the water in the reservoir is maintained by replacing the warmer tank water with the cooler building makeup water. Then air enters the screen box. This screen box is made up of four nylon screens, which help redistribute the flow profile before it reaches the nozzle (Gandavarapu, 2011).

When the flow leaves the screen box, it encounters a nozzle. There are different types of nozzles to achieve the different desired turbulence levels of the flows. The low turbulence nozzle stabilizes the flow by decreasing the cross-sectional flow by about 72.22% (Gandavarapu, 2011). The interior design of the nozzle surface was designed to be smooth and be flush with the interior of the spool, turbulent generator, or the test section to reduce unwanted disturbances in the flow.

The changes to the free streams fluid properties occur by switching the grid assemblies or the mock aero derivative combustor assemblies. The grid assembly generates a smaller scale turbulence intensity. The grid assembly includes the spool and some grid meshes. Square aluminum bars adhered by JB weld helped make the square mesh.

Table 1. Distance from the Cylindrical Leading Edge.

		Distance	
Flow Condition	L_{mesh}	X (inch)	X(meter)
Large Grid	10	25	63.5
Small Grid Far	32	40	1.016
Small Grid Near	10	12.5	0.3175

The meshes come in two sizes, the small grid located either at 10 or 32 mesh lengths upstream from the leading edge plane and a large grid also located ten mesh lengths upstream. This is shown in Table 1. The small grid is constructed using 0.635 cm square bars spaced 3.175 cm apart. The large grid construction consisted of double the size square bars set apart by twice the distance as the small grid. (Gandavarapu, 2011)

$$L_{mesh} = x/Pitch_{mesh} \qquad [10]$$

The spool is a Plexiglas rectangular extension of the test section located between the test section and the Mock Aero-Derivative Combustor shown in Figure 3 and is 36 inches in length. From the spool, the grids slip into notches drilled through the Plexiglas. The spool can also add additional distance between the turbulence generator and the test section. This addition of the spool to the mock derivative aero combustor assembly allows the observance on how turbulence decays.

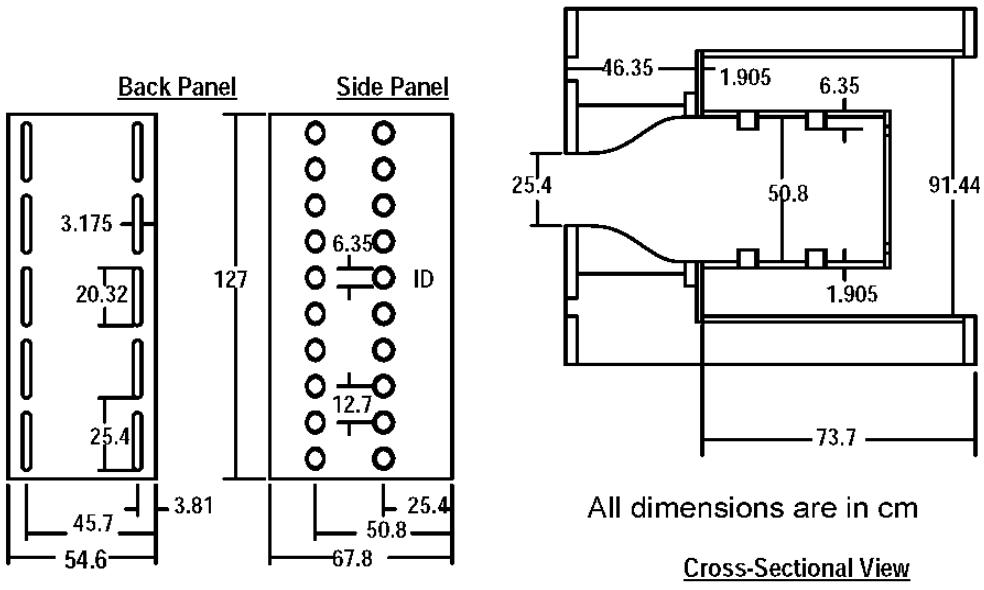

Figure 3. Mock Aero-Derivative Combustor (cm).

The Mock Aero-Derivative Combustor produces an accelerated, high turbulence intensity flow of about 13.5 percent and an energy length scale of about 7 centimeters. The existing flow accelerates through the nozzle to the Mock Aero Derivative-Combustor, which decreases the cross-sectional area by an additional fifty percent (Gandavarapu & Ames, 2013).

Table 2 shows are the flow conditions averaged from results for the 0.4064 m cylinder presented by J E Kingery at the ASME Turbo Conference and his paper in the turbomachinery journal. (Kingery & Ames, 2015)

Table 2. Flow Properties of the Free Stream Velocity.

Condition	Property	2.5 m/s	5 m/s	10 m/s	20 m/s
Low Turbulence	ReD	60864	121397	243759	485410
Low Turbulence	Tu	0.0069	0.0069	0.0076	0.0060
Low Turbulence	Lu (m)	0.154	0.154	0.154	0.154
Low Turbulence	TRL	0.94	1.25	1.84	1.95
Small Grid Near	ReD	60237	122154	245950	493636
Small Grid Near	Tu	0.0773	0.0808	0.0781	0.0792
Small Grid Near	Lu (m)	0.018	0.01785	0.018458	0.0197
Small Grid Near	TRL	21.43	30.16	38.59	51.20
Mock Aero-Derivative Combustor	ReD	60123	120954	245615	499359
Mock Aero-Derivative Combustor	Tu	0.1235	0.1235	0.1302	0.1259
Mock Aero-Derivative Combustor	Lu (m)	0.0724	0.0724	0.0636	0.0735
Mock Aero-Derivative Combustor	TRL	21.51	28.78	42.56	52.71
Large Grid	ReD	60762	121585	243178	484976
Large Grid	Tu	0.0755	0.0755	0.0790	0.0813
Large Grid	Lu (m)	0.033	0.033	0.034	0.0355
Large Grid	TRL	17.16	22.92	31.69	42.86
Small Grid Far	ReD	60486	121779	246348	493294
Small Grid Far	Tu	0.0350	0.0384	0.0352	0.0348
Small Grid Far	Lu (m)	0.0338	0.03808	0.032311	0.0285
Small Grid Far	TRL	7.88	11.12	14.45	19.88
Mock Aero-Derivative Combustor With Spool	ReD	61367	121698	244871	479686

Table 2. Continued

Mock Aero-Derivative Combustor With Spool	Tu	0.0883	0.0883	0.0916	0.0897
Mock Aero-Derivative Combustor With Spool	Lu (m)	0.0903	0.0903	0.0881	0.0949
Mock Aero-Derivative Combustor With Spool	TRL	14.41	19.17	26.83	33.92

After the flow exits the nozzle, it enters the rectangular wind tunnel cross section called the 'Test Section.' The wind tunnel's construction from 0.5 and 0.75 inch Plexiglas. The location of equipment and the small space available required the addition of access holes. These holes were cut using a dulled whole saw. Cutting the holes in the Plexiglas required a large amount of caution. The caution is due to the nature of Plexiglas. The hole's edges were wet sanded by hand to smooth out the roughness and to allow the windows and or hole covers to fit tightly.

The access holes had Plexiglas windows to cover the holes allowing visibility into the test section while sealing the wind tunnel. The location of the holes was picked to allow ease of access to the equipment. Figure 4 shows how the holes looked against the test apparatus. The hole located on the exterior of the test apparatus allowed installation and adjustment to the hot wire anemometer. We installed the hot wire to the exterior of the test apparatus to avoid damage to the hot wire. The hole located in the interior on the inside of the tip allowed adjustments to positions of the bracing equipment for the hotwire and to secure test equipment. The third hole allowed access for another project where measurements were acquired along the stagnation streamline.

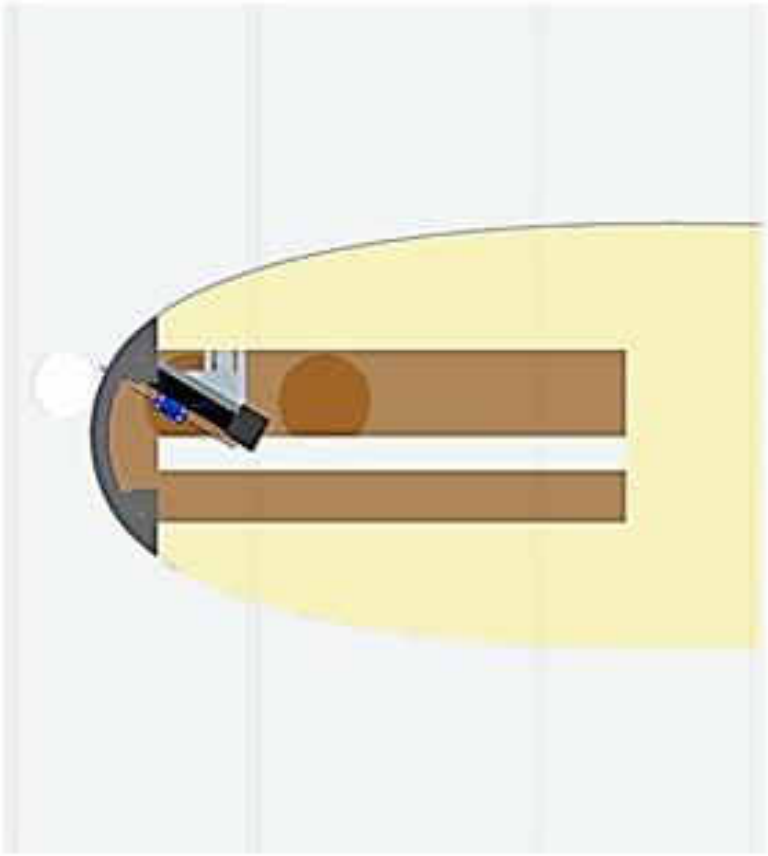

Figure 4. Three-dimensional test section model with 0.4064 meter cylindrical leading edge.

Small windows were designed to seal the holes during testing. Figure 5 shows how the windows looked in the experimental setup. These windows or covers were cut from Plexiglas using a CNC milling machine. The windows were designed using three-dimensional design software PRO- Engineering to fit snuggly over the hole. Compression helped prevent any fracturing while drilling the holes through the Plexiglas material. A large quantity of water was used to prevent locking of the drill bit in the hole. If the drill bit locked in the hole, it would result in cracking. To decrease fracturing of the Plexiglas the friction of a dull drill bit heated to the surrounding area. These covers had machine screws cut flush to the surface of the wind tunnel to fix the cover to the wind tunnel. The

purpose of these windows was to allow testing without the presence of the cylindrical leading edge test apparatuses and seal the surface.

Figure 5. Test section's window cover.

Two cylindrical leading edge vanes designed had two different diameters: one was a 0.1016 meter and the second was a 0.4064 meter vane. Only the 0.4064 meter cylindrical edge was utilized for this experimentation though a cylindrical leading edge is where a cylindrical edge has a traversing radius. Both the cylindrical leading edges had a radius that would increase as the surface location traversed after the thirty degrees offset.

Information in the appendix for the smaller 0.1016 meter cylindrical leading edge described its design process. The smaller cylindrical leading edge was left out because the acceleration of the 0.1016 meter cylinder would have produced a boundary layer that was too small for our current equipment to collect enough information in the near wall region for reliable analysis. The smaller diameter cylinder ended up used in the experimentation for another student's thesis research that focused on the stagnation line. However, the smaller cylinder had a port designed to collect information at the about a twenty-seven degrees offset. This way this information could be collected if the new equipment becomes available.

Figure 6. The 0.4064 meter cylindrical leading edge vane.

The cylindrical leading edge vanes had four components: the cylinder tip, the cylinder base, and two cylinder plywood sides. This is shown in Figure 6. The cylindrical tip's design allowed space for the traversing equipment. The cylinder base construction was also hollowed out, and the tip was removed. The plywood sides were made similar to previous sides, but one of the sides had a window inside of the cylinder. These plywood sides held the tip and back portion of the cylinder together.

Figure 7. The assembled 0.4064 meter cylindrical leading edge tip.

These cylindrical leading edge tips as shown in Figure 7, have both internal and external design features that allowed application of the cylinders for different research projects: testing at the stagnation region and the thirty degrees downstream.

The cylindrical leading edge's tip design allowed room for two different screw drive apparatuses mounted in the test apparatus. The imported profile from Excel used the points in a spline fit function in Pro Engineering. These data included the desired thickness of the cylinder tip. The three-dimensional modeling software 'Pro Engineering' was used to design the tip. The cylinder tip consisted of six pieces, including the two anchors, the tip, and the plugs. Figure 8 shows how the cylinder tip and the brace where connected by a pin.

The construction of the tip included pieces from a three-dimensional printer using Acrylonitrile-Butadiene-Styrene 'ABS' plastic. Creating the part from ABS allows the tip to withstand the high aerodynamic forces with much less material since ABS has high impact strength and is light. ABS Plastic allowed us to have a thin structure and more room to maneuver within the test apparatus.

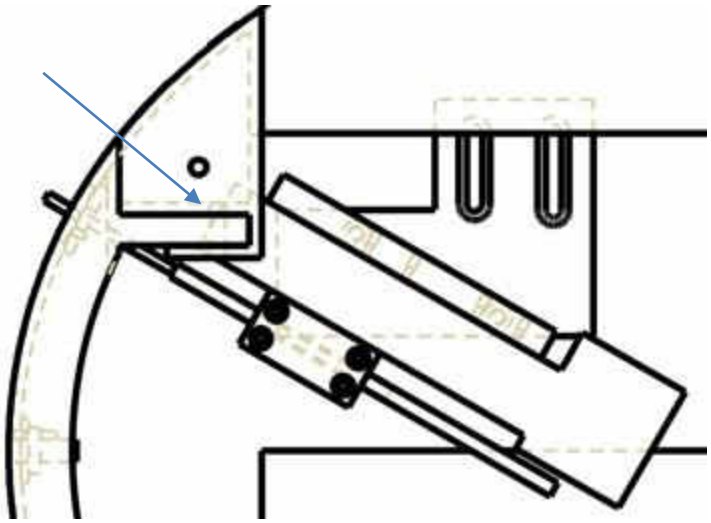

Figure 8. Pin location on 0.4064 meter cylindrical leading edge tip.

Both designs of the cylindrical leading edge vanes mounted the apparatus in the wind tunnel walls. These two-dimensional cylindrical leading edge surfaces were designed to be similar to first stage turbine vanes. Data were collected in the normal direction to the surface at the stagnation line and thirty degrees downstream. The data analyzed in this thesis is a downstream location from a stagnation line.

The cylinder tip exterior design followed the curvature of the previous cylindrical leading edge test surface for heat transfer (Gandavarapu & Ames, 2013) and velocity at the stagnation region (Chowdhury M. N., 2012). A smooth transition was necessary from the tip section to the base of the cylindrical leading edge. The curvature was designed to have an increasing diameter once the cylinder reaches thirty degrees downstream of the cylinder to help foster a stabilizing, accelerating flow.

The 0.4064 meter cylindrical leading edge had about 26.9 degrees offset from the stagnation region. This offset is instead of thirty degrees because the limitations of the three-dimensional printer's height, width and depth and the required space for the epoxy

board to adhere to. After the Part was printed, the exterior surface was scraped by hand and then buffed to have an even smooth surface. Additionally “pitting” can occur if the positioning is done in the wrong way. This is because of how the printer is programmed to hollow out the inside of the printed model.

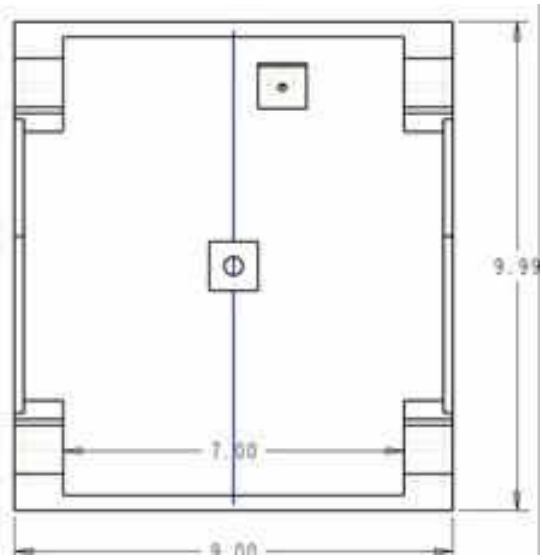

Figure 9. Back of cylinder tip (hole offsets).

The placement of the hole at 26.9 degrees was offset an inch away as shown in Figure 9, from the center, and the access hole located in the stagnation region. This design feature gave each location its streamline to collect data. The physical limitation of the three-dimensional printer was 10”x10”x12.” This limitation resulted in the 0.4064 meter cylinder having two more parts that are called the “Tip Braces.” The tip braces allowed the large diameter cylinder to be interchangeable with other tips for future use by removing the machine screws that act as pins. The thickness of the cylinder was designed by subtracting the same distance from the radius of the cylinder.

Figure 10. Picture of assembled tip after buffing.

Inserts were made to cover the holes at the two sites the probes would be collecting the data as shown in Figure 10. Because experimentation only requires one of these holes used at a time, inserts were created to plug the unused probe hole to prevent air leaks during the experiment. To avoid affecting the development of the fluid dynamic boundary layer, the location of the hole in the stagnation region was placed in the center of the cylindrical leading edge. The tape was placed along the streamline of the approach velocity to prevent surface imperfections from interfering with the boundary layer.

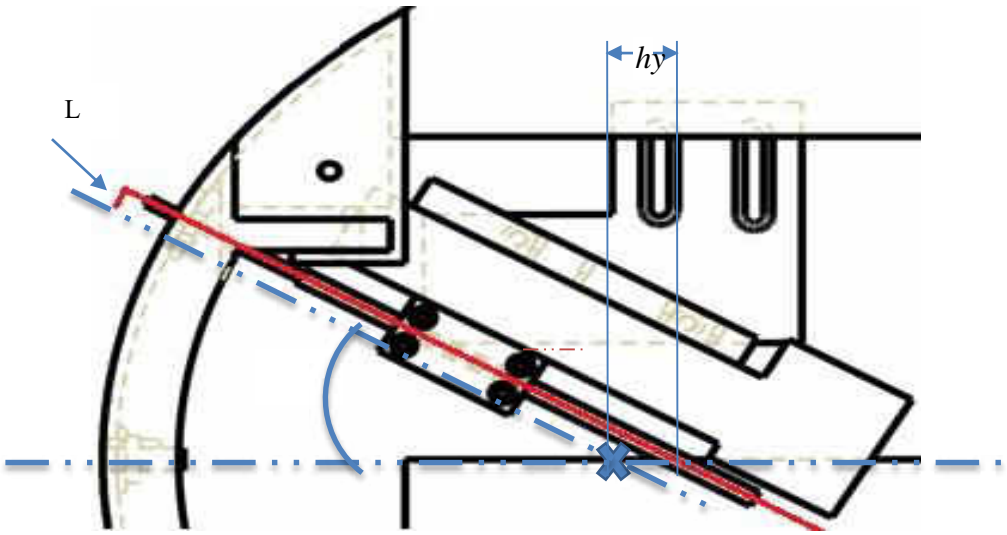

Figure 11. The true distance of the hot wire probe away from the probe holder

The location between the probe holder and the measurements as shown by Figure 11 were fixed by geometrical analysis the hot wire shape. According to the manufacturer, the Length of the Hotwire prong is 0.2165 inches. This required information also helped place the machine screw inserts for the probe brace system. Equation 11 shows how much distance "hy" was needed to properly align the probe. The distance ended up 0.433 inches.

$$Sin\ (30) = \frac{Oposite\ side}{Hypotenuse} = \frac{Length\ of\ Prong}{Offset\ of\ the\ axis} = \frac{0.2165\ inches}{hy} \quad [11]$$

The construction of the back end of the cylinder involved several steps. The first step used an aluminum jig with the cylinders profile. This jig's outline allowed a plunge router to cut isocyanate insulation foam boards into the shape of the cylindrical leading edge. Next pieces of plywood used the same jig as the insulation boards to cut the desired forms. The resulting pieces had matching profiles. These plywood boards are a half inch thick, high strength wood. Once the boards were cut, anchor inserts were installed to the

boards. These inserts allowed the boards to mount to the wind tunnel with machine screws. Then insulation boards were glued together on top of the back end of the pieces of plywood.

The next step was to remove the tip of the foam portion. A new design of tip needed to allow space for the measurement equipment. The removal was achieved by designing a three-dimensional printed tip that mounts to the foam and ply board. The rear of the cylinder was trimmed to have a cleaner edge. The center had the foam removed to allow room for experimental equipment. With the foam trimmed to specification, the cylinder tip bracket was glued to where the tip was removed from the foamed section.

The top piece of the plywood was then glued to the foam. Once the glue was set, the plywood pieces allow mounting of the traversing devices. The tip bracket was glued afterward to the tip of the cylinder. Once the tip bracket was installed, the 0.038 cm thick fiberglass epoxy board was adhered with cement glue over the flow surface. The tip bracket had a recess to allow the epoxy board to reside. A thin piece of Kapton tape covered the area where the epoxy board and the cylinder tip meet to prevent the epoxy board to be peeled off the insulation by the free stream velocity.

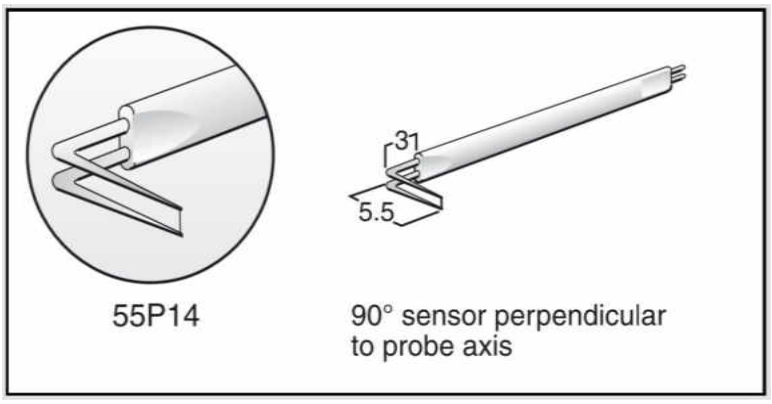

Figure 12. Dantec catalog's description of standard 55p14 dantec probe from catalog.

The specially modified, calibrated Dantec hot wire anemometer 55P14, shown in Figure 10, was used to measure data on the surface of the cylindrical leading edge surface. A standard 55P14 probe is a platinum plated single tungsten wire that has a diameter of 5 micrometers and a length of 1.25 mm. This probe is extremely delicate because of the thin diameter. Handling the probe required extreme care. By our request, the manufacturer modified the hot wire to measure data on the concaved surface by decreasing the angle from ninety degrees to eighty degrees. If not done the probe would not reach the curved surface. The resulting angle between the prong and the stem of the hot wire measured between 84-86 degrees.

This hot wire was calibrated using a smaller wind tunnel set up. Here the velocity and the corresponding pressure drop were used to calibrate the probe. The TSI IFA 300 constant temperature anemometry bridge conditions and amplifies the recorded drop in voltage from the hot wire while pressure taps are used to sense the drop in pressure. The calibration set up had two velocity settings 0.7 m/s to 1.25 m/s, and 1.15 m/s to about 28 m/s. Although measurements taken at velocities less than 0.7m/s would help increase the range of velocities, the uncertainties become much higher as velocity drops in the flow. These low velocity uncertainties are due to how the lower velocity values were calculated and calibrated. This can be reviewed in earlier work written by L. Dvorak. The two calibrated curves at the two velocity settings were combined to develop a complete relationship over the entire curve. Each probe went through calibration before it can be used to collect data on the surface. The velocity was measured using the pressure drop across the orifice and used the relationship described in Equation 12. The orifice was

designed to minimize the viscous effects, especially for the lower velocities from blockage effects caused by the boundary layer growth (Dvorak, 2003).

$$P = 0.5\rho(U^2)\,[12]$$

The calibration methodology used to calibrate the hot wire anemometers followed the same steps outlined in L. Dvorak's Master's Thesis. The equipment and the software were the same, and the inputs for the software were the same. The only difference was the modification of the 55P14 that was manually adjusted. Therefore, the two hot wire anemometers would have slightly different geometry. The set up allowed the calibration to occur by the error of two percent. The calibration was done by making adjustments to the setup that allowed velocities to be accurately measured within two percent (Dvorak, 2003).

Although it would be ill advised to use the same calibration curve for the hot wire anemometers, it would be wrong to not do separate calibrations for the two probes. Any time the probes needed repair calibrations were redone to ensure a good fit.

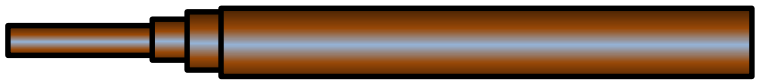

Figure 13. Home made probe holder.

The equipment used in this experiment to transverse the hotwire was the "Velmex XSLIDE" assembly that held the probe using a 4mm diameter Probe Support, and the XSLIDE's brace. The probe support, shown in Figure 13, was homemade from four brass tubes soldered together. This Probe design was chosen for the best fit of the hot wire, as

the manufacturers' probe holder did not work for what the function required. The brass tubing sizes are 5/32", 3/16", and 1/4" an inch. The 5/32" inch tube had a distance of 2.5 inches, the next two were a quarter of an inch, and the largest 1/4 inch tube was about five inches long. The hotwire slipped in the 5/32 inch tube and was taped to the probe support. The probe support was attached by a clamp that was mounted onto the XSLIDE.

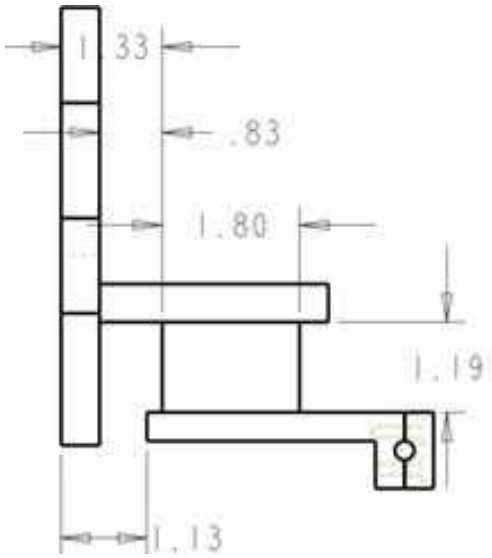

Figure 14. Brace system for traversing system and probe holder.

The traversing device needed to be attached firmly, because of the weight of the slide and the sensitivity of the equipment when making very small measurements. The traversing device was firmly attached to the brace system as shown in Figure 14. The brace held the X-SLIDE at the desired location and angle to collect the data. This brace was designed to adjust the angle, height, and vertical distances slightly so that the probe can be aligned perfectly normal to surface. This occurrence is because dimensional differences of the different cylindrical leading edge vane, two different supports for the different cylinders.

These supports were cut by the in-house CNC from aluminum and a third dimension model printer. The pieces of machined aluminum were attached by machine screws to the X slide and mounted on the plywood. Figure 15 shows how these where attached. All of the fastening areas were counter bored to prevent locking and allow more space to maneuver inside the test apparatus.

Figure 15. Traversing equipment mounted in test apparatus.

This traversing device, X-Slide made by Velmex, was designed to make extra fine movements. The device can travel a total of two inches (0.0508 meters). This device is also small enough to fit inside of the cylinder thanks to the smaller traversing distance. Values of velocity, location, “u,” and “Tu” were acquired from the probe and later analyzed.

The temperature sensors made from type K fine wire thermocouples measured the recovery temperatures upstream of the test apparatus. These thermocouples are accurate to two-tenths of a Celsius. The reference temperature used an ice bath to maintain a

constant temperature. This temperature helped establish the properties of the air. The total pressure was measured upstream at the test section entrance. The pressure measured at the test section entrance helped determine the pressure drop. From these pressures, the calculation of the exit and approach velocity was estimated. Pressure transmitters were used to obtain these pressures.

The HP-3497 data acquisition was used to acquire a voltage signal from the Rosemount pressure transducers that varied from 2 to 10 volts. The conversion from the voltage output to pressure included subtracting the zero pressure voltage from the signal. The computer converted the array of hot wire anemometry voltages into velocities using the calibration correlation. The pressure transmitters sent signals to the Data Acquisition System, and the computer converted the signal into a pressure reading.

Figure 16. Picture of hot wire probe on the surface.

During experimentation, the probe would start taking measurements at 0.3 inches (0.00762 meters) normal from the cylinder's surface and move in small increments to the surface. Figure 16 shows the probe near the surface. Because the limitations of the

equipment and acquiring data in small enough increments to read the flow in the near wall region, the equipment could not take measurements in fine enough increments. Reynolds numbers of about 500,000 case had thinner boundary layers. This effect resulted in the acquirement of a less resolved boundary layer. Therefore higher Reynolds numbers had fewer data collected near the wall. The location of the probe was later estimated by the process explained in the analysis, where the comparison of the predicted velocity to the actual velocity helped estimate values of the probe location and wall shear stress.

The location of the surface was determined when the viscous shear stress fell off instead of increased. The shear stress in the near wall region would only appear to fall off if the probe were touching the surface. Because this procedure results in an uncertain location, adjustments to the offset value had to be made in the iteration process described in the analysis to determine better the actual location of the measurements. One check ensured determination of the correct offset location. The last point measured was between 0.045 and 0.055 or 0.0080 to 0.009 thousandths of an inch (0.001143-0.001397 meters), which are the increments that the X-Slide was taking. The uncertainty of this location stems from a human error in the resetting the probe in the program and "slips" that may happen with the "XSLIDE."

During the experimentation, approach velocities will reached approximately 2.5 m/s, 5 m/s, 10 m/s and 20 m/s and resulted in flows that reached Reynolds numbers of 62,500, 125,000, 250,000 and 500,000. The air temperatures were constantly monitored to keep it constant, by using the heat exchanger. Once the data was collected, they were analyzed and crossed checked with data collected earlier. All data were analyzed using

non-dimensional conditions like the Reynolds number and free stream turbulence. Data collected was obtained by N. Chowdhury in 2012.

CHAPTER IV

ANALYSIS

Once the data was collected, it was converted into an Excel spreadsheet for analysis. All of the data analyzed went through the same steps. For simplicity, the analysis procedure will be reviewed with the data from the Aero-Combustor. The analysis portion is summarized and will have a more in-depth mathematical explanation in the appendix. Once the Equations were set up in the spreadsheet, the results were iterated until all of the results converged.

Some of the values were estimated by iterating the results until the solution is as close as possible. The velocity gradient normal to the surface, "$\frac{dU}{dy}$,"was estimated using the shooting method which will be explained later. Reynold's numbers: Re_D 62500, Re_D 125,000, Re_D 250,000, and Re_D 500,000 had an initial values of the velocity gradient normal to the surface of: 3500, 10,000, 35,000, and 90,000 1/s. This velocity gradient multiplied by the viscosity is the shear at the wall.

Because data collection that began in the free stream moved toward the surface of the cylindrical, leading edge there is an offset between the recorded value and the actual measured distance. You probably have too much in this sentence. This offset is important in developing the shear distribution. The fitting of the shear distribution involved both specifying an offset and the velocity gradient at the wall. The dimensionless shear stress

profile from White was used help determine this shear distribution, particularly in the near wall region. The offset is assumed to be zero at the beginning of the analysis.

Some of the data were determined from the measured velocity. The boundary layer thickness"δ" was determined from the first peak of the velocity profile results. The approach velocity was determined from the exit velocity. This was done by finding the Mach number "M" from the total and static pressure and the specific heat ratio of air is 1.4. This Mach number was determined from the measured air velocity leaving the test section and using the definition of a Mach number as described in Equation 13 and 14 (William Kays, 2005).

$$M = \sqrt{\frac{2}{1.4-1} \times \left(\left(\left(\frac{P_T}{P_S} \right)^{\frac{1.4-1}{1.4}} \right) - 1 \right)} \quad [13]$$

$$M = \sqrt{5 \times \left(\left(\left(\frac{P_T}{P_S} \right)^{\frac{1}{3.5}} \right) - 1 \right)} \quad [14]$$

The speed of sound "c" was derived from its definition using the gas constant "R" and the temperature of the air as shown in Equation 15.

$$c = \sqrt{1.4RT} \quad [15]$$

Then the speed of sound and the Mach number are used to find the velocity "U_{out}" which is the velocity of the air exiting the test chamber. The Equation 16 is from the definition of the Mach number.

$$U_{out} = M \times c \; [16]$$

From the exit velocity the velocity of the flow along the surface, the approach velocity "$U_{approach}$" can be determined using the acceleration parameter and the velocity. The presence of a leading edge is known to effect the velocity field well upstream of the stagnation region. Consequently, the conceptual approach velocity could not be determined from upstream measurements of total and static pressure. Consequently, a CFD prediction was performed to develop the relationship between the conceptual approach velocity and the test section exit velocity. The ratio develop from the analysis is provided by Equation 17 (Gandavarapu, 2011).

$$U_{app} = 0.4835 \times U_{out} \qquad [17]$$

The maximum velocity in the boundary layer was taken as "U_{∞}" for the analysis. The next parameter was the skin friction of the flow. This was determined using the parameters from Equation 18 (William Kays, 2005).

$$\frac{C_f}{2} = \frac{\tau_w}{\rho \times U_{\infty}^2} \qquad [18]$$

The measured velocity "U" profile was fit to a set of functions to analyze better the data, like a better velocity gradient prediction. The process of fitting the lines is explained in the appendix. After the fit for the velocity "U" is found that profile becomes "u(x)." The data were fit to a fourth order polynomial. From this fit, the difference was taken between the fit and the results. This difference was then fit and added to the fourth order polynomial. This process continued until the differences between the fits and the results stopped improving or was less than two percent. Each new fit had an increase of the polynomial order of two to catch the place where the data shifts across the "X" axis.

The resulting fit was the average velocity of the boundary layer that could be used for analysis. Please see Appendix IV for more information.

After the fit for the velocity "u(x)" is found, the dimensionless forms of the results can be determined using the shear velocity. The shear velocity."u_τ" is the free stream velocity multiplied by the square root of the skin friction. The non-dimensional velocity and the normal distance can be found by the Equations 19 and 20 (William Kays, 2005).

$$Y^+ = \frac{y \times \rho \times U_\infty \times \sqrt{\frac{C_f}{2}}}{\mu} \qquad [19]$$

$$U^+ = \frac{u(x)}{u_\tau} \qquad [20]$$

The converted data is then plotted on a U^+ verses Y^+Graph as shown below. The mock aero-combustor velocity profile graphs were then combined into one graph as shown below. This graph shown on Figure 17, helps to provide a visual representation of how to find the best Y offset and shear stress.

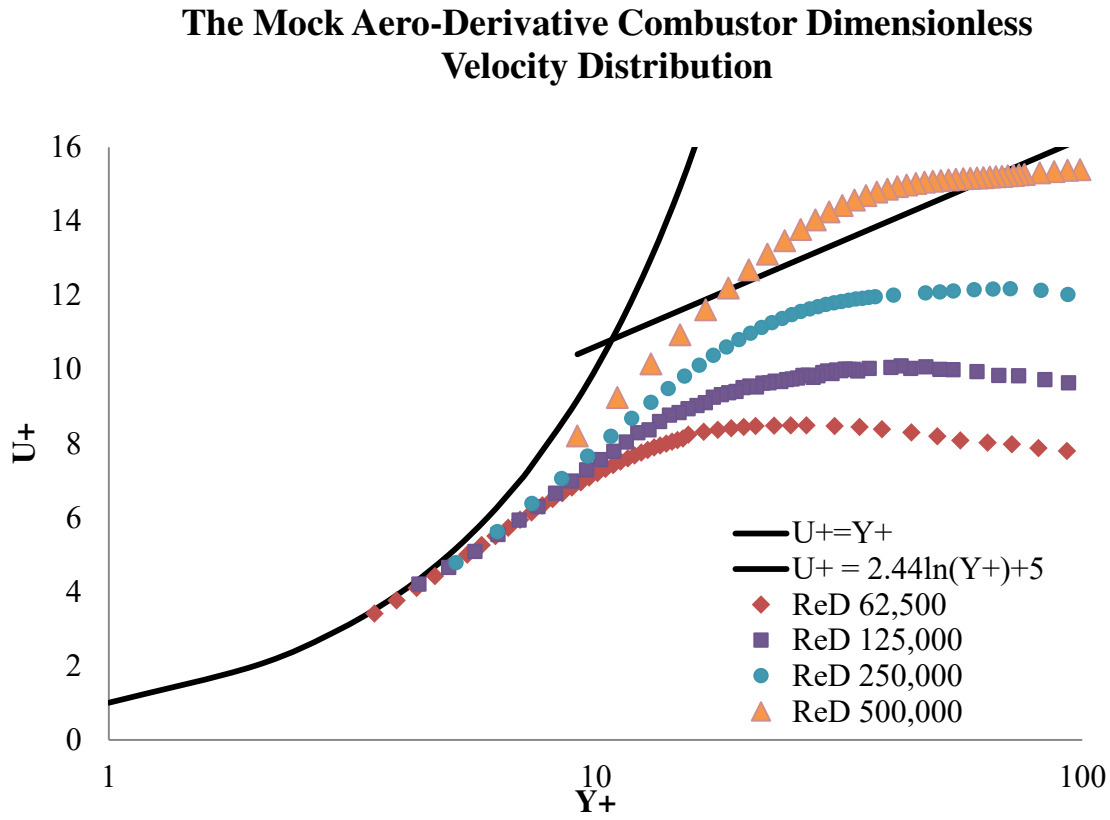

Figure 17. The velocity profile for the Mock Aero-Derivative Combustor.

The velocity gradient across the boundary layer "$\frac{dU}{dy}$" is determined from the derivative of the velocity fit. This approach was used to determine the local velocity gradient and reduce scatter due to the random uncertainty in the velocity measurements. The velocity gradient was also determined in excel by taking the difference in velocity and dividing it by the difference in height for comparisons purposes. Equation 21 shows how this was done.

$$\frac{dU}{dy}_{average(n,n-1)} = \frac{u(x)_{n-1} - u(x)_n}{x_{n-1} - x_n} \qquad [21]$$

The average distances $Y_{Average}$ and $Y^+_{Average}$ were determined to better align the data so that relationships using $\frac{du(y)}{dx}$ would be correctly plotted. This also must be

done to any result obtained through averaging. This way the correct locations of the derivatives and averages are taken.

A file that contained the computed surface velocity distribution along the surface helped determined the flow's acceleration along the cylindrical leading edge surface. The pressure gradient is determined from the derivative of Bernoulli's rule along a streamline described by Equation 22 below.

$$\frac{dP}{dx} = -\frac{dU}{dx} \times U_\infty \times \rho \quad [22]$$

This pressure gradient is used in helping to determine the shear stress "τ" distribution. In Frank Whites Text Viscous Fluid Flow, he had a relationship between the location from the surface to the dimensionless shear stress "τ^+". The definition of the dimensionless shear stress is the measured shear stress divided by the shear stress at the wall "τ_{wall}" as shown in Equations 23 and 24 (White, 1974).

$$\tau^+(x) = 1 + \xi\frac{x}{\rho} + (3 + 2\xi)\left(\frac{x}{\frac{c_f}{2}}\right)^2 + (2 + \xi)\left(\frac{x}{\frac{c_f}{2}}\right)^3 \qquad [23]$$

$$\xi = \frac{\rho\frac{dP}{dx}}{\tau_w} \qquad [24]$$

The total shear stress is the viscous shear stress plus the apparent turbulent shear stress. From this relationship, the eddy diffusivity will be obtained by dividing the velocity gradient and the density from the total shear stress and then subtracting the kinematic viscosity as shown in Equation 24.

$$\frac{\tau}{\rho} = (\upsilon + \varepsilon_m)\frac{du}{dy} \text{ (William Kays, 2005)} \qquad [24]$$

The viscous shear stress distribution was determined by multiplying this velocity gradient to the dynamic viscosity. It can be assumed that in the near wall region, that this

portion of the shear stress is the most dominant. The Equation 25 describes the viscous shear stress.

$$\tau_{viscous} = \mu \frac{du}{dy} \text{ (William Kays, 2005)} \qquad [25]$$

The apparent turbulent shear stress plays a larger role in the shear stress when further away from the wall. Therefore, data is collected to far from the wall are influenced by the turbulent shear stress component shown in Equation 26.

$$\tau_{Turbulent} = -\overline{u'v'} = \varepsilon_m \frac{du}{dy} \quad [26]$$

Then the total shear stress "τ" is determined from the definition of the dimensionless shear stress shown in Equation 27.

$$\tau = \tau^+ \times \tau_{wall} \qquad [27]$$

When the viscous shear stress is subtracted from the shear stress, the result is the turbulent shear stress. Then the turbulent shear stress is divided by the density of air to get the average of the fluctuating velocity components "$-\overline{u'v'}$." Then the eddy diffusivity "$\varepsilon_{M\ (measured)}$" is determined from the Equation 28 (William Kays, 2005).

$$\varepsilon_{M\ (measured)} = \frac{-\overline{u'v'}}{\frac{du}{dy}} \qquad [28]$$

Then the data was compared to the Algebraic Turbulence Model (ATM) developed by Ames et al. in "An Algebraic Model for High-Intensity Large Scale Turbulence." the ATM model predicts the flow's eddy viscosity using predicted turbulent conditions of the flow to find the eddy diffusivity shown in Equation 29 (Ames, Kwon, & Moffat, 1999).

$$\nu_{M,o} = 1.5 \times C_\mu \times Tu_\infty \times u_\infty \times Lu_\infty \left[1 - e^{\left(\frac{-2.9 \times y}{Lu_\infty}\right)}\right]^{4/3} D_v \qquad [29]$$

The constant "$C_{\mu-ATM}$" shown in the above Equation is 0.09. This Equation also accounts for the near wall dampening by adding the dampening "D_v" coefficient seen in Equation 30. The constant "C_η" was taken to be 6.7. "η" is the Kolmogoroff micro length scale which is dependent of the kinematic velocity and the turbulent dissipation as shown in Equation 31 (Ames, Kwon, & Moffat, 1999).

$$D_v = 1 - e^{\frac{-y}{C_{(\eta-ATM)\times\eta}}} \quad [30]$$

$$\eta = \left(\frac{\nu^3}{\varepsilon}\right)^{0.25} \quad [31]$$

With elevated external turbulent, laminar flows, this can be used to predict the eddy diffusivity throughout the boundary layer. It is expected that this should accurately predict the eddy viscosity, except where local acceleration is moderate to low. The flow characteristics were taken from the work done by Nafiz Chowdhury in his Master's thesis with Dr. Forrest Ames, which preceded mine. These data were analyzed to determine similar flow conditions as this experiments. This data were averaged data from Nafiz Chowdhury's and Preethi Gandavarapu's work. (Chowdhury M. N., 2012)

From these data the turbulence dissipation "ε" was determined by taking the relationship the turbulence dissipation rate with the turbulent length scale "Lu" and the free stream velocity variance "u'". This relationship is derived from the Reynolds average transport shown in Equation 32 (William Kays, 2005).

$$\varepsilon = 1.5\frac{u'^3}{Lu} \quad [32]$$

Once the ATM model for the eddy viscosity was calculated, it was converted to the Eddy diffusivity. Please note Equation 33 and 34 which clarifies Ames et al. definition of eddy diffusivity from the eddy viscosity. Where the eddy viscosity divided

by the eddy diffusivity is equal to the eddy diffusivity. The symbol for eddy diffusivity can equal "ε_M" or "$\nu_{M,o}$", but not "υ_m" which is the eddy viscosity. "ε_M" will be used FO the eddy diffusivity to clarify any confusion moving forward.

$$\varepsilon_M = \frac{\upsilon_m}{\rho} \qquad \text{(Ames, Kwon, \& Moffat, 1999)} \qquad [33]$$

$$\varepsilon_M = \nu_{M,o} \qquad [34]$$

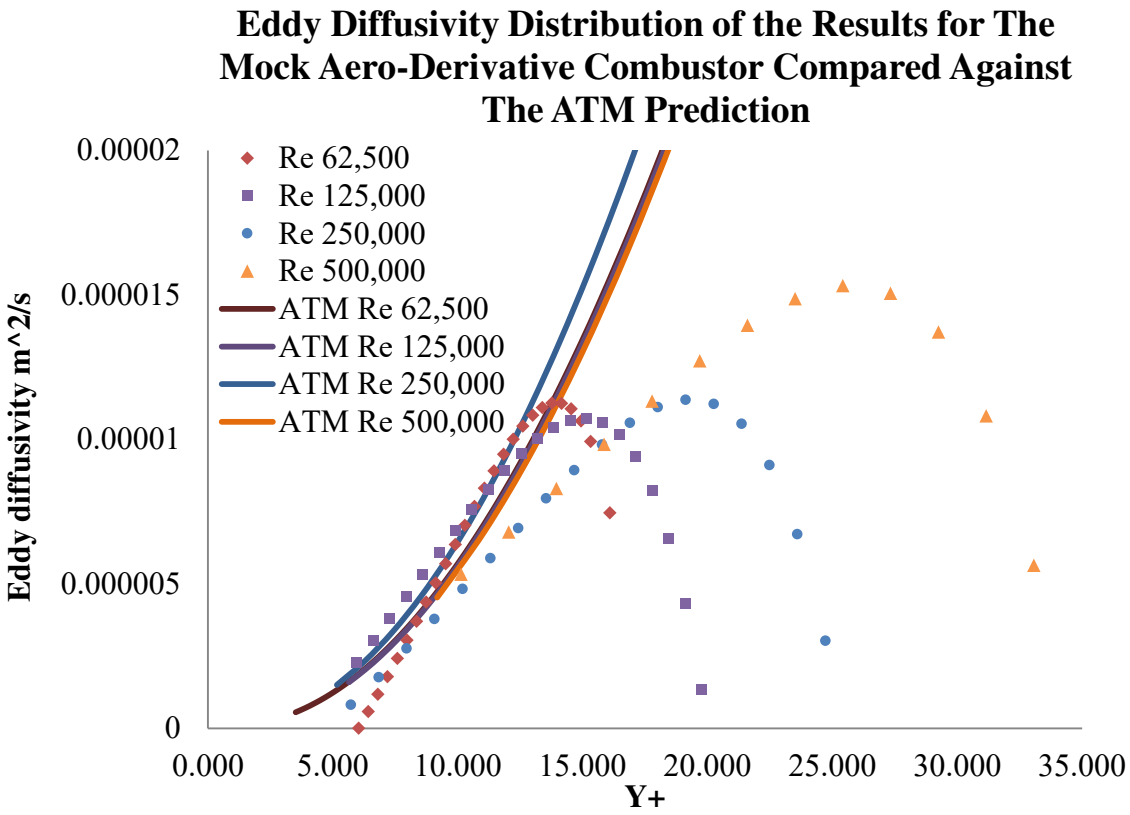

Figure 18. Eddy diffusivity distribution for the Mock Aero-Derivative Combustor.

Then the eddy diffusivity from experiment and the ATM model's prediction are then converted into the dimensionless form by dividing by the kinematic viscosity. Afterward, the results are plotted on a $\varepsilon_M{}^+$ verses Y^+graph. The eddy diffusivity helps show the relative levels of intensification for the result.

Because the values of the shear stress at the wall and the offset in the distance are uncertain, the shooting method was used to help iterate the values until the Equations came close to an agreement. The first set of Equations predicts the velocity gradient, defined by Equation 35, at the wall by dividing the dimensionless shear stress by the viscous shear stress. These work well when points are obtained within the near wall laminar boundary layer with external turbulence imposed.

$$\frac{dU}{dy}_{wall} \sim \frac{\frac{du(x)}{dy}}{\tau^+} \quad [35]$$

However, when applied to the higher Reynolds numbers this analysis is less accurate because of the limitations of the equipment to traverse in small enough steps near the wall. In these cases, the effective near-wall boundary layer or shear thickness is much thinner, the apparent turbulent shear stress has greater influence over the results of the data beyond the near wall region.

In these cases the predicted velocity using the shooting method. The shooting method will be gone over in more detail in the appendix. The predicted velocity is estimated from using Simpsons Rule of Integration on the shear distribution shown in Equation 36. A correcting constant C_{ε_m} accounted for the effect on the velocity gradient due to the ratio of viscous to total shear stress as shown in Equation 37.

$$u(x)_{n+1} = \left(\frac{\frac{\tau^+{}_{n+1}}{C_{\varepsilon_M,n+1}} + \frac{\tau^+{}_n}{C_{\varepsilon_M,n}}}{2} \right) (Y_{n+1} - Y_n) \frac{dU}{dy}_{wall} + u(x)_n \quad [36]$$

$$C_{\varepsilon_M} = \frac{\upsilon + \varepsilon_M}{\upsilon} \quad [37]$$

The predicted velocity gradient is then determined from the predicted velocity gradient. The next step is to adjust the offset and the shear stress at the wall until the

experimental and predicted velocity gradients come as close as possible to each other. This process will help establish where the offset is located. Then the predicted velocity gradient and the measured velocity gradient are compared to estimate the velocity gradient at the wall.

The table below shows an example of the Mock Aero-Derivative Combustor's iterative solutions. I also observed these values at other nearby points to make sure the rate of change makes sense. If the rate of change in the velocity gradient is too different between the estimated and the predicted values, then the location or velocity gradient at the surface may not be accurate. Table 3 shows the solutions to these processes.

Table 3. The iterative solutions for the Mock Aero-Derivative Combustor.

Reynolds Number	Measured Velocity (m/s)	Predicted Velocity (m/s)	Estimated du/dy at The Last Point (1/s)	Predicted du/dy at The Last Point (1/s)	Last Point Measured (inch)
62,131	0.855	0.879	3,650	3648	0.009079
127,012	1.296	1.289	9,018	9011	0.0046
252,939	3.973	3.925	22,276	22,243	0.00462
489,139	11.435	11.513	48,152	48,063	0.004803

The location of the last measured point was typically between either 0.0045 to 0.0055 inches (0.0001143-0.0001397 meters), or 0.0075 to .0085 (0.0001905-0.0002159 meters) depending which probe was used. So that the last measured point is the measured distance plus the offset. It is assumed that the last point is taken has this value due to the geometry of the probe. The iterations stop when I reach a point that validates the "checks" the best as shown in table 4.

Table 4. The results for The Mock Derivative Aero-Derivative Combustor at a Re_D of 62,500.

Reynolds Number	Offset (m)	Shear Stress at The Wall (1/s)	Boundary Layer (m)	Last Point Measured (m)
62,131	0.000002	3,810	0.00156	0.009079
127,012	0.00032	10,700	0.001285	0.0046
252,939	-0.000162	31,200	0.001235	0.00462
489,139	0.000009	94,500	0.12396	0.004803

The uncertainty was determined from the experimental results. Some factors created the complications in determining the uncertainty were traditional methods were possibly not correct by the adjustments to the "Y" offset and the known shear stress distribution that occurs in an accelerating laminar boundary layer. Many of the errors from equipment and measurement are affected by this process. Also instead of fitting a traditional line to the data a set of fits to the errors were completed until no improvements were made, or differences between the fit and the actual results were two percent or less. Therefore, traditional methods of uncertainty analysis may mislead on what is occurring. The differences were squared based on the root sum square method described by Moffat in Equation 38 (Moffat, 1988).

$$\pm\delta R = \sqrt{\frac{\sum_{i=1}^{i=n} {R_i}^2}{n}} \qquad [38]$$

The resulting fitted values were subtracted from the measured results. This difference between the fit and the measured points was then squared along all of the points. The resulting values were then the average of these values were square rooted to obtain the standard deviation. When reviewing the data, the largest areas of error are on the ends of the fits. Therefore when looking at the standard deviations instead of decreasing proportionally to the velocity the standard deviation reduces slightly indicating proportionally more uncertainty near the wall.

The uncertainty of the results was determined by identifying the sources of error. It is known that the pressure gauges have an error of 0.1% of the result (Dvorak, 2003). Also that the thermocouples have an error of 0.2 degrees Celsius. Also, it is known that the calibration set up which was discussed by Lindsey Dvorak was the same calibration process used. Table 5 shows the error results for the Mock Aero-Derivative Combustor at a Reynolds number of 62,500.

Table 5. Uncertainty analysis of the sources of uncertainty for the Mock Aero-Derivative Combustor at Re_D of 62,500.

	Nominal	Units	Unc.	Nom+ Unc.
T_{air}	302.3	K	0.2000	302.51
P_{in}	98283	Pa	20.0000	98303
P_{out}	98268	Pa	20.0000	98288
$U_{y\ fit}$	1.8	m/s	0.0122	2
$U_{y\ hot\ wire}$	1.8	m/s	0.0357	1.8198
D	0.4064	m	0.0016	0.4080
Y	0.0007	m	0.000005	0.0007
du/dy_{wall}	3810	1/s	190.5	4000.5
$du/dy_{y=10}$	1184	1/s	87.0	1271

Some of these errors are from calibration, fitting the lines and uncertainty in predicted values. The thought when fitting a curve to the data was that the fit had to be as close to the actual data as possible, and the measured variances were part of the boundary layer. This fitting method is why I had fit the error and added it to the fit polynomial. Both the fits for the boundary layer velocity and the velocity gradient had an uncertainty based on the differences between the measured results and the fit results.

The uncertainty of the results was averaged over the length of the boundary layer where the fit would be the best. Often the last one to three points from the surface had the

largest variances. These variances were squared, averaged and square rooted. These values were used as the average uncertainty from the fit.

Since some of the data were predicted to find the solution, there is an error from that as well. For example, the two hot wires had a measured range of 0.005 inches or 0.008 inches for the location of the last point. Therefore when the data were analyzed through iterations that the data lands in these locations within plus or minus of 0.0005 inches. This resolution was used in the analysis. In table 6, the uncertainty is calculated for the Mock Aero-Derivative Combustor using the perturbation "Pert".

Table 6. The Perturbation and Propagation of Uncertainty of the Mock Aero-Derivative Combustor at Re_D of 62,500.

Density	Nominal	Units	Uncertainty	Nom+ Uncert.	Pert	Calc. (kg/m^3)	(Pert-Calc.)^2	
P_{in}	98283	Pa	20.0000	98303	1.1329	1.133	5.313E-08	
T_{air}	302.3	K	0.2000	303	1.1319	1.133	5.608E-07	
				Standard Deviation			0.000784	kg/m^3

Also, the velocity gradient at the wall also had an uncertainty of the value. However, the known shear profile was used. The amount of uncertainty depended in how many points were collected within the near wall region. Also, the quality of the integration also plays a key role in improving the range of uncertainty of the data.

After the general uncertainties had been collected, the errors were propagated and then the process of perturbation was used to calculate the error of the results. The perturbations were broken down into steps to prevent error and check the results. In Table 7 the momentum eddy diffusivity measured at a Y+ of 10 is shown to have an uncertainty "Unc."of about 25%. For more information please see Appendix V. The Uncertainty analysis was derived from the root sum square combination method described by Robert

Moffat (Moffat, 1988) and excerpts from the text "Theory and Design For Mechanical Measurements" (Figiola & Beasley, 2006). Where the Perturbation "Pert." And the calculation of the average value "Calc." were used to find the uncertainty.

Table 7. The perturbation and propagation of the momentum eddy diffusivity's uncertainty for Re_D of 62,500.

$\varepsilon_{M(y+=10)}$	Nominal	Units	Unc.	Nom+ Unc.	Pert	Calc.	(Pert.-Calc.)^2	
ρ	2.462	kg/m^3	0.000784	2.463	-1.7E-06	-1.70E-06	2.936E-19	
$\tau_{visc.(y+=10)}$	0.0220	Pa	0.0016	0.0236	-1.4E-06	-1.70E-06	8.521E-14	
$\tau_{wall\ (y+=10)}$	0.0314	Pa	0.001632	0.0330	-2.0E-06	-1.70E-06	8.702E-14	
$\frac{dU}{dy}_{(y+=10)}$	2248	1/s	86.98	2334.5	-1.6E-06	-1.70E-06	4.027E-15	
					Standard Deviation		4.198E-07	m^2/s
					Standard Deviation		25%	

CHAPTER V

EXPERIMENTAL RESULTS

The results discussed in this section encompass the data collected from the Mock Aero-Derivative Combustor “AC1”, the Mock Aero-Derivative Combustor with spool “ACS”, the small grid near “GS2”, the small grid far”GS1”, the large grid “GR”, and the low turbulence inlet conditions “LT”. The goal is to identify the effect these different flow conditions have on the resulting boundary layer. The analysis of the data included checking the results to make sure they were logical, and then reviewing the eddy diffusivity across the boundary layer. The results for each flow condition could have intensification caused by eddy straining, the results were also compared with previous work to see any interesting patterns occurred.

Since the boundary layer data were taken downstream from the stagnation region, the stagnation eddy diffusivity amplification field must reach the location of the probe for it to be detected. Further, the amplification is expected to increase the velocity gradient in the near-wall region of the boundary layer since this turbulence enhances mixing. The mixing in the momentum boundary layer is modeled by the ATM correlation (Ames, Kwon, & Moffat, 1999) which models a turbulent mixing across a flow field adjacent to a surface, without amplification due to a strain field. It may be assumed that a thin boundary layer on a convex curved surface can be modeled as a boundary layer over a flat plate taken the acceleration around the surface is accounted for. Therefore notable

increases in momentum eddy diffusivity surpassing prediction could indicate amplification. Further recent studies show this model is still valid in modeling mixing in the momentum boundary layers. (Mayle, Schultz, & H.J., 2008)

Because of the assumptions we made in the analysis, there will be a peak observed in the results. This peak is from deriving the $-\overline{u'v'}$ component from the velocity gradient. The velocity gradient is assumed to be zero at the location of the boundary layer edge. This is not exactly the case. Mixing actually continues to increase away from the surface, also increasing the eddy diffusivity. This analytical method limits the useful range when comparing the data to the ATM. Therefore the maximum of the eddy diffusivity is where the validity of the analytical method ends. The closer the values to the wall the more accurate it is expected to be. Since I am observing the near wall behavior this is fine.

The first condition, the Mock Aero-Derivative Combustor (AC), produced the following results on the 0.4064 meter cylindrical leading edge diameter test surface. When reviewing the momentum eddy diffusivity in Figure 19, the results aligned closely with the ATM model located between Y+ from five to fifteen. The larger Reynolds number values fell away from the predicted ATM Model sooner. Further, it appears that the eddy diffusivity would peak by location in progressive order as the Reynolds number increases. Instead of the eddy diffusivity increasing, the dU/dy approaches zero. In reality, the eddy diffusivity would continue to increase. This difference is because dU/dy was used to calculate the eddy diffusivity. This drop off or maximum indicates this relationship begins to be invalid beyond this point. The momentum eddy diffusivity

diagram below shows close agreement. Therefore, this location does not appear to be influenced by the amplification field.

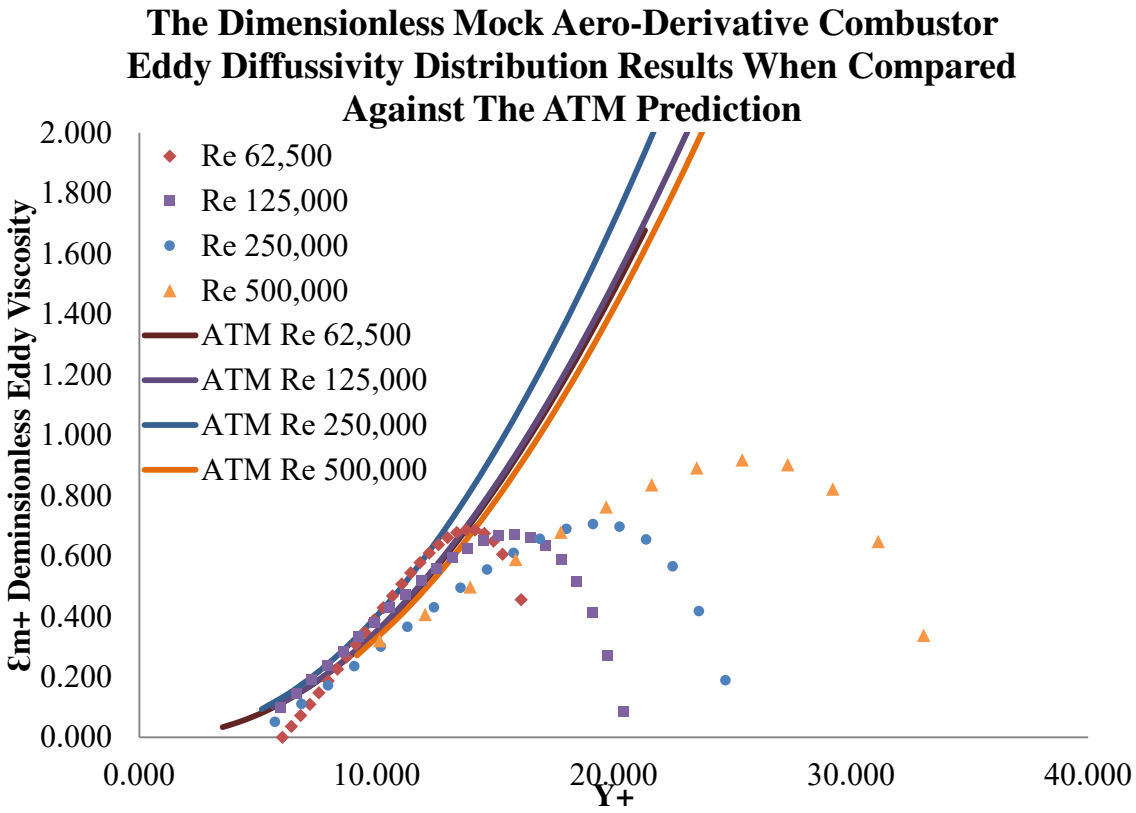

Figure 19. Dimensionless eddy diffusivity distribution for the Mock Aero-Derivative Combustor.

When the results are compared with the Tu and Lu collected by Nafiz Chowdhury certain patterns occur. This information comes from his masters thesis (Chowdhury N. H., 2012). When comparing the energy length scale to the constants, there is a general trend where it dips in value at the Re_D250,000 case, while the momentum eddy diffusivity slopes appear to drop in slope along Y+ = 10 in Figure 19 as the Reynolds numbers increase. Further, the dimensionless maximum momentum eddy diffusivity drops from the ATM correlation and the analysis method becomes invalid away from the wall as the Reynolds number increases.

The Mock Aero-Derivative Combustor with the Spool produced strong amplification of the momentum eddy diffusivity, specifically at the Reynold's number of 125,000 as shown in Figure 20. At this location, the experimentally determined eddy diffusivity increases at a steeper rate than the other Reynolds numbers. Interestingly, the Reynolds number case of 62,500 case appears to agree with the ATM model and is less influenced by the stagnation amplification zone.

Additionally the Re_D500,000 case appears to agree with the prediction over a greater distance than the condition without the spool as shown in Figure 20. Further, the maximum momentum eddy diffusivity appears to occur in progressive locations. Another feature is that the Re_D 62,500 case maximum is much lower than the other peaks and occurs about the same location as the same case in Figure 19, while the Re_D 250,000 and Re_D 500,000 case have the same the same peak magnitude between the Re_D equal to 62,500 and Re_Dequal to 125,000. The larger dimensionless momentum eddy diffusivities match in magnitude with the values in the case without the spool.

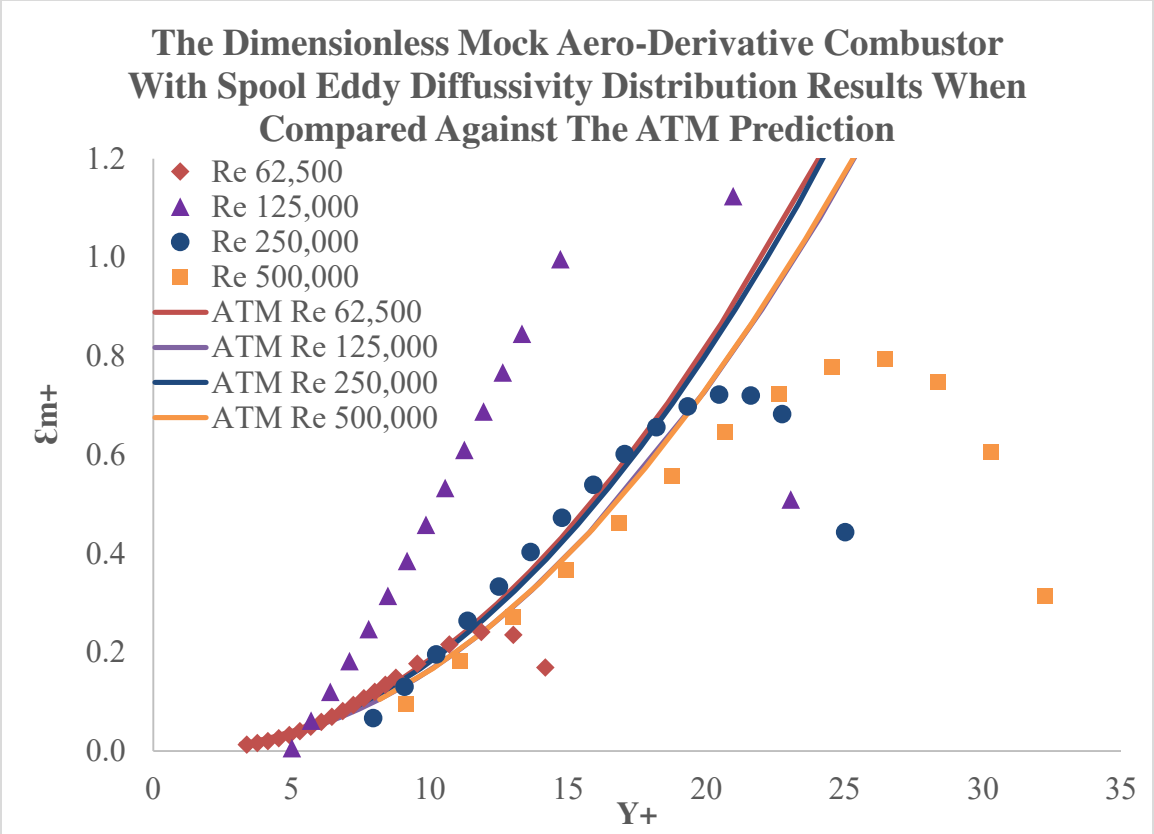

Figure 20. The eddy diffusivity for the derivative mock aero combustor with the spool.

Comparing the results between the experimentally derived diffusivities and ATM predicted values, using the Tu and Lu by Chowdhury, the results from the Mock Aero-Derivative Combustor showed some patterns (Chowdhury N. H., 2012) for the Mock Aero-Derivative Combustor showed some patterns. The maximum momentum eddy diffusivity occurs at the Re_D of 125,000 case. The Lu measured for Re_D 250,000 case was shown to be less than the Lu for Re_D 125,000.

The large grid results in Figure 21 showed that intensification also occurred for the lower Reynold's numbers while the models nearly overlap each other. Intensification occurs for the Re_D of 62,500 case and possibly Re_D 250,000 case. Additionally the maximum momentum eddy diffusivity does not peak in progressive order but appears to be shifted for the lowest value case. The results for the largest Reynolds number values

agree strongly with the ATM model in Figure 21, but agree with a further distance than the Mock Aero-Derivative Combustor condition shown in Figure 19.

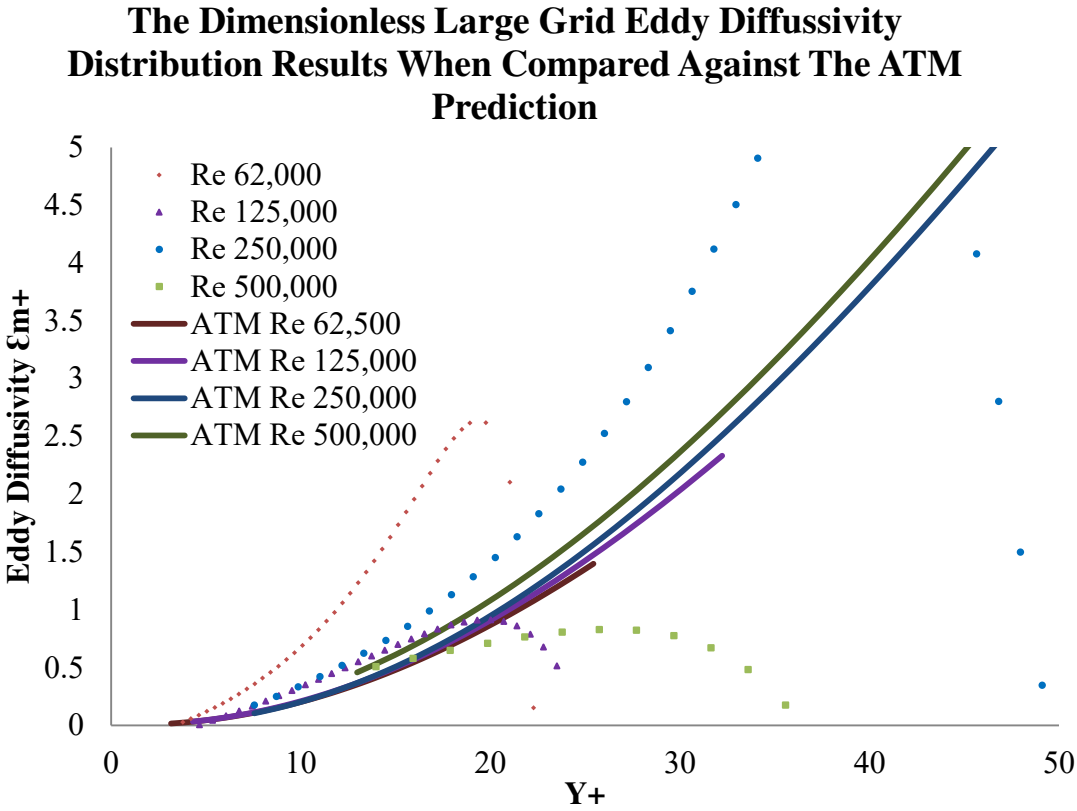

Figure 21. The dimensionless momentum eddy diffusivity for the large grid flow condition.

Interestingly, in this case, the Lu value does not drop at a Re_D 250,000 case like the previous cases in Figure 20. Instead, the slopes appear to agree with the predictions for a further distance except Re_D 62,500 case which sees amplification. The Lu at this Re_D of 62,500 case was assumed to be the same as a Re_D of 125,000 case. All momentum eddy diffusivity slopes appear to decrease as Reynolds numbers increase in Figure 21.

The small grid at the location nearest to the test apparatus, shown in Figure 22, showed the maximum dimensionless momentum eddy diffusivity decrease with the

Reynolds number increase Re_D increase. Amplification occurs at the Re_D of 62,500 and possibly at Re_D 125,000 cases. The largest values of Re_D fall from the predicted ATM model between the locations of Y+ = 10 to Y+ = 15. Also, the ATM models appear to overlap in this case.

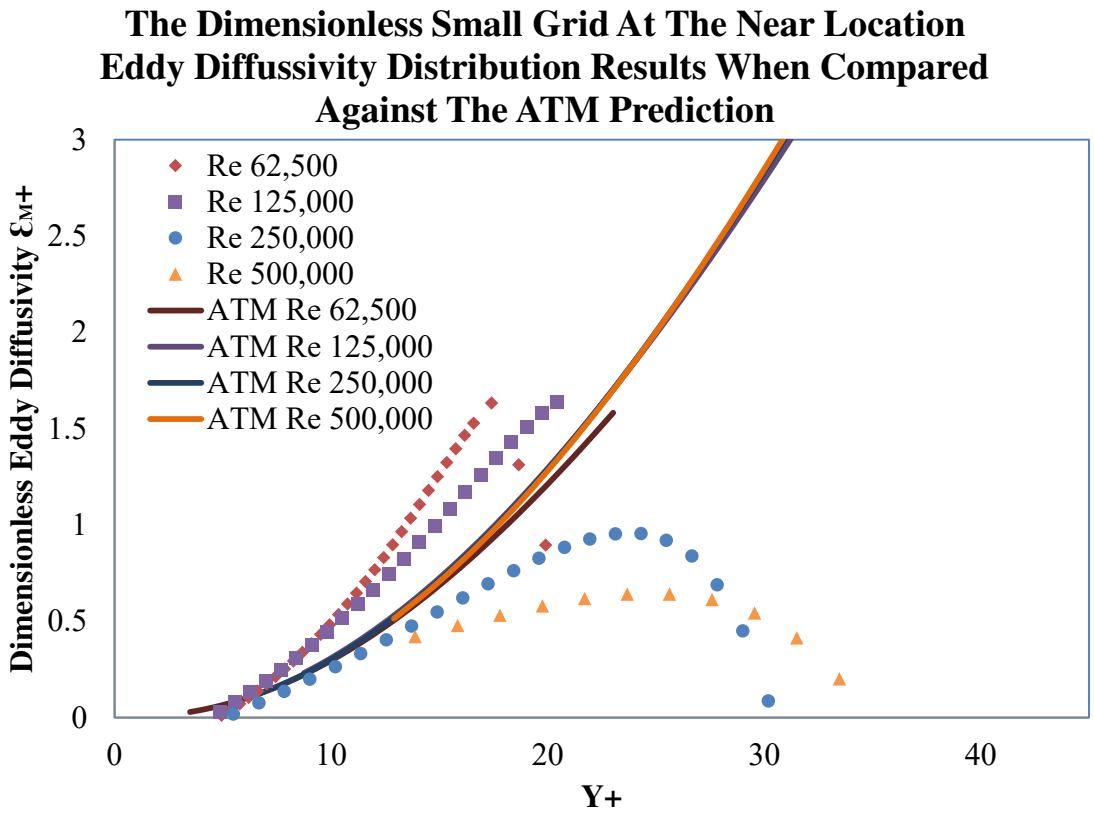

Figure 22. Eddy diffusivity of the small grid at the near location.

In this case shown in Figure 22, there is no drop in Lu for the Re_D 250,000 case. Here both of the slope and the magnitude of the dimensionless momentum eddy diffusivity drop as Reynolds number increases. The location of the maximum momentum eddy diffusivity occurs in progressive order. The two fastest flows fall away from the prediction sooner. The value of the Lu appears to drop as the Reynolds number increases. It appears that Figure 22 agrees with earlier work, where span of stagnation region

intensification decreases as Reynolds number increases for this case (Gandavarapu, 2011).

An increased level of eddy diffusivity was determined by a Reynolds number case of 125,000 in Figure 23. These increased levels of eddy diffusivity extend to higher y+ values than the peaks at higher Reynolds number for this turbulence condition. This is interesting since this location of the small grid had more heat transfer relative intensification in earlier work for this case (Gandavarapu & Ames, 2013). Like the case of the Mock Aero-Derivative Combustor with the spool, the maximum value occurs on the ATM prediction. Except the Re_D 125,000, the maximums occur in a progressive fashion.

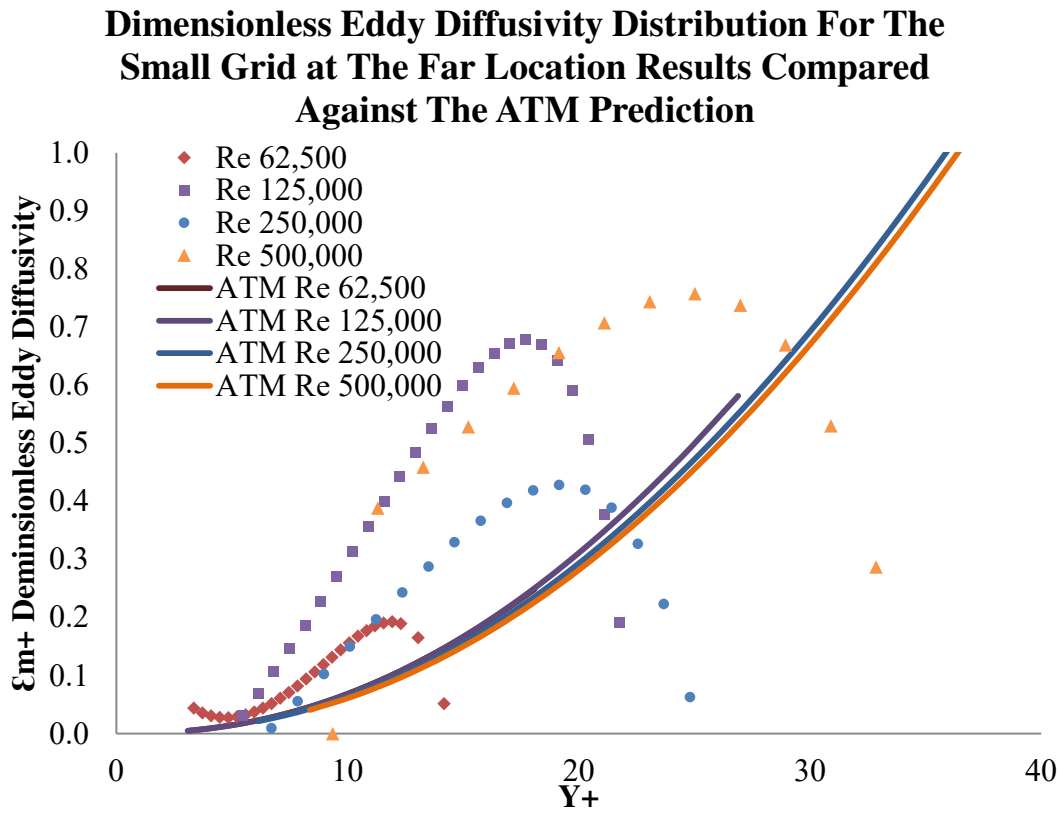

Figure 23. Eddy diffusivity of the small grid at the far location.

In the small grid in the far location case shown in Figure 23, the value of Lu was measured at Re_D 62,500 which showed, for this case, Lu increased with the amplification of Re_D 125,000. The slope and the magnitude of the momentum eddy diffusivity also show this amplification. Also, Lu does not recover at Re_D 500,000 but drops off. The values also appear smaller across the board. Therefore even though there is a relative intensification shown in the in Re_D of 125,000 case the overall magnitude of eddy diffusivity in Figure 23 is less than previous cases.

The low turbulence model shown in Figure 24 performed as expected with heightened diffusivity. Earlier work on the same curvature showed that TRL on the low turbulence study was in the range of 0.94 to 2.0. Therefore, these results were expected. Although the relative intensification occurs in Figure 24, the dimensionless momentum eddy diffusivity is still less than the other flow conditions.

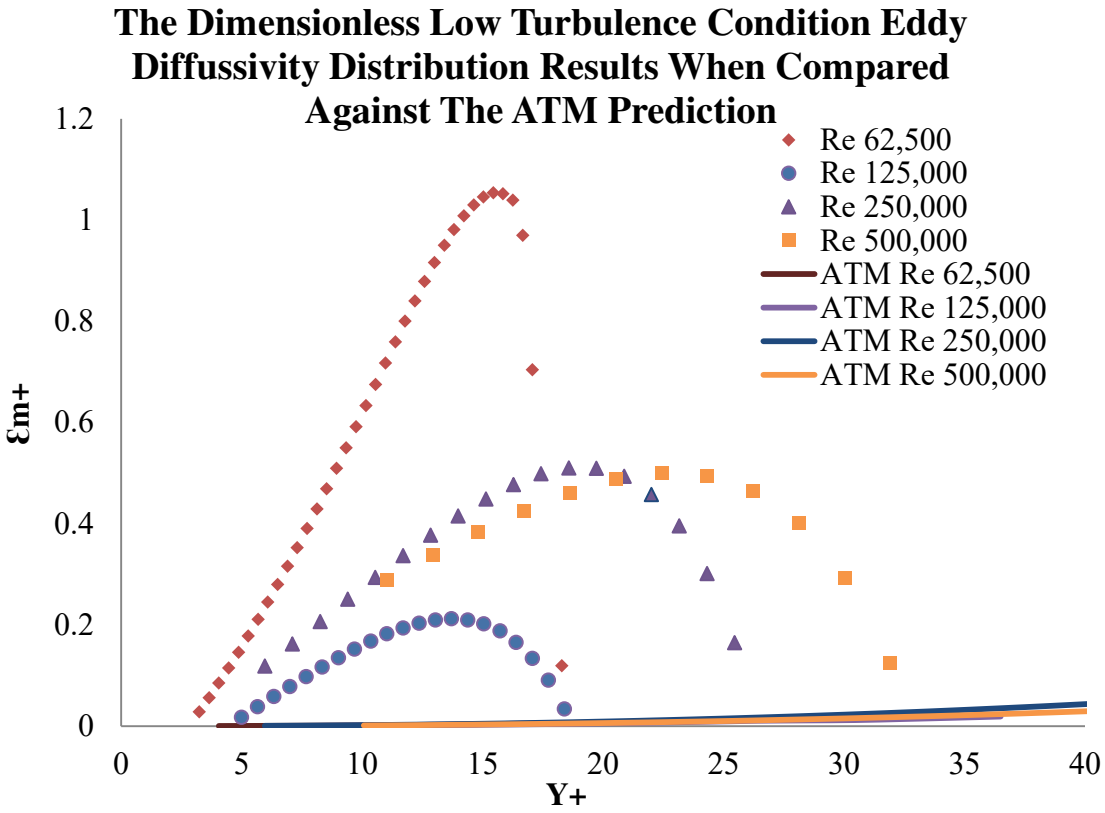

Figure 24 The dimensionless momentum eddy diffusivity of the low turbulence condition.

The TRL for these values are very low, so there is an amplification that is predicted to occur (Gandavarapu, 2011). Here the slopes still tend to decrease as the Reynolds number increases. The magnitude of the momentum eddy diffusivity appears to drop at the Re_D125,000 case and then appear to be the same for the two largest Reynolds number cases.

Earlier work has shown that broadening of the Nusselt number values along the surface occurred in the stagnation region of the small grid and the Mock Aero-Derivative Combustor in the far position for the Re_D 125,000 case. Also, as the Reynolds numbers and turbulence intensities increased the stagnation intensification field decreased for small length scale flow conditions (Gandavarapu, 2011). This seems to imply that a

relative intensification of the stagnation intensification field reaches a smaller region at higher Reynolds number and FSTI levels for small length scale. This makes sense because higher FSTI values add more strain against eddies from the free stream shortening the stagnation amplification range. Also, Lu likely plays a role, but it is hard to determine since it was not measured for the lowest Reynolds number. What's likely, is that larger length scale flows strengthen the stagnation intensification field. This strengthening results in a broadening of the field. The intensification not being seen by the probe for the GS2 and ACS conditions at 250,000 and higher Reynolds numbers is probably from the shearing in the free stream being stronger. This strain field is probably strengthened as the velocity increases, but sheared by the free stream flow.

Typical intensification of the eddy diffusivity appears to occur in the near wall region and the results quickly fall off at about "Y+" of 20. This has to do with where the maximum velocity occurs in the velocity profile which we claimed was the edge of the boundary layer. Intensification appears to fall off or dampen eddy diffusivity as either FSTI or Reynolds number is increased. There was no additional relative intensification measured for the Mock Aero-Derivative Combustor condition at the downstream location

The two flow conditions ACS and GS2 where the amplification occurred at the Re_D 125,000 cases could be explained by the data collected by N. Chowdhury. The data collected at the stagnation region showed the increase of the RMS values of fluctuating velocity for these cases, higher than what's observed in the free stream (Chowdhury N. H., 2012).

There is a sharp drop in both the integral length scale and also the energy scale near the stagnation region. There was also a slight increase in relative dissipation which

indicates an intensification of the stagnation turbulence also seen by increased mixing. This sharp drop in turbulence scales is from the blocking caused by the cylindrical leading edge (Chowdhury N. H., 2012). Further, it is important to point out that the length scale for the aero combustor with the spool was three times higher than the small grid at the far position case. This would imply that Lu is not the only factor in predicting the peak momentum eddy diffusivity.

CHAPTER VI

CONCLUSIONS

The results support the concept of amplification being the function of the FSTI, Lu in the free stream, and the balance between the shearing across the surface and the shearing from the free stream. Although there are other factors, the scope of the experiment focused on only the 0.4064 meter diameter cylinder and only measured the velocity parallel to the surface. The distance from the location of the measured velocity to the surface plays a part as well. Three different types of amplification in a laminar boundary layer on a cylindrical leading edge was observed. The first has low turbulence intensity levels with high turbulent time scales. This type will have higher TRL values than the prediction and much higher eddy diffusivity than the ATM model prediction. The second type of higher relative intensification is driven by the high Reynolds number and high FSTI flows. This second type sees a shorter span of influence, but higher relative intensification thus making a "peaky" appearance when graphed as a function of distance. The third case for stagnation region intensification has the field of stagnation region intensification broadened or covers a greater distance and is less "peaky." In this cases, the free stream has high turbulence and high turbulent length scale values. The dissipation measured near the stagnation region increases above the free stream while the second cases it stays below the dissipation in the free stream. This type of higher relative intensification strengthens and broadens of the stagnation intensification field.

The first type is seen occurring with the low turbulence condition. Here the momentum eddy diffusivity is significantly higher than the predicted ATM model cylinders leading edges have an accelerating boundary layer that helps stabilize the flow. However, the overall magnitude of eddy diffusivity is less than the rest of the flow conditions.

The second type is seen with the Mock Aero-Derivative Combustor, the Large Grid and the Small Grid at the near location flow conditions. Here the fields influence was seen to decrease at the downstream location as the Reynolds number increases. From P. Gandavarapu's work, we know that the higher relative intensification of the heat transfer increased as Reynolds number increased. Though the eddy diffusivity is higher, relative intensification is showeynolds number is increased. The span of the stagnation intensification field would decrease as Reynolds numbers increased. The observed reduction in the slope of the eddy diffusivity as the Reynolds number increased may show agreement with Gandavarapu's results (Gandavarapu, 2011), where the free stream limits the relative intensification.

In the third type, displayed by the Mock Aero-Derivative Combustor with Spool and Small Grid at the Far Location flow conditions for the Re_D of 125, 000 case. Here intensification is not solely dependent on Reynolds number and turbulence intensity. When reviewing N. Chowdhury's Master's Thesis results showed the turbulent time scale was higher and the dissipation increased as the wall was approached. In the literature review, several authors described this type of relative intensification of the stagnation intensification field as likely influenced by the free stream characteristics. In N. Chowdhury's master's thesis, the third case has higher dissipation and an relative

intensification of u' then the second case. In fact, these values appeared to surpass the free stream's measured u' and dissipation near the stagnation point. In N. Chowdhury's master's thesis, shows these characteristics are introduced, since the free stream RMS velocity fluctuations are not insulated from the stagnation region like the other cases.

Also from P. Gandavarapu's work the higher Reynolds numbers may increase the heat flux, but tends to shorten the stagnation amplification field. So for the higher Reynolds numbers, it is possible that intensification is occurring just upstream over a limited region where the fields are "peaky" and just not measured by the probe in this thesis. It is also shown that the third case also shown a broadening in P. Gandavarpu's master's thesis.

Future studies that may answer this question would look into measuring the Lu for the cases with a Re_D 62,500 case for the rest of the turbulence conditions. Also measuring the v', w' and u' with an x probe may give some more insight into the mixing. One downside to this is that the x wire is dimensionally limited to how close it can reach to the surface. Even looking at a closer location to the stagnation region may give more insight into the boundary layers behavior under the stagnation field of intensification and how these free stream characteristics effect the development of the laminar boundary layer. Also it would be interesting to look into what is happening with the low turbulence case in more depth along the width of the cylinder.

APPENDICES

Appendix A
Derivation of the Reynolds Analogy Value $1/Pr_t$

The definition of the turbulent Prandtl number is defined by William and Kays Convective Heat and Mass Transfer, as the fraction of the eddy diffusivity of momentum transfer to the eddy diffusivity of heat transfer. The book defined the definition in two ways as shown in Equations 39 and 40 (William Kays, 2005). This is derived to explain what the constant meant in the literature review section. The solution of this derivation implies author was looking to see how well his data matched up with Reynolds analogy.

$$Pr_t = \frac{\varepsilon_m}{\varepsilon_H} = \frac{\overline{u\prime v\prime}\times\frac{d\bar{T}}{dy}}{\overline{v\prime T\prime}\times\frac{d\bar{u}}{dy}} \quad [39]$$

$$Pr_t = \frac{\varepsilon_m}{\varepsilon_H} = \frac{\frac{\tau_t}{\rho}\times\frac{d\bar{T}}{dy}}{\frac{\dot{q}''}{\rho C}\times\frac{d\bar{u}}{dy}} \quad [40]$$

Inverting this first Equation results in the comparison of the eddy diffusivity of heat transfer to the eddy diffusivity of momentum transfer. Equation 41 shows this result.

$$\frac{1}{Pr_t} = \frac{\overline{v\prime T\prime}\times\frac{d\bar{u}}{dy}}{\overline{u\prime v\prime}\times\frac{d\bar{T}}{dy}} \quad [41]$$

When you substitute the second definition of the turbulent shear stress, the Equation becomes more simple as shown in Equation 42.

$$\frac{1}{Pr_t} = \frac{\overline{v\prime T\prime}\times\frac{\tau_t}{\rho}}{\overline{u\prime v\prime}\times\frac{\dot{q}''}{\rho C}} \quad [42]$$

Then when you substitute out the definition of the turbulent shear stress in Equation 42 with Equation 43 (William Kays, 2005).

$$\frac{\tau_t}{\rho} = \overline{u'v'} \quad [43]$$

Then the relationship becomes Equation 44 shown below.

$$\frac{1}{Pr_t} = \frac{\overline{v\prime T\prime}}{\frac{\dot{q}''}{\rho C}} \quad [44]$$

Appendix B
Design of the 0.1016 Meter (Four Inch) Cylinder

The design of the 0.1016 meter cylindrical leading edge vane began in excel. Here the design concepts began on where and how the equipment would be placed inside the cylinder so that the probe would be able to measure at the 30 degrees location. Also, the amount of insulation board that would be needed to be cut away was picked here. There was a limited amount of space available to design the overlay. This had to be designed to house both the experiments for the stagnation measurements and the offset measurements.

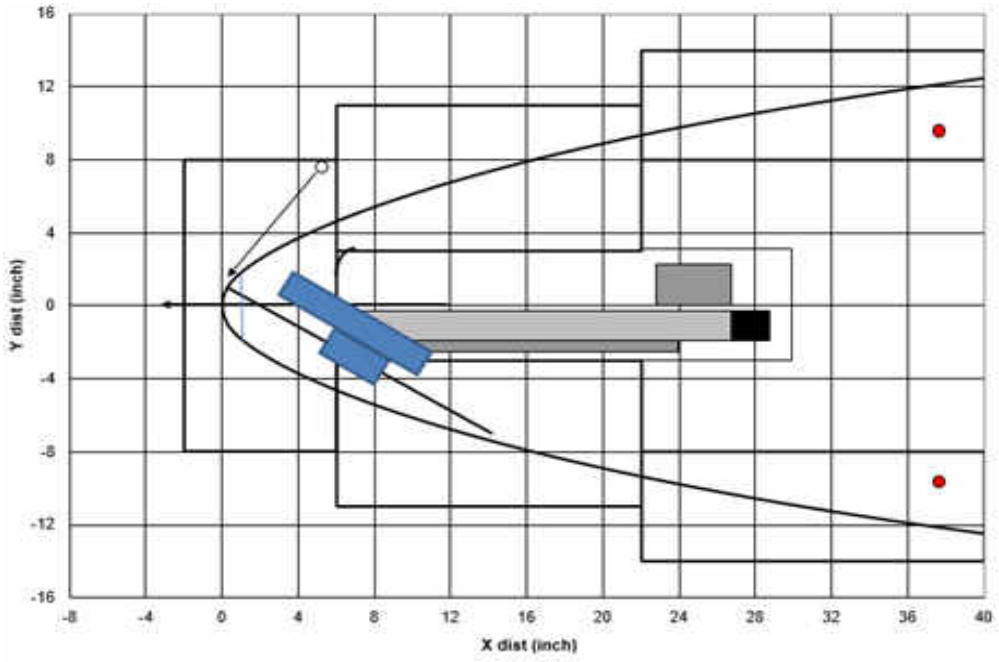

Figure 25. Excel preliminary design.

Once the general layout was decided the in-depth design work was completed in Pro E., this helped with proper alignment of equipment would prevent a stall. As illustrated above the cylinders had to be designed to take measurements for the measurements at the stagnation point and also thirty degrees downstream of the

stagnation line. Also, we wanted to make sure all equipment and also the cylinder could be mounted to the wind tunnel. Below is an example of the cylinder tip, which was designed on Pro-E.

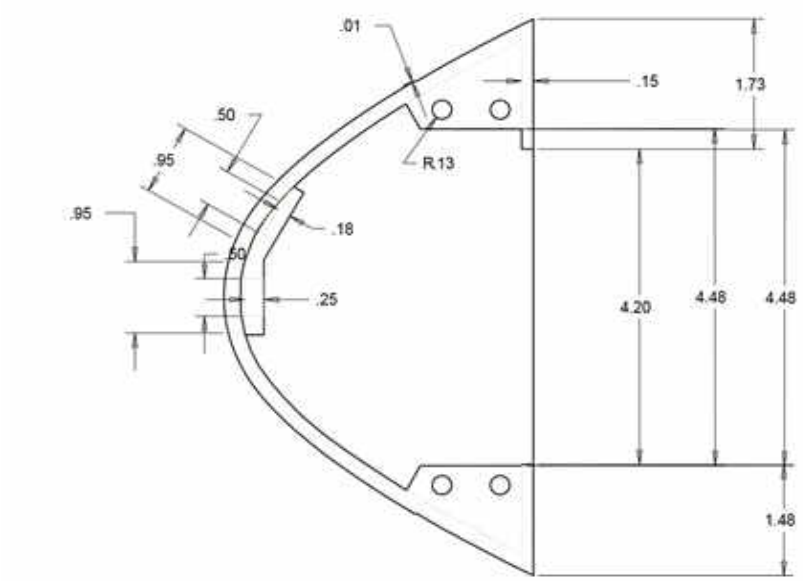

Figure 26. 0.1016 meter cylindrical leading edge tip design.

Because we did not want the streamline to experience section in the flow, covers were designed to plug the flow. Below is the design of both of the plugs. There was also another set with no holes in the streamline.

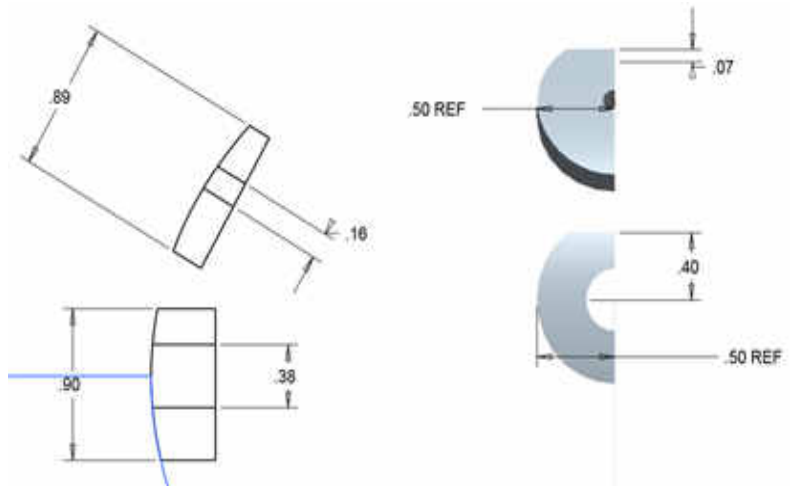

Figure 27. Probe hole cover designs.

The locations of the equipment were double checked, and only slight variations in the mounting equipment were made from the 0.4064 meter cylindrical leading edge. The biggest issue with the 0.1016 meter cylindrical leading edge was small space available to mount the traversing equipment assembly within the test surface. Fortunately, there was enough space to play with the geometry and make it work.

The locations of the window holes were picked as the best location between both the 0.4064 meter cylinder and the 0.1016 meter cylinder. As shown the area to move was pretty tight, so some additional material was removed from the 0.1016 meter cylinder.

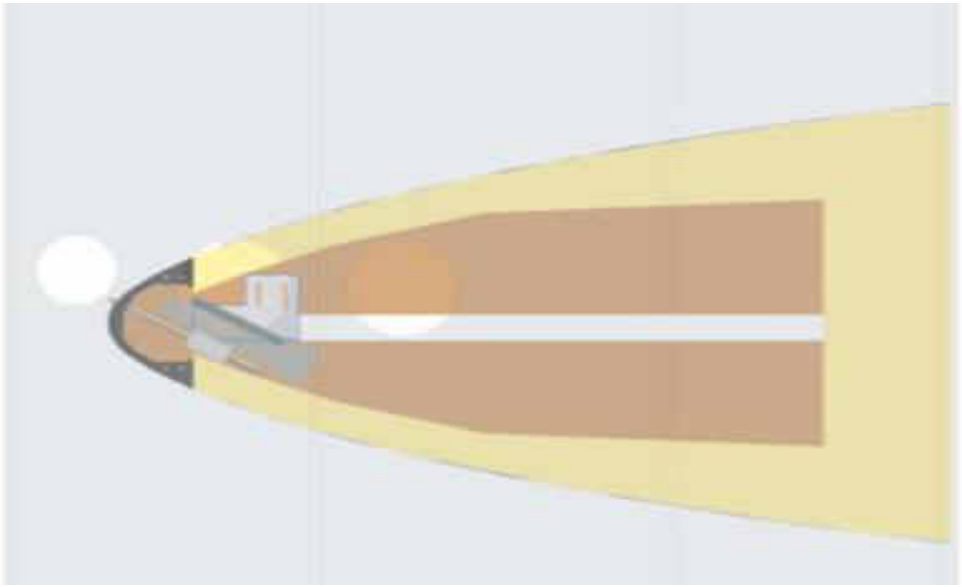

Figure 28. The 0.1016 meter cylindrical leading edge test section model.

The traversing assembly was the same equipment as the 0.4064 meter cylindrical leading edge vane only there was an attachment that helped the probe have alignment. The probe holder for the 0.1016 meter cylindrical leading edge was shorter than the 0.4064 meter cylindrical leading edge version for the purpose of fitting in the cylinder. The 0.4064 meter cylindrical leading edge needed the extra length to get the probe to reach the desired location.

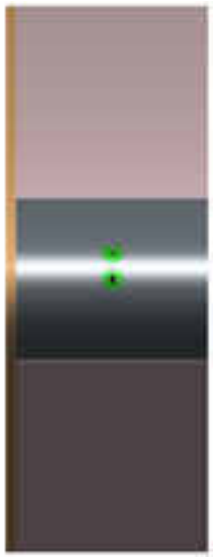

Figure 29. The 0.1016 meter cylindrical leading edge model front view.

The cylinder also had to fit the equipment needed to take measurements at the stagnation region. Pro E was used to ensure everything fit, and all of the angles were correct. In Pro-E, I checked all of the moving parts for possible binding or other fit issues that could occur.

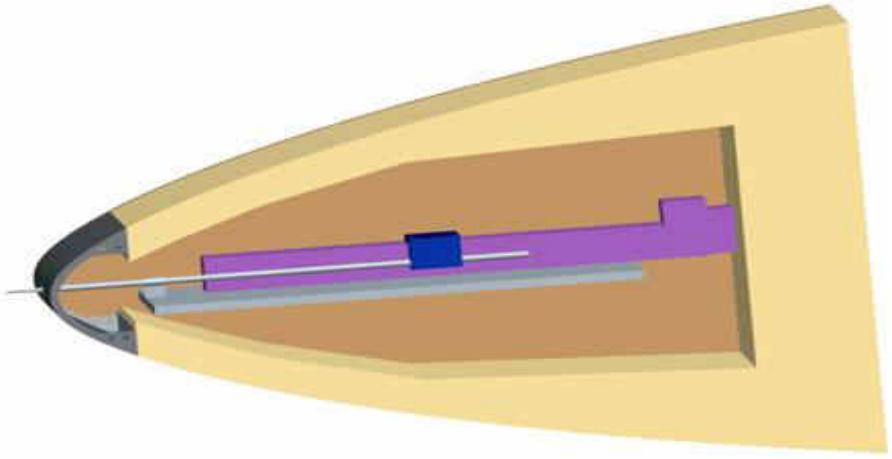

Figure 30. The 0.1016 meter cylindrical leading edge model with other test set up.

The 0.1016 meter cylindrical leading edge was created the same way as the 0.4064 meter cylindrical leading edge vane. The only major difference was that the 0.1016 meter cylindrical tip was able to fit in the three-dimensional printer without needing to break up the part into several pieces. The surface was scraped down by hand since the surface was not smooth after the printing process. A machine could not confidently do this since minor changes to the surface would affect the acceleration. I used a clean buffing piece to finish off the surface.

Figure 31. Front view of the 0.1016 meter cylindrical leading edge vane.

After they were assembled it was easier just to place tape over the hole on the thirty degrees downstream location, because it was small. The Clear scotch tape was placed along the streamline improved the measurements, by providing a smooth surface for the boundary layer. This also prevented any leaks from the plugs creating leaks on the streamline and any imperfections caused by the three-dimensional printing process.

Appendix C
Dimensionless Velocity Profiles

These are the dimensionless velocity profiles. These were done to help see what the values of the wall shear stress and the offset of the probe from the recorded distance. The Figure 32 below illustrates the profile of the velocities at various Reynolds numbers for the small grid case which was located in the position farthest from the test section.

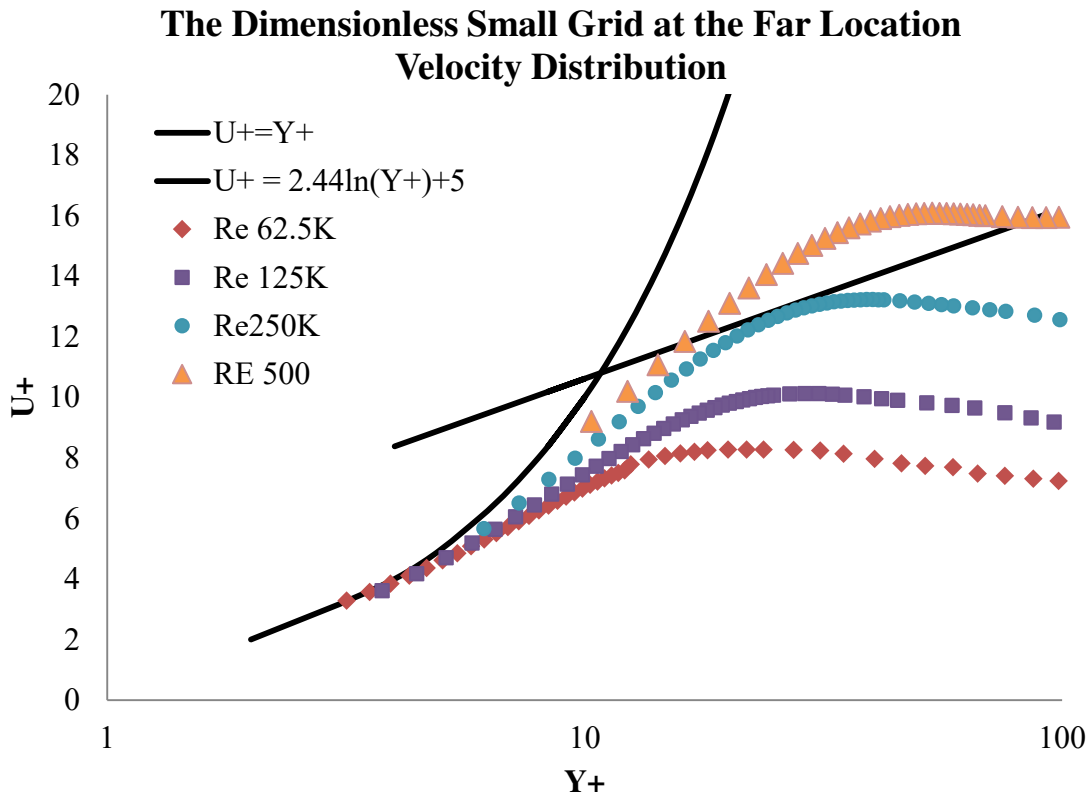

Figure 32. The velocity profile for the small grid located in the far location.

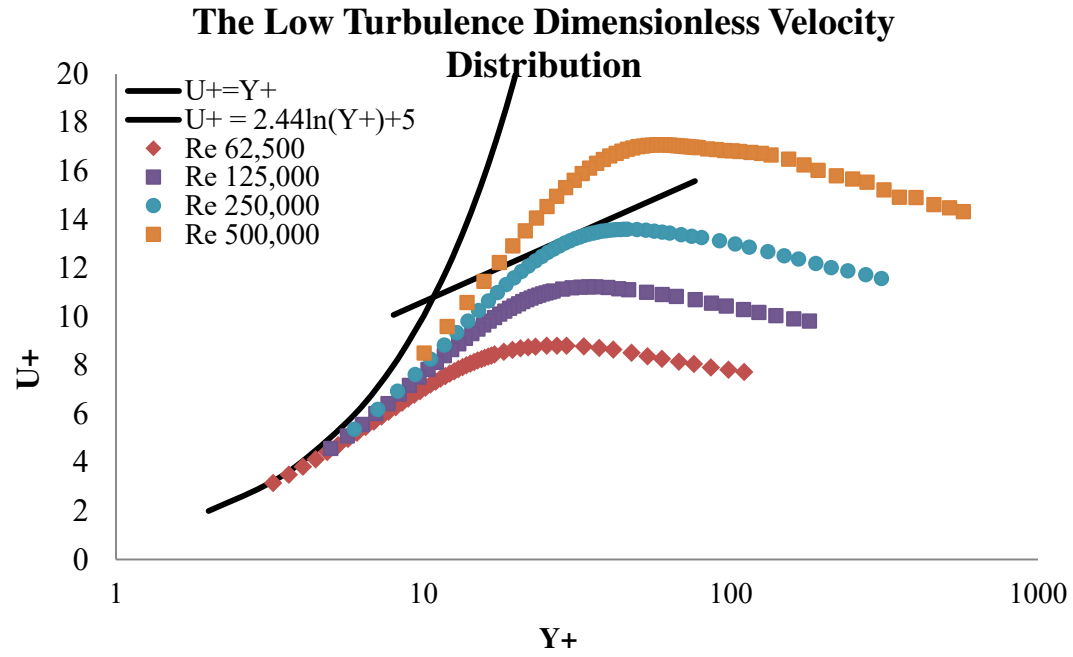

Figure 33. The velocity profile for the low turbulence condition.

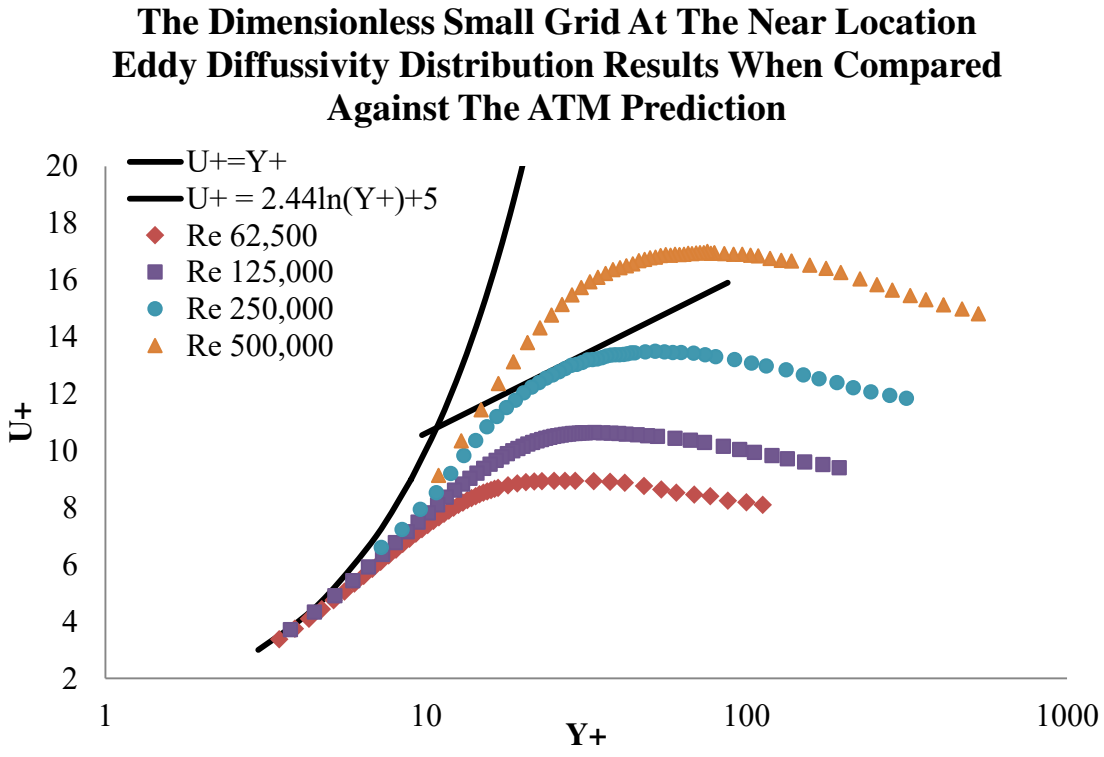

Figure 34. The velocity profile for the small grid in the location near the test surface.

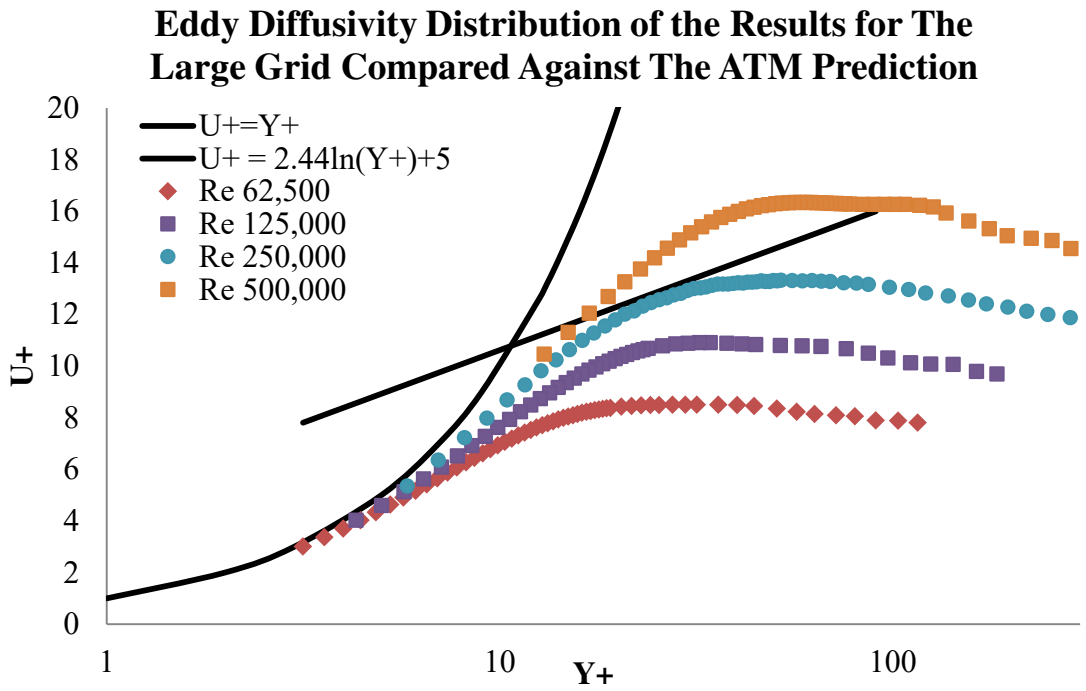

Figure 35. The velocity distribution for the large grid.

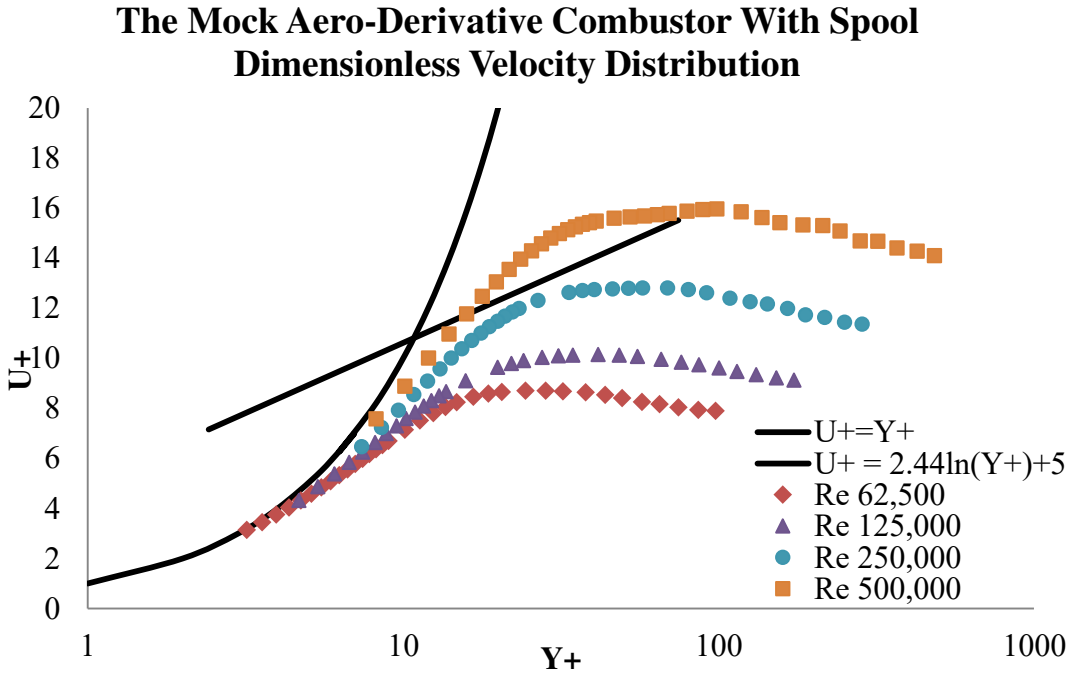

Figure 36. The velocity distribution for the mock derivative aero-combustor with the spool.

Appendix D
Fitting the Velocity and Velocity Gradient for Analysis.

The data had to be fit to a curve to improve the calculation of the velocity gradient. This velocity gradient is the change of velocity in the boundary layer. The fit was determined by first removing the velocity datum point taken nearest to the wall because it touches the wall. The velocity profile result "U" was fit to a fourth order (n = 4rth) polynomial equation "u(y)." After an acceptable (difference of 2% of the actual data) fit is made with the velocity, we can calculate the velocity gradient "dU/dy." Next the fit for the velocity gradient "dU/dy" was fit to a third order equation "du(y)/dy."

$$\frac{dU}{dy} = \frac{u(y)_{n-1} - u(y)_n}{y_{n-1} - y_{n-1}} \quad [45]$$

The resulting data "F" was fit (for both velocity and the velocity gradient) to function "f(x)"of "nth" power through linear regression. If the difference between the fit and the datum near the wall at x is greater than 2%, then the difference is fit "F" with a two order greater Equation. "F" denotes a result and f(y) the fit.

$$F^{n+2}{}_2 = F - f^n(x)_1 \ [46]$$

$$F^{n+4}{}_3 = F^{n+2}{}_2 - f^{n+2}(x)_2 \ [47]$$

$$F^{n+6}{}_4 = F^{n+4}{}_3 - f^{n+4}(x)_3 \ [48]$$

$$F \cong f^n(x)_1 + f^{n+2}(x)_2 + f^{n+4}(x)_2 + \ \ldots + f^{n+2m}(x)_m$$

This is repeated until the differences between the fits are less than two percent.

$$\frac{F - (f^n(x)_1 + f^{n+2}(x)_2 + f^{n+4}(x)_3 + \ldots + f^{n+2m}(x)_m)}{F} \leq 2\% \quad [49]$$

The resulting fits are then summed and used in the spreadsheet for analysis.

$$F \cong f^{n}(x)_1 + f^{n+2}(x)_2 + f^{n+4}(x)_2 + \ ... + f^{n+2m}(x)_m \quad [50]$$

Appendix E
Uncertainty Analysis

The calculation of the uncertainty in the results used information from the analysis of the results and the equipment limitations. Some factors created a complication in determining the uncertainty were traditional methods were possibly not correct by the adjustments to the "Y" offset and the known shear stress distribution that occurs in a laminar boundary layer. Many of the errors from equipment and measurement are affected by this process. Also instead of fitting a traditional line to the data a set of fits to the errors had improved the fit to the data. The curve had the error fits added until improvements stopped, or differences between the fit and the actual results were two percent or less. The uncertainty analysis used a combination of methods.

The first step was to establish the root sources of uncertainty. The largest uncertainty comes from the pressure gauges, the hot wire anemometer calibration, and the thermocouples. The sum of these errors are from calibration, fitting the velocity and velocity gradient curves and uncertainty in predicted values.

The equipment used in this experiment had manufacturer given uncertainties. The results' uncertainty used information from the equipment resolution included the pressure gauges and the thermal couples. The pressure gauges have an error of 1% of the range (Dvorak, 2003). Also that the thermocouples have an error of 0.2 degrees Celsius (Dvorak, 2003). Calibration of the hotwire velocity curve allowed for an uncertainty of 2%.

When a curve is fit to a data set, there is an uncertainty in its. When the errors of the curve's fit were then fit to a polynomial this accounted for the gap. Then the error fit

could be added to better represent these values. In addition, when fitting the data an offset was added to the distances when the regression fit was done in Excel. This helps reduce errors from coincidental common zero values. Both the fits for the boundary layer velocity and the boundary layer's velocity gradient had an uncertainty based on the differences between the measured results and the fit results. When the point occurred where no single point had a difference more than 2% or no improvements occurred then I used this final set of data for the error analysis. In the formula, "R" is the results and "δR" is the difference between the measured result and the regression fit. The values away from the outer region of the boundary layer and near the surface so to have a better representative account of the error. The reason is that the error was fit several times, therefore the values may be more greatly affected by being the "ends of the fits."

$$\pm\delta R = \sqrt{\frac{\sum_{i=1}^{i=n} {\delta R_i}^2}{n}} \qquad [51]$$

Then the data's differences are squared and averaged to get the standard deviation for the fit. Here the assumption that the definition of standard deviation is as the square root of the variance (Figiola & Beasley, 2006).

From aligning the predicted velocity gradient profile discussed in the analysis section to the actual velocity- the "y" offset and the wall's shear stress can be determined. The results of the shear stress at the wall should be within 5%

The last point measured happened to occur at two different ranges consistently. The point occurred either at 0.0055 thousandths of an inch or 0.0085 thousandths of an inch. The deviations of these values stayed within plus or minus 0.0005 thousandths and usually very close to those values. The reason behind this may be because the

modification in the angle of the hotwire probe was done by hand for both probes. Then it is possible that geometry differences in the probe resulted in this. Table 8 shows how the uncertainty "Unc." Was calculated

Table 8. The Mock Derivative Aero-Combustor base uncertainty results at Re_D 62,500.

	Nominal	Units	Unc.	Nom+ Unc.
T_{air}	302.3	K	0.2000	302.51
P_{in}	98283	Pa	20.0000	98303
P_{out}	98268	Pa	20.0000	98288
$U_{y,\ fit}$	1.8	m/s	0.0122	2
$U_{y,\ Hot\ wire}$	1.8	m/s	0.0357	1.8198
D	0.4064	m	0.0016	0.4080
Y	0.0007	m	0.000005	0.0007
$\frac{dU}{dy}_{wall}$	3810	1/s	190.5	4000.5
$\frac{dU}{dy}_{\text{y+ = 10 fit}}$	1184	1/s	87.0	1271

After the general uncertainties had been collected, the errors were propagated (Moffat, 1988) and perturbation. Since the calculation of the momentum eddy diffusivity took many steps, the calculations were broken down into steps. First the solution of the deviation values of density, free stream velocity, the velocity of the laminar velocity distribution, viscosity, shear velocity, and any others dependent on the main sources of error; the table below illustrates the calculations.

Table 9. Example of how uncertainty in density was calculated for the Mock Derivative Aero-Combustor at Re_D 62,500.

Density	Nominal	Units	Unc.	Nom+ Unc.	Pert	Calc (kg/m^3)	(Pert-Calc)^2	
Pin	98283	Pa	98283	Pa	20.0000	98303	1.1329	
Temp	302.3	K	302.3	K	0.2000	303	1.1319	
					Standard Deviation		0.000784	kg/m^3

When calculating the uncertainty in the density to be used in later calculations both the errors in temperature and the pressure had to be used. The perturbations and

propagations were broken down into steps to prevent error and check the results. Below shows the Equations that showed how the perturbations were used to find the variances and how they were used to find the deviation from the density. The first two Equations show how the perturbation minus the calculations were obtained.

$$\delta\rho_{Pressure} = \left(\frac{P_{in}+\delta P}{T*R_{gas}}\right) - \rho \quad [52]$$

$$\delta\rho_{Temperature} = \left(\frac{P_{in}}{(T+\delta T)*R_{gas}}\right) - \rho \quad [53]$$

Finally, the uncertainty of the density can be calculated.

$$\delta\rho = \sqrt{\delta\rho_{Pressure}{}^2 + \delta\rho_{Temperature}{}^2} \quad [54]$$

Using the same method as above, the deviation in Reynolds number boundary layer velocity, the different shear stresses, and any other variables. This table below illustrates how the shear stresses were calculated. Using the same process shown above the deviation is found. The uncertainty of the velocity distribution was about 0.051 m/s.

Table 10. The Mock Aero-Derivative Combustor Velocity Profile Uncertainty at Re_D = 62,500.

U_y	*Nominal*	*Units*	*Unc.*	*Nom+ Unc.*	*Pert .*	*Calc. (m/s)*	*(Pert- Calc)^2*	
$U_{y,\ fit}$	2.46	Pa	0.01	2.474	2.47	2.46	0.000152	
$U_{y,\ Hot\ wire}$	2.46	Pa	0.05	2.511	2.51	2.46	0.00242	
						Stdev	0.0508	m/s

The Reynolds number was found to have an error of about 178.25.

Table 11. The Mock Aero-Derivative Combustor Re_D Uncertainty at Re_D = 62,500.

Re_D	Nominal	Units	Unc.	Nom+ Unc.	Pert	Calc	(Pert-Calc)^2
Density	1.133	kg/m^3	0.00078	1.133	44258	44228	936
Viscosity	1.857E-05	Pa s	9.4E-09	1.86E-05	44205	44228	504
Diameter	0.4064	m	0.0016	0.408	44400	44228	29848
U_∞	1.8	m/s	0.0009	1.785	44250	44228	485
				Standard Deviation			178.25

Because for the Mock Aero-Derivative Combustor at Re_D 62,500 case seems to vary similarly in the center of the velocity gradient distribution fit I picked a Y+ often to calculate the data. Also, the uncertainty must be propagated out. The error for the velocity gradient is about 395 1/s.

Table 12. The Mock Aero-Derivative Combustor velocity gradient uncertainty at Re_D = 62,500.

dU/dy	***Nom.***	***Units***	***Unc.***	***Nom+ Unc.***	***Pert***	***Calc***	***(Pert-Calc)^2***
$\frac{dU}{dy}_{y+=10\ fit}$	1184	1/s	87.0	1271	1271	1183	7566
				Standard Deviation		87.0	1/s

These calculations were used to calculate the eddy viscosity as shown below. These calculations are from the same discussed flow condition. The below table makes sense because of the uncertainty in both the last point locations. The Uncertainty is found to be about 25% for the eddy diffusivity.

Table 13. Deviation results for the momentum eddy diffusivity for the Mock Aero-Derivative Combustor at Re_D62,500.

εm(y+ = 10)	Nominal	Units	Unc.	Nom+ Unc.	Pert	Calc	(Pert-Calc)^2	
Density	2.462	kg/m^3	0.00078	2.4627	-1.7E-06	-1.70E-06	2.93E-19	
τ_visc(y+ = 10)	0.0220	Pa	0.0016	0.0236	-1.4E-06	-1.70E-06	8.5209E-14	
τ(y+ = 10)	0.0314	Pa	0.00163	0.0330	-2.0E-06	-1.70E-06	8.7016E-14	
Du/Dy (y+ =10)	2248	1/s	86.98	2334.5	-1.6E-06	-1.70E-06	4.0270E-15	
						Stdev	4.19E-07	m^2/s

Appendix F
Raw Data

Table 14. Low Turbulent flow properties with Re_D of 62,500.

Item	Value	Units
File Name	BLT1R1Y1	
Reynolds D	62219.54	
Temperature air	303.2101	K
Pressure_in	99351.71	Pa,
Pressure Drop	14.67399	Pa,
Velocity	2.495779	m/s

Table 15. Low Turbulent profile measurements for Re_D of 62,500.

Y (inch)	U (m/s)	u' (m/s)	Tu
0.3	1.99423	0.016	0.00803
0.27	2.01595	0.00733	0.00364
0.24	2.03912	0.00498	0.00244
0.21	2.06944	0.00694	0.00335
0.185	2.09838	0.00396	0.00189
0.165	2.12852	0.01162	0.00546
0.145	2.16203	0.0162	0.00749
0.13	2.18767	0.00967	0.00442
0.115	2.21949	0.01122	0.00506
0.1	2.2515	0.00425	0.00189
0.09	2.27245	0.00429	0.00189
0.08	2.29449	0.01424	0.0062
0.07	2.30356	0.0133	0.00578
0.065	2.30451	0.01507	0.00654
0.06	2.30233	0.01617	0.00702
0.055	2.29367	0.0188	0.0082
0.052	2.28397	0.01797	0.00787
0.049	2.26978	0.01563	0.00689
0.046	2.24658	0.01665	0.00741
0.043	2.22225	0.02011	0.00905
0.04	2.18966	0.01924	0.00879
0.039	2.18893	0.02015	0.00921
0.038	2.17676	0.02135	0.00981
0.037	2.16699	0.02315	0.01068

Continue Table 15

0.036	2.15329	0.02301	0.01069
0.035	2.13907	0.02341	0.01095
0.034	2.12585	0.02298	0.01081
0.033	2.10934	0.02146	0.01017
0.032	2.09219	0.01905	0.0091
0.031	2.07236	0.01935	0.00934
0.03	2.05462	0.01929	0.00939
0.029	2.0309	0.01878	0.00925
0.028	2.00154	0.01976	0.00987
0.027	1.9784	0.01651	0.00834
0.026	1.94817	0.00849	0.00436
0.025	1.91855	0.0124	0.00646
0.024	1.8833	0.02351	0.01248
0.023	1.84776	0.02232	0.01208
0.022	1.81267	0.02262	0.01248
0.021	1.77155	0.02276	0.01285
0.02	1.72534	0.02145	0.01243
0.019	1.67964	0.02122	0.01263
0.018	1.64655	0.01934	0.01175
0.017	1.593	0.01767	0.01109
0.016	1.53699	0.01893	0.01231
0.015	1.47933	0.01893	0.0128
0.014	1.416	0.01785	0.01261
0.013	1.35209	0.01928	0.01426
0.012	1.29033	0.01812	0.01404
0.011	1.22505	0.0184	0.01502
0.01	1.15766	0.01712	0.01479
0.009	1.08419	0.01621	0.01495
0.008	1.00311	0.01437	0.01433
0.007	0.91442	0.0143	0.01564
0.006	0.82542	0.01221	0.01479
0.005	0.75123	0.01027	0.01368

Table 16. Low Turbulent Profile flow properties with Re_D of 125,000.

Item	Value	Units
File Name	BLT1R2Y1	
Reynolds D	127930.8	
Temperature air	301.8051	K
Pressure_in	99351.71	Pa,
Pressure Drop	61.32019	Pa,
Velocity	5.08966	m/s

Table 17. Low Turbulent Profile measurements with Re_D of 125,000.

Y (inch)	U (m/s)	u' (m/s)	Tu
0.3	4.122	0.01816	0.00441
0.27	4.15474	0.02186	0.00526
0.24	4.19323	0.02663	0.00635
0.21	4.24277	0.02643	0.00623
0.185	4.30258	0.02414	0.00561
0.165	4.35691	0.0261	0.00599
0.145	4.42037	0.01451	0.00328
0.13	4.45544	0.01416	0.00318
0.115	4.51595	0.01399	0.0031
0.1	4.57899	0.01881	0.00411
0.09	4.62295	0.01242	0.00269
0.08	4.66406	0.0486	0.01042
0.07	4.70784	0.04972	0.01056
0.065	4.73059	0.05041	0.01066
0.06	4.73684	0.05131	0.01083
0.055	4.74393	0.04903	0.01034
0.052	4.74582	0.05049	0.01064
0.049	4.73859	0.05224	0.01102
0.046	4.72066	0.05728	0.01213
0.043	4.69895	0.05965	0.01269
0.04	4.66447	0.05841	0.01252
0.039	4.65123	0.05441	0.0117
0.038	4.63655	0.0531	0.01145
0.037	4.61346	0.04818	0.01044
0.036	4.59784	0.04984	0.01084
0.035	4.57533	0.05255	0.01149
0.034	4.55557	0.05071	0.01113
0.033	4.52749	0.05571	0.0123

Table 17 Continued

0.032	4.49936	0.05356	0.0119
0.031	4.46408	0.05539	0.01241
0.03	4.42749	0.05578	0.0126
0.029	4.38459	0.05345	0.01219
0.028	4.34111	0.0529	0.01219
0.027	4.28803	0.05202	0.01213
0.026	4.23745	0.05903	0.01393
0.025	4.17485	0.0591	0.01416
0.024	4.10742	0.05947	0.01448
0.023	4.02935	0.06013	0.01492
0.022	3.94022	0.05496	0.01395
0.021	3.85268	0.05511	0.01431
0.02	3.75209	0.05203	0.01387
0.019	3.65001	0.04991	0.01367
0.018	3.54629	0.04908	0.01384
0.017	3.42952	0.04846	0.01413
0.016	3.30264	0.04811	0.01457
0.015	3.16763	0.0462	0.01458
0.014	3.01558	0.04195	0.01391
0.013	2.85769	0.03384	0.01184
0.012	2.69077	0.03907	0.01452
0.011	2.52429	0.03202	0.01269
0.01	2.3605	0.0339	0.01436
0.009	2.18049	0.02915	0.01337
0.008	1.95773	0.02041	0.01042
0.007	1.71044	0.02299	0.01344
0.006	1.50506	0.01765	0.01173

Table 18. Low Turbulent flow properties for Re_D of 250,000.

Item	Value	Units
File Name	BLT1R3Y1	
Reynolds D	250976	
Temperature_air	302.6979	K
Pressure_in	99182.45	Pa,
Pressure Drop	238.3349	Pa,
Velocity	10.05435	m/s

Table 19. Low Turbulent profile measurements for Re_D of 250,000.

Y (inch)	U (m/s)	u' (m/s)	Tu
0.3	8.49582	0.07663	0.00902
0.27	8.51017	0.07837	0.00921
0.24	8.62644	0.06018	0.00698
0.21	8.74257	0.04246	0.00486
0.185	8.84527	0.06628	0.00749
0.165	8.96381	0.05159	0.00576
0.145	9.09051	0.05004	0.00551
0.13	9.20414	0.0417	0.00453
0.115	9.33231	0.0383	0.0041
0.1	9.46029	0.03827	0.00405
0.09	9.54592	0.05756	0.00603
0.08	9.64484	0.04763	0.00494
0.07	9.73881	0.04111	0.00422
0.065	9.80282	0.04471	0.00456
0.06	9.86986	0.05091	0.00516
0.055	9.90099	0.05945	0.006
0.052	9.92665	0.06524	0.00657
0.049	9.9508	0.06677	0.00671
0.046	9.96199	0.07177	0.0072
0.043	9.97277	0.07569	0.00759
0.04	9.98191	0.09501	0.00952
0.039	9.98159	0.08898	0.00891
0.038	9.98832	0.08988	0.009
0.037	9.95459	0.09728	0.00977
0.036	9.9598	0.09651	0.00969
0.035	9.96376	0.10105	0.01014
0.034	9.96022	0.11248	0.01129
0.033	9.94005	0.11006	0.01107
0.032	9.91486	0.1182	0.01192
0.031	9.89583	0.12149	0.01228
0.03	9.85799	0.13084	0.01327
0.029	9.83798	0.1328	0.0135
0.028	9.78798	0.13662	0.01396
0.027	9.73278	0.14917	0.01533
0.026	9.66398	0.15117	0.01564
0.025	9.60004	0.16226	0.0169
0.024	9.53688	0.1684	0.01766
0.023	9.4104	0.16899	0.01796
0.022	9.28832	0.17603	0.01895

Table 19 Continued

0.021	9.1784	0.18387	0.02003
0.02	9.02784	0.19317	0.0214
0.019	8.89038	0.18613	0.02094
0.018	8.69448	0.19485	0.02241
0.017	8.52382	0.19267	0.0226
0.016	8.31754	0.18591	0.02235
0.015	8.09262	0.17798	0.02199
0.014	7.80976	0.17266	0.02211
0.013	7.53902	0.1624	0.02154
0.012	7.22288	0.15688	0.02172
0.011	6.89156	0.13228	0.01919
0.01	6.4748	0.13106	0.02024
0.009	6.06943	0.12379	0.0204
0.008	5.60108	0.11358	0.02028
0.007	5.11074	0.09816	0.01921
0.006	4.55939	0.08084	0.01773
0.005	3.93617	0.06725	0.01708
0.004	3.59493	0.06405	0.01782

Table 20. Low Turbulent flow properties for Re_D of 500,000.

Item		Value	Units
File Name	BLT1R4Y1		
Reynolds D	490892.1		
Temperature air	305.4984	K	
Pressure_in	99351.71	Pa,	
Pressure Drop	934.0439	Pa,	
Velocity	19.95415	m/s	

Table 21. Low Turbulent profile measurements for Re_D of 500,000.

Y (inch)	U (m/s)	u' (m/s)	Tu
0.3	17.72038	0.07806	0.00441
0.27	17.89444	0.10495	0.00586
0.24	18.10472	0.06702	0.0037
0.21	18.33569	0.09404	0.00513
0.185	18.57752	0.12059	0.00649

Table 21 Continued

0.165	18.81285	0.08182	0.00435
0.145	19.09037	0.10793	0.00565
0.13	19.33921	0.13639	0.00705
0.115	19.6404	0.14539	0.0074
0.1	19.92561	0.12887	0.00647
0.09	20.12931	0.13045	0.00648
0.08	20.28628	0.12645	0.00623
0.07	20.48247	0.15097	0.00737
0.065	20.58648	0.15884	0.00772
0.06	20.67633	0.1652	0.00799
0.055	20.74743	0.15943	0.00768
0.052	20.82245	0.15427	0.00741
0.049	20.9014	0.14272	0.00683
0.046	20.96816	0.15742	0.00751
0.043	21.01208	0.15211	0.00724
0.04	21.04611	0.16503	0.00784
0.039	21.05115	0.15838	0.00752
0.038	21.06684	0.17404	0.00826
0.037	21.07402	0.18258	0.00866
0.036	21.07584	0.18974	0.009
0.035	21.08684	0.18664	0.00885
0.034	21.09779	0.17766	0.00842
0.033	21.08165	0.19574	0.00928
0.032	21.08593	0.20611	0.00977
0.031	21.07041	0.20899	0.00992
0.03	21.05742	0.22696	0.01078
0.029	21.0324	0.2312	0.01099
0.028	21.06524	0.24367	0.01157
0.027	21.0349	0.27246	0.01295
0.026	20.97569	0.28697	0.01368
0.025	20.94131	0.29849	0.01425
0.024	20.90558	0.32546	0.01557
0.023	20.8235	0.35715	0.01715
0.022	20.74224	0.39161	0.01888
0.021	20.6437	0.40268	0.01951
0.02	20.50589	0.44723	0.02181
0.019	20.35699	0.4897	0.02406
0.018	20.17971	0.51657	0.0256
0.017	19.93794	0.5474	0.02746

Table 21 Continued

0.016	19.66339	0.5809	0.02954
0.015	19.34358	0.60859	0.03146
0.014	18.96347	0.63432	0.03345
0.013	18.56539	0.65843	0.03547
0.012	18.0475	0.68644	0.03804
0.011	17.46639	0.71139	0.04073
0.01	16.77815	0.72711	0.04334
0.009	16.02064	0.78661	0.0491
0.008	15.16835	0.82405	0.05433
0.007	14.19067	0.8419	0.05933
0.006	13.0528	0.88702	0.06796
0.005	11.66844	0.89703	0.07688
0.004	10.52491	0.83294	0.07914
0.003	10.0682	0.78648	0.07812

Table 22. Mock Derivative Aero-Combustor flow properties for Re_D of 62,500.

Item	Value	Units
File Name	Bac1R1Y3	
Reynolds D	62131.35	
Temperature_air	302.3084	K
Pressure_in	98268.48	Pa,
Pressure Drop	14.68246	Pa,
Velocity	2.506485	m/s

Table 23. Mock Derivative Aero-Combustor profile measurements for Re_D of 62,500.

Y (inch)	U (m/s)	u' (m/s)	Tu
0.3	1.94289	0.27093	0.13945
0.27	1.95001	0.28242	0.14483
0.24	1.9673	0.28469	0.14471
0.21	2.00243	0.28107	0.14036
0.185	1.98935	0.28492	0.14322
0.165	2.03504	0.29046	0.14273
0.145	2.04945	0.29796	0.14539
0.13	2.07107	0.31131	0.15031
0.115	2.09684	0.31256	0.14906
0.1	2.10908	0.31389	0.14883
0.09	2.11406	0.32472	0.1536

Table 23 Continued

0.08	2.12552	0.31727	0.14927
0.07	2.1246	0.33096	0.15578
0.065	2.12405	0.33067	0.15568
0.06	2.11453	0.31205	0.14757
0.055	2.1292	0.32773	0.15392
0.052	2.09813	0.33235	0.1584
0.049	2.09745	0.32891	0.15681
0.046	2.09378	0.31533	0.1506
0.043	2.04764	0.31272	0.15272
0.04	2.02636	0.31338	0.15465
0.039	2.02851	0.32408	0.15976
0.038	2.00192	0.32164	0.16067
0.037	1.97245	0.31162	0.15799
0.036	1.97056	0.31188	0.15827
0.035	1.962	0.30933	0.15766
0.034	1.9348	0.3084	0.1594
0.033	1.94069	0.32114	0.16548
0.032	1.9125	0.30369	0.15879
0.031	1.90822	0.3076	0.1612
0.03	1.89393	0.29422	0.15535
0.029	1.85927	0.29301	0.15759
0.028	1.84052	0.29385	0.15965
0.027	1.82005	0.28761	0.15802
0.026	1.78412	0.2851	0.1598
0.025	1.7327	0.28029	0.16176
0.024	1.72272	0.27724	0.16093
0.023	1.68808	0.27456	0.16265
0.022	1.62877	0.26942	0.16541
0.021	1.58796	0.2607	0.16417
0.02	1.54238	0.24922	0.16158
0.019	1.48362	0.23673	0.15956
0.018	1.42544	0.23311	0.16353
0.017	1.36558	0.21837	0.15991
0.016	1.29702	0.20881	0.16099
0.015	1.2287	0.19229	0.1565
0.014	1.16756	0.17916	0.15345
0.013	1.08697	0.1693	0.15575
0.012	1.02049	0.15783	0.15466
0.011	0.9427	0.14525	0.15408
0.01	0.85528	0.13227	0.15465

Table 23 Continued

0.009	0.78128	0.11527	0.14754
0.008	0.71323	0.09769	0.13696

Table 24. Mock Derivative Aero-Combustor flow properties with Re_D of 125,000.

Item	Value	Units
File Name	BAC1R2Y3	
Reynolds D	127012	
Temperature_air	297.6698	K
Pressure_in	97997.68	Pa,
Pressure Drop	59.16814	Pa,
Velocity	4.999378	m/s

Table 25. Mock Derivative Aero-Combustor profile measurements for Re_D of 125,000.

Y (inch)	U (m/s)	u' (m/s)	Tu
0.7959852	3.74255	0.58022	0.15503
0.7197852	3.76425	0.56176	0.14924
0.6435852	3.79501	0.56731	0.14949
0.5673852	3.84029	0.58021	0.15108
0.5038852	3.862	0.59992	0.15534
0.4530852	3.92731	0.60563	0.15421
0.4022852	3.95788	0.59487	0.1503
0.3641852	3.98795	0.61523	0.15427
0.3260852	4.02319	0.63396	0.15758
0.2879852	4.06582	0.62955	0.15484
0.2625852	4.07007	0.6404	0.15734
0.2371852	4.11379	0.63472	0.15429
0.2117852	4.13501	0.65235	0.15776
0.1990852	4.14033	0.65013	0.15702
0.1863852	4.16605	0.66832	0.16042
0.1736852	4.14826	0.66767	0.16095
0.1660652	4.17775	0.6629	0.15867
0.1584452	4.16203	0.67218	0.1615
0.1432052	4.14942	0.66437	0.16011
0.1355852	4.12035	0.67195	0.16308
0.1330452	4.13776	0.67525	0.16319
0.1305052	4.13978	0.68458	0.16537

Table 25 Continued

0.1279652	4.14169	0.67934	0.16403
0.1254252	4.12538	0.67531	0.1637
0.1228852	4.13139	0.68716	0.16633
0.1203452	4.09083	0.6785	0.16586
0.1178052	4.12188	0.67668	0.16417
0.1152652	4.10374	0.67573	0.16466
0.1127252	4.06832	0.69722	0.17138
0.1101852	4.05049	0.67304	0.16616
0.1076452	4.07376	0.66414	0.16303
0.1051052	4.07036	0.67985	0.16702
0.1025652	4.04106	0.67626	0.16735
0.1000252	4.03025	0.67828	0.1683
0.0974852	4.02462	0.67818	0.16851
0.0949452	4.0027	0.67585	0.16885
0.0924052	4.00484	0.67542	0.16865
0.0898652	3.98848	0.6717	0.16841
0.0873252	3.98477	0.67594	0.16963
0.0847852	3.94274	0.67043	0.17004
0.0822452	3.95327	0.68281	0.17272
0.0797052	3.93599	0.65887	0.1674
0.0771652	3.89034	0.68344	0.17568
0.0746252	3.87928	0.67352	0.17362
0.0720852	3.85665	0.66508	0.17245
0.0695452	3.82933	0.66516	0.1737
0.0670052	3.76862	0.6513	0.17282
0.0644652	3.73388	0.64914	0.17385
0.0619252	3.70073	0.65307	0.17647
0.0593852	3.65619	0.64496	0.1764
0.0568452	3.62821	0.6387	0.17604
0.0543052	3.55626	0.63342	0.17811
0.0517652	3.46381	0.61734	0.17823
0.0492252	3.43214	0.60967	0.17764
0.0466852	3.3256	0.58246	0.17514
0.0441452	3.22282	0.57994	0.17995
0.0416052	3.13075	0.55892	0.17853
0.0390652	3.01455	0.54021	0.1792
0.0365252	2.89172	0.51155	0.1769
0.0339852	2.75483	0.49096	0.17822
0.0314452	2.60413	0.45652	0.17531
0.0289052	2.45584	0.42898	0.17468

Table 25 Continued

0.0263652	2.29301	0.39245	0.17115
0.0238252	2.10504	0.34575	0.16425
0.0212852	1.92612	0.30522	0.15846
0.0187452	1.73831	0.26173	0.15056
0.0162052	1.52086	0.22114	0.14541
0.0136652	1.29627	0.17395	0.13419
0.012446	1.18432	0.14575	0.12306

Table 26. Mock Derivative Aero-Combustor flow properties with Re_D of 250,000.

Item	Value	Units
File Name	Bac1R3Y1	
Reynolds D	252939.8	
Temperature air	298.8737	K
Pressure in	97997.68	Pa,
Pressure Drop	237.2291	Pa,
Velocity	10.02748	m/s

Table 27. Mock Derivative Aero-Combustor profile measurements for Re_D of 250,000.

Y (inch)	U (m/s)	u' (m/s)	Tu
0.3	7.71588	1.09658	0.14212
0.27	7.80887	1.11087	0.14226
0.24	7.81564	1.09607	0.14024
0.21	7.90902	1.13204	0.14313
0.185	8.04644	1.13255	0.14075
0.165	8.07516	1.14346	0.1416
0.145	8.21811	1.15844	0.14096
0.13	8.28143	1.16754	0.14098
0.115	8.38268	1.20089	0.14326
0.1	8.42639	1.22202	0.14502
0.09	8.51276	1.22788	0.14424
0.08	8.58411	1.23941	0.14438
0.07	8.58765	1.2542	0.14605
0.065	8.60906	1.25515	0.14579
0.06	8.63033	1.25653	0.14559
0.055	8.63196	1.27485	0.14769
0.052	8.59829	1.30138	0.15135
0.049	8.58708	1.27988	0.14905

Table 27 Continued

0.043	8.54613	1.3173	0.15414
0.04	8.5281	1.3008	0.15253
0.039	8.48234	1.30555	0.15391
0.038	8.46887	1.31654	0.15546
0.037	8.40398	1.30533	0.15532
0.036	8.39413	1.29402	0.15416
0.035	8.37693	1.30608	0.15591
0.034	8.34721	1.31087	0.15704
0.033	8.32409	1.31931	0.15849
0.032	8.27376	1.31336	0.15874
0.031	8.21284	1.26576	0.15412
0.03	8.23924	1.31355	0.15943
0.029	8.11289	1.28875	0.15885
0.028	8.02651	1.25669	0.15657
0.027	7.97855	1.25864	0.15775
0.026	7.85979	1.26953	0.16152
0.025	7.77588	1.24102	0.1596
0.024	7.65469	1.24117	0.16215
0.023	7.52574	1.21303	0.16118
0.022	7.38549	1.22284	0.16557
0.021	7.2009	1.19837	0.16642
0.02	6.98767	1.16241	0.16635
0.019	6.7443	1.12292	0.1665
0.018	6.51478	1.0916	0.16756
0.017	6.19295	1.06228	0.17153
0.016	5.82578	0.98604	0.16926
0.015	5.4181	0.90811	0.16761
0.014	4.98132	0.81539	0.16369
0.013	4.50351	0.72459	0.1609
0.012	3.97291	0.61484	0.15476
0.011	3.38602	0.50301	0.14856
0.01	3.07126	0.43872	0.14285
0.01	0.85528	0.13227	0.15465
0.009	0.78128	0.11527	0.14754
0.008	0.71323	0.09769	0.13696

Table 28. Mock Derivative Aero-Combustor flow properties for Re_D of 500,000.

Item	Value	Units
File Name	BAC1R4Y3	
Reynolds D	489139.3	
Temperature air	305.3761	K
Pressure in	98268.48	Pa,
Pressure Drop	936.7019	Pa,
Velocity	20.08787	m/s

Table 29. Mock Derivative Aero-Combustor profile measurements for Re_D of 500,000.

Y (inch)	U (m/s)	u' (m/s)	Tu
0.3	17.14616	2.29577	0.13389
0.27	17.23864	2.36189	0.13701
0.24	17.34686	2.30078	0.13263
0.21	17.57322	2.32326	0.1322
0.185	17.71158	2.35231	0.13281
0.165	17.89034	2.37583	0.1328
0.145	18.17182	2.41363	0.13282
0.13	18.31018	2.41975	0.13215
0.115	18.46797	2.43268	0.13172
0.1	18.73717	2.53444	0.13526
0.09	18.83116	2.4505	0.13013
0.08	18.98056	2.53613	0.13362
0.07	19.08589	2.53528	0.13284
0.065	19.18277	2.51972	0.13135
0.06	19.18925	2.53045	0.13187
0.055	19.30604	2.57825	0.13355
0.052	19.3148	2.58977	0.13408
0.049	19.34303	2.53579	0.1311
0.046	19.23584	2.62871	0.13666
0.043	19.24942	2.56329	0.13316
0.04	19.23386	2.59213	0.13477
0.039	19.21163	2.63603	0.13721
0.038	19.14344	2.60402	0.13603
0.037	19.19721	2.59107	0.13497
0.036	19.15914	2.60015	0.13571
0.035	19.114	2.60479	0.13628
0.034	19.11231	2.641	0.13818
0.033	19.15836	2.60016	0.13572

Table 31 Continued

0.032	19.07019	2.63021	0.13792
0.031	19.10124	2.61618	0.13696
0.03	19.03897	2.66132	0.13978
0.029	19.04977	2.58056	0.13546
0.028	19.00596	2.64324	0.13907
0.027	19.00415	2.61532	0.13762
0.026	18.88479	2.61144	0.13828
0.025	18.89568	2.67949	0.1418
0.024	18.85165	2.64306	0.1402
0.023	18.77227	2.61765	0.13944
0.022	18.72074	2.65792	0.14198
0.021	18.53589	2.65873	0.14344
0.02	18.44332	2.61097	0.14157
0.019	18.32945	2.60289	0.14201
0.018	18.20679	2.61441	0.1436
0.017	18.03597	2.55693	0.14177
0.016	17.8849	2.61995	0.14649
0.015	17.67944	2.56076	0.14484
0.014	17.34681	2.52398	0.1455
0.013	17.0146	2.51531	0.14783
0.012	16.57528	2.50264	0.15099
0.011	16.05209	2.42273	0.15093
0.01	15.46383	2.35525	0.15231
0.009	14.70527	2.24563	0.15271
0.008	13.77655	2.12117	0.15397
0.007	12.6921	1.97584	0.15567
0.006	11.43514	1.77028	0.15481
0.005	10.26505	1.57182	0.15312
0.004	9.39052	1.44334	0.1537

Table 30. Mock Derivative Aero-Combustor with Spool flow properties for Re_D of 62,500.

Item	Value	Units
File Name	BACSR1Y1	
Reynolds D	64162.73	
Temperature air	298.691	K
Pressure in	98843.95	Pa,
Pressure Drop	15.09869	Pa,
Velocity	2.519145	m/s

Table 31. Mock Derivative Aero-Combustor with Spool profile measurements for Re_D of 62,500.

Y (inch)	U (m/s)	u' (m/s)	Tu
0.3	1.88663	0.22285	0.11812
0.27	1.91587	0.22728	0.11863
0.24	1.92411	0.23323	0.12121
0.21	1.95059	0.22805	0.11691
0.185	1.97641	0.24163	0.12226
0.165	2.00048	0.23584	0.11789
0.145	2.04974	0.24932	0.12163
0.13	2.06238	0.24812	0.12031
0.115	2.08836	0.25362	0.12144
0.1	2.1074	0.26018	0.12346
0.09	2.11557	0.25723	0.12159
0.08	2.11235	0.25397	0.12023
0.07	2.09876	0.27006	0.12868
0.065	2.07839	0.26628	0.12812
0.06	2.05658	0.26261	0.12769
0.055	1.98789	0.26763	0.13463
0.052	1.94185	0.25824	0.13298
0.049	1.89917	0.25174	0.13255
0.046	1.82568	0.25001	0.13694
0.043	1.73396	0.23328	0.13454
0.04	1.63432	0.23762	0.14539
0.039	1.59232	0.23245	0.14598
0.038	1.55271	0.20372	0.1312
0.037	1.50187	0.19472	0.12965
0.036	1.44797	0.18974	0.13104

Table 31 Continued

0.035	1.38838	0.17759	0.12791
0.034	1.34574	0.16919	0.12572
0.033	1.2863	0.1646	0.12797
0.032	1.23475	0.15511	0.12562
0.031	1.16819	0.144	0.12327
0.03	1.10884	0.13821	0.12464
0.029	1.04888	0.12419	0.11841
0.028	0.97435	0.11194	0.11489
0.027	0.9119	0.09939	0.10899
0.026	0.8408	0.08808	0.10475
0.025	0.76753	0.07432	0.09684
0.024	0.71324	0.05988	0.08395
0.023	0.68899	0.04607	0.06687

Table 32. Mock Derivative Aero-Combustor with Spool flow properties for Re_D 125,000.

Item	Value	Units
File Name	BACSR2Y2	
Reynolds D	129680.8	
Temperature air	297.97	K
Pressure in	98505.44	Pa,
Pressure Drop	61.5207	Pa,
Velocity	5.087186	m/s

Table 33. Mock Derivative Aero-Combustor with Spool profile measurements for Re_D 125,000.

Y (inch)	U (m/s)	u' (m/s)	Tu
0.3	3.96319	0.43001	0.1085
0.27	3.97748	0.42805	0.10762
0.24	4.01552	0.43896	0.10932
0.21	4.0745	0.44919	0.11024
0.185	4.12593	0.44296	0.10736
0.165	4.19556	0.44799	0.10678
0.145	4.23391	0.45061	0.10643
0.13	4.2987	0.45755	0.10644
0.115	4.345	0.46685	0.10745

Table 33 Continued

0.1	4.37963	0.48449	0.11062

0.09	4.42048	0.48657	0.11007
0.08	4.41656	0.4823	0.1092
0.07	4.40922	0.48976	0.11108
0.065	4.40726	0.50182	0.11386
0.06	4.38875	0.50596	0.11529
0.055	4.31025	0.5069	0.1176
0.052	4.2519	0.50259	0.1182
0.049	4.18621	0.51005	0.12184
0.043	3.97171	0.50146	0.12626
0.04	3.79215	0.49356	0.13015
0.039	3.71313	0.47665	0.12837
0.038	3.61872	0.46926	0.12968
0.037	3.52327	0.45329	0.12866
0.036	3.42438	0.43371	0.12665
0.035	3.31963	0.43053	0.12969
0.034	3.18234	0.41197	0.12945
0.033	3.04257	0.39581	0.13009
0.032	2.87719	0.41504	0.14425
0.031	2.71575	0.37081	0.13654
0.03	2.54461	0.33107	0.13011
0.029	2.34436	0.29369	0.12528
0.028	2.11722	0.25885	0.12226
0.027	1.89628	0.21951	0.11576
0.026	1.65356	0.1858	0.11237
0.025	1.39387	0.15158	0.10875
0.024	1.26254	0.1311	0.10384

Table 34. Mock Derivative Aero-Combustor with Spool flow properties for Re_D 250,000.

Item	Value	Units
File Name	BACSR3Y1	
Reynolds D	252179.5	
Temperature air	300.1249	K
Pressure in	98505.44	Pa,
Pressure Drop	237.0901	Pa,
Velocity	10.0196	m/s

Table 35. Mock Derivative Aero-Combustor with Spool profile measurements for Re_D 250,000.

Y (inch)	U (m/s)	u' (m/s)	Tu

0.3	8.09607	0.88272	0.10903
0.27	8.21776	0.91324	0.11113
0.24	8.28668	0.89656	0.10819
0.21	8.3938	0.91431	0.10893
0.185	8.53729	0.92033	0.1078
0.165	8.64889	0.94182	0.10889
0.145	8.75334	0.93467	0.10678
0.13	8.91048	0.96234	0.108
0.115	9.00575	0.97718	0.10851
0.1	9.12778	0.97104	0.10638
0.09	9.17898	0.98897	0.10774
0.08	9.21374	0.99143	0.1076
0.07	9.29837	0.99586	0.1071
0.065	9.2646	1.03424	0.11163
0.06	9.27802	1.05066	0.11324
0.055	9.24386	1.04218	0.11274
0.052	9.21891	1.03614	0.11239
0.049	9.1505	1.05548	0.11535
0.043	8.85996	1.05378	0.11894
0.04	8.63702	1.05304	0.12192
0.039	8.56084	1.05136	0.12281
0.038	8.44345	1.04906	0.12425
0.037	8.26458	1.04131	0.126
0.036	8.10457	1.03555	0.12777
0.035	7.92654	1.00651	0.12698
0.034	7.76955	0.98072	0.12623
0.033	7.52322	0.94449	0.12554
0.032	7.28442	0.92784	0.12737
0.031	6.98985	0.88922	0.12722
0.03	6.6425	0.8655	0.1303
0.029	6.23939	0.80135	0.12843
0.028	5.78067	0.73758	0.12759
0.027	5.21266	0.65753	0.12614
0.026	4.57983	0.5339	0.11658
0.025	3.8664	0.42891	0.11093
0.024	3.40519	0.37146	0.10909
0.023	7.52574	1.21303	0.16118
0.022	7.38549	1.22284	0.16557

Table 35 Continued

0.021	7.2009	1.19837	0.16642
0.02	6.98767	1.16241	0.16635

0.019	6.7443	1.12292	0.1665
0.018	6.51478	1.0916	0.16756
0.017	6.19295	1.06228	0.17153
0.016	5.82578	0.98604	0.16926
0.015	5.4181	0.90811	0.16761
0.014	4.98132	0.81539	0.16369
0.013	4.50351	0.72459	0.1609
0.012	3.97291	0.61484	0.15476
0.011	3.38602	0.50301	0.14856
0.01	3.07126	0.43872	0.14285
0.01	0.85528	0.13227	0.15465
0.009	0.78128	0.11527	0.14754
0.008	0.71323	0.09769	0.13696

Table 36. Mock Derivative Aero-Combustor with Spool flow properties for Re_D 500,000.

Item	Value	Units
File Name	BACSR4Y1	
Reynolds D	499055.7	
Temperature air	302.3945	K
Pressure in	98843.95	Pa,
Pressure Drop	945.6014	Pa,
Velocity	20.02563	m/s

Table 37. Mock Derivative Aero-Combustor with Spool profile measurement for Re_D 500,000.

Y (inch)	U (m/s)	u' (m/s)	Tu
0.3	17.33543	1.77508	0.1024
0.27	17.42514	1.8037	0.10351
0.24	17.62797	1.77049	0.10044
0.21	17.83873	1.80088	0.10095
0.185	18.00492	1.80726	0.10038
0.165	18.32465	1.81442	0.09902
0.145	18.56676	1.82969	0.09855
0.13	18.77773	1.84536	0.09827

Table 37 Continued

0.115	18.9731	1.87607	0.09888
0.1	19.20913	1.87773	0.09775
0.09	19.33398	1.9252	0.09958

0.08	19.47796	1.90361	0.09773
0.07	19.55146	1.95732	0.10011
0.065	19.63071	1.96647	0.10017
0.06	19.57309	1.94893	0.09957
0.055	19.66447	1.96542	0.09995
0.052	19.56549	1.99571	0.102
0.049	19.55218	2.02949	0.1038
0.046	19.42438	2.03599	0.10482
0.043	19.31862	2.09256	0.10832
0.04	19.08691	2.05996	0.10793
0.039	18.96626	2.05124	0.10815
0.038	18.85918	2.0466	0.10852
0.037	18.70795	2.06031	0.11013
0.036	18.54908	2.01626	0.1087
0.035	18.44215	2.07436	0.11248
0.034	18.15705	2.05573	0.11322
0.033	17.89846	1.99551	0.11149
0.032	17.62172	2.05396	0.11656
0.031	17.22308	2.02802	0.11775
0.03	16.78231	1.99788	0.11905
0.029	16.21855	1.97095	0.12152
0.028	15.62772	1.91457	0.12251
0.027	14.80764	1.83791	0.12412
0.026	13.80385	1.75598	0.12721
0.025	12.35968	1.54387	0.12491
0.024	10.6642	1.33068	0.12478
0.023	9.27255	1.09551	0.11815
0.022	8.48417	0.98288	0.11585
0.0265	19.02669	2.71534	0.14271
0.0255	18.9156	2.73918	0.14481
0.0245	18.87562	2.75607	0.14601
0.0235	18.82285	2.73191	0.14514
0.0225	18.76383	2.77487	0.14788
0.0215	18.6589	2.75675	0.14774
0.0205	18.5176	2.74736	0.14837
0.0195	18.48999	2.73796	0.14808
0.0185	18.33304	2.73749	0.14932

Table 37 Continued.

0.0175	18.17713	2.75036	0.15131
0.0165	17.9997	2.68571	0.14921
0.0155	17.8372	2.70589	0.1517

0.0145	17.57764	2.69027	0.15305
0.0135	17.35319	2.65277	0.15287
0.0125	16.99776	2.60995	0.15355
0.0115	16.62006	2.58898	0.15577
0.0105	16.14104	2.47358	0.15325
0.0095	15.55073	2.50885	0.16133
0.0085	14.87716	2.40411	0.1616
0.0075	13.89593	2.2463	0.16165
0.0065	12.65093	2.06346	0.16311
0.0055	10.98308	1.78133	0.16219
0.0045	9.63601	1.52411	0.15817

Table 38. Small Grid at Near Position flow properties for Re_D 62,500.

Item	Value	Units
File Name	BGS1R1Y3	
Reynolds D	64520.01	
Temperature air	301.9459	K
Pressure in	99013.2	Pa,
Pressure Drop	15.66632	Pa,
Velocity	2.577796	m/s

Table 39. Small Grid at Near Position profile measurements for Re_D 62,500.

Y (inch)	U (m/s)	u' (m/s)	Tu
0.3	2.13982	0.10966	0.05124
0.27	2.15265	0.11069	0.05142
0.24	2.17481	0.11231	0.05164
0.21	2.19685	0.11305	0.05146
0.185	2.22461	0.11528	0.05182
0.165	2.24792	0.1166	0.05187
0.145	2.27479	0.11715	0.0515
0.13	2.29638	0.12484	0.05436
0.115	2.32904	0.12195	0.05236
0.1	2.34652	0.13051	0.05562
0.09	2.35889	0.13257	0.0562

Table 39 Continued.

0.08	2.38058	0.13511	0.05676
0.07	2.3888	0.14383	0.06021
0.065	2.38745	0.14959	0.06266

0.06	2.38066	0.15295	0.06425
0.055	2.38319	0.15433	0.06476
0.052	2.36911	0.16158	0.0682
0.049	2.36566	0.16437	0.06948
0.046	2.34626	0.16444	0.07009
0.043	2.32368	0.16983	0.07309
0.04	2.3008	0.17443	0.07581
0.039	2.28926	0.17284	0.0755
0.038	2.27853	0.1765	0.07746
0.037	2.26886	0.17437	0.07685
0.036	2.24917	0.17531	0.07794
0.035	2.23993	0.17949	0.08013
0.034	2.22808	0.17688	0.07939
0.033	2.21156	0.17992	0.08136
0.032	2.19419	0.1793	0.08172
0.031	2.18113	0.17835	0.08177
0.03	2.15439	0.17784	0.08255
0.029	2.13555	0.17835	0.08352
0.028	2.11426	0.17756	0.08398
0.027	2.08302	0.17615	0.08456
0.026	2.05196	0.17543	0.0855
0.025	2.01836	0.17127	0.08486
0.024	1.98226	0.17263	0.08709
0.023	1.9336	0.17043	0.08814
0.022	1.89369	0.1628	0.08597
0.021	1.8384	0.16311	0.08873
0.02	1.78624	0.15597	0.08732
0.019	1.73729	0.14652	0.08434
0.018	1.67701	0.14448	0.08615
0.017	1.6119	0.13845	0.08589
0.016	1.55053	0.1297	0.08365
0.015	1.47807	0.12326	0.08339
0.014	1.40279	0.11288	0.08047
0.013	1.32612	0.10532	0.07942
0.012	1.24736	0.09721	0.07794
0.011	1.16904	0.08783	0.07513
0.01	1.08208	0.08004	0.07397

Table 39 Continued.

0.009	0.99432	0.07214	0.07255
0.008	0.90547	0.06458	0.07132
0.007	0.82014	0.05536	0.0675

0.006	0.74423	0.04454	0.05984
0.005	0.70786	0.03634	0.05134

Table 40. Small Grid at Near Position flow properties for Re_D 125,000.

Item	Value	Units
File Name	BGS1R2Y3	
Reynolds D	126489.3	
Temperature air	302.4451	K
Pressure in	99013.2	Pa,
Pressure Drop	60.47496	Pa,
Velocity	5.068465	m/s

Table 41. Small Grid at Near Position profile measurements for Re_D 125,000.

Y (inch)	U (m/s)	u' (m/s)	Tu
0.3	4.27359	0.26986	0.06315
0.27	4.35034	0.27012	0.06209
0.24	4.39506	0.273	0.06211
0.21	4.43863	0.27538	0.06204
0.185	4.49141	0.27731	0.06174
0.165	4.54532	0.27806	0.06118
0.145	4.60129	0.28051	0.06096
0.13	4.64506	0.28794	0.06199
0.115	4.70273	0.29156	0.062
0.1	4.75821	0.29726	0.06247
0.09	4.79168	0.30215	0.06306
0.08	4.83046	0.31067	0.06431
0.07	4.86002	0.3276	0.06741
0.065	4.87746	0.32874	0.0674
0.06	4.8865	0.3349	0.06854
0.055	4.89081	0.3421	0.06995
0.052	4.88137	0.34983	0.07167
0.049	4.881	0.36424	0.07462
0.046	4.84566	0.35868	0.07402
0.043	4.8304	0.37237	0.07709

Table 41 Continued

0.04	4.80573	0.37264	0.07754
0.039	4.79745	0.37789	0.07877
0.038	4.79845	0.39368	0.08204

0.037	4.77242	0.38352	0.08036
0.036	4.76888	0.39012	0.08181
0.035	4.74165	0.39464	0.08323
0.034	4.72417	0.39904	0.08447
0.033	4.71064	0.3951	0.08387
0.032	4.68734	0.40185	0.08573
0.031	4.6477	0.39816	0.08567
0.03	4.61684	0.4083	0.08844
0.029	4.58484	0.40685	0.08874
0.028	4.55069	0.40873	0.08982
0.027	4.51209	0.4115	0.0912
0.026	4.43725	0.40882	0.09213
0.025	4.38337	0.4074	0.09294
0.024	4.30542	0.4095	0.09511
0.023	4.22426	0.402	0.09516
0.022	4.13964	0.39393	0.09516
0.021	4.03727	0.38885	0.09631
0.02	3.93454	0.38188	0.09706
0.019	3.81678	0.37054	0.09708
0.018	3.68605	0.35959	0.09755
0.017	3.54698	0.34597	0.09754
0.016	3.40065	0.3268	0.0961
0.015	3.22613	0.31051	0.09625
0.014	3.05549	0.27979	0.09157
0.013	2.86083	0.25552	0.08932
0.012	2.66672	0.22627	0.08485
0.011	2.46351	0.19814	0.08043
0.01	2.26071	0.17525	0.07752
0.009	2.03972	0.14915	0.07312
0.008	1.78542	0.12355	0.0692
0.007	1.58993	0.10458	0.06577
0.0466852	3.3256	0.58246	0.17514
0.0441452	3.22282	0.57994	0.17995
0.0416052	3.13075	0.55892	0.17853
0.0390652	3.01455	0.54021	0.1792
0.0365252	2.89172	0.51155	0.1769
0.0339852	2.75483	0.49096	0.17822

Table 41 Continued

0.0314452	2.60413	0.45652	0.17531
0.0289052	2.45584	0.42898	0.17468
0.0263652	2.29301	0.39245	0.17115

0.0238252	2.10504	0.34575	0.16425
0.0212852	1.92612	0.30522	0.15846
0.0187452	1.73831	0.26173	0.15056
0.0162052	1.52086	0.22114	0.14541
0.0136652	1.29627	0.17395	0.13419
0.012446	1.18432	0.14575	0.12306

Table 42. Small Grid at Near Position flow properties for Re_D 250,000.

Item	Value	Units
File Name	BGS1R3Y3	
Reynolds D	250697.4	
Temperature air	302.386	K
Pressure in	99013.2	Pa,
Pressure Drop	237.5906	Pa,
Velocity	10.04205	m/s

Table 43. Small Grid at Near Position profile measurements for Re_D 250,000.

Y (inch)	U (m/s)	u' (m/s)	Tu
0.3	8.8612	0.57477	0.06486
0.27	8.93087	0.57673	0.06458
0.24	9.00456	0.57425	0.06377
0.21	9.09878	0.59042	0.06489
0.185	9.21124	0.5791	0.06287
0.165	9.33922	0.5911	0.06329
0.145	9.445	0.59353	0.06284
0.13	9.54605	0.59446	0.06227
0.115	9.67809	0.60915	0.06294
0.1	9.78619	0.61404	0.06275
0.09	9.86018	0.621	0.06298
0.08	9.95595	0.63391	0.06367
0.07	10.02889	0.64447	0.06426
0.065	10.08149	0.6583	0.0653
0.06	10.1229	0.64969	0.06418
0.055	10.13765	0.66797	0.06589

Table 43 Continued

0.052	10.13918	0.69143	0.06819
0.049	10.15834	0.68694	0.06762
0.046	10.17037	0.69953	0.06878

0.043	10.1608	0.71967	0.07083
0.04	10.13274	0.73287	0.07233
0.039	10.13428	0.74145	0.07316
0.038	10.10874	0.74246	0.07345
0.037	10.09048	0.74988	0.07432
0.036	10.08375	0.74691	0.07407
0.035	10.07809	0.75707	0.07512
0.034	10.06858	0.758	0.07528
0.033	10.04842	0.77111	0.07674
0.032	10.00481	0.77101	0.07706
0.031	9.97025	0.78109	0.07834
0.03	9.95058	0.77239	0.07762
0.029	9.94176	0.78751	0.07921
0.028	9.87372	0.79113	0.08012
0.027	9.82903	0.7989	0.08128
0.026	9.80182	0.81752	0.08341
0.025	9.71296	0.82502	0.08494
0.024	9.63539	0.81593	0.08468
0.023	9.55009	0.83047	0.08696
0.022	9.46268	0.84221	0.089
0.021	9.34275	0.8392	0.08982
0.02	9.22051	0.84166	0.09128
0.019	9.07313	0.84616	0.09326
0.018	8.87868	0.8562	0.09643
0.017	8.68026	0.82537	0.09509
0.016	8.44193	0.83825	0.0993
0.015	8.17125	0.80964	0.09908
0.014	7.80809	0.78789	0.10091
0.013	7.41144	0.75501	0.10187
0.012	6.93616	0.69711	0.1005
0.011	6.42831	0.6603	0.10272
0.01	5.98914	0.59267	0.09896
0.009	5.45435	0.51091	0.09367
0.008	4.97527	0.4408	0.0886
0.007	4.31404	0.3528	0.08178
0.006	3.84785	0.29831	0.07753
0.005	3.57835	0.26203	0.07323

Table 44. Small Grid at Near Position property measurements for Re_D 500,000.

Item	Value	Units
File name	BGS1R4Y3	
Reynolds D	494290.8	

Temperature air	304.0224	K
Pressure in	99013.2	Pa,
Pressure Drop	938.7026	Pa,
Velocity	19.98927	m/s

Table 45. Small Grid at Near Position profile measurement for Re_D 500,000.

Y (inch)	U (m/s)	u' (m/s)	Tu
0.3	18.65775	1.11907	0.05998
0.27	18.77729	1.1217	0.05974
0.24	18.9913	1.13057	0.05953
0.21	19.17708	1.1197	0.05839
0.185	19.405	1.10682	0.05704
0.165	19.57822	1.12171	0.05729
0.145	19.83163	1.14895	0.05794
0.13	20.07506	1.14395	0.05698
0.115	20.32646	1.16057	0.0571
0.1	20.60739	1.14907	0.05576
0.09	20.78892	1.16921	0.05624
0.08	20.94244	1.17252	0.05599
0.07	21.11821	1.20896	0.05725
0.065	21.15675	1.20431	0.05692
0.06	21.24127	1.22439	0.05764
0.055	21.3518	1.25606	0.05883
0.052	21.38524	1.24987	0.05845
0.049	21.42147	1.27127	0.05935
0.046	21.41607	1.29651	0.06054
0.043	21.45848	1.29006	0.06012
0.04	21.48866	1.32412	0.06162
0.039	21.46617	1.34361	0.06259
0.038	21.55091	1.33704	0.06204
0.037	21.49192	1.34067	0.06238
0.036	21.50072	1.34631	0.06262
0.035	21.48597	1.35567	0.0631
0.034	21.45358	1.35033	0.06294
0.033	21.45989	1.35922	0.06334

Table 45 Continued.

0.032	21.42766	1.38233	0.06451
0.031	21.40888	1.38725	0.0648
0.03	21.42549	1.38588	0.06468
0.029	21.38509	1.42043	0.06642

0.028	21.40315	1.41255	0.066
0.027	21.36145	1.43483	0.06717
0.026	21.29323	1.45335	0.06825
0.025	21.26143	1.47461	0.06936
0.024	21.18994	1.48421	0.07004
0.023	21.13327	1.49158	0.07058
0.022	20.98906	1.49088	0.07103
0.021	20.90568	1.53002	0.07319
0.02	20.82988	1.5511	0.07446
0.019	20.73698	1.54521	0.07451
0.018	20.57322	1.57349	0.07648
0.017	20.39216	1.57178	0.07708
0.016	20.19775	1.60978	0.0797
0.015	19.93414	1.63413	0.08198
0.014	19.61531	1.65599	0.08442
0.013	19.18883	1.67798	0.08745
0.012	18.7187	1.65826	0.08859
0.011	18.1461	1.67596	0.09236
0.01	17.48776	1.66589	0.09526
0.009	16.62667	1.58001	0.09503
0.008	15.6707	1.53143	0.09773
0.007	14.49729	1.4164	0.0977
0.006	13.1056	1.24977	0.09536
0.005	11.57193	1.05025	0.09076
0.004	10.63067	0.96227	0.09052

Table 46. Small Grid at Far Position flow properties for Re_D 62,500.

Item	Value	Units
File Name	BGS2R2Y1	
Reynolds D	129570.2	
Temperature air	298.8134	K
Pressure in	98505.44	Pa,
Pressure Drop	61.85845	Pa,
Velocity	5.108343	m/s

Table 47. Small Grid at Far Position profile measurement for Re_D 62,500.

Y (inch)	U (m/s)	u' (m/s)	Tu
0.3	3.65469	0.11788	0.03225
0.27	3.68615	0.1208	0.03277
0.24	3.72274	0.11922	0.03202
0.21	3.78408	0.12417	0.03281
0.185	3.84221	0.12218	0.0318
0.165	3.89448	0.12373	0.03177
0.145	3.96127	0.12571	0.03174
0.13	4.00681	0.13238	0.03304
0.115	4.06388	0.13132	0.03231
0.1	4.12731	0.13704	0.0332
0.09	4.16911	0.13499	0.03238
0.08	4.21615	0.14548	0.0345
0.07	4.28195	0.15249	0.03561
0.065	4.29203	0.15701	0.03658
0.06	4.31823	0.16196	0.03751
0.055	4.33601	0.17245	0.03977
0.052	4.33092	0.17715	0.0409
0.049	4.32912	0.18471	0.04267
0.046	4.33416	0.19813	0.04571
0.043	4.32723	0.20151	0.04657
0.04	4.30795	0.21633	0.05022
0.039	4.29863	0.22102	0.05142
0.038	4.2968	0.22084	0.0514
0.037	4.28911	0.22604	0.0527
0.036	4.26004	0.23119	0.05427
0.035	4.24881	0.23412	0.0551
0.034	4.22155	0.23887	0.05658
0.033	4.20729	0.24417	0.05803

Table 47 Continued.

0.032	4.18838	0.24705	0.05898
0.031	4.15502	0.24919	0.05997
0.03	4.12076	0.26081	0.06329
0.029	4.08232	0.25485	0.06243
0.028	4.03533	0.26356	0.06531
0.027	3.98663	0.26257	0.06586
0.026	3.9293	0.263	0.06693
0.025	3.87576	0.2569	0.06628
0.024	3.80298	0.25902	0.06811
0.023	3.72664	0.25767	0.06914
0.022	3.63404	0.25515	0.07021
0.021	3.54022	0.25244	0.07131
0.02	3.4436	0.23927	0.06948
0.019	3.31197	0.23432	0.07075
0.018	3.1848	0.21902	0.06877
0.017	3.06798	0.20138	0.06564
0.016	2.90738	0.18872	0.06491
0.015	2.75214	0.17388	0.06318
0.014	2.57077	0.15782	0.06139
0.013	2.38942	0.13654	0.05714
0.012	2.2053	0.12408	0.05626
0.011	2.0046	0.10242	0.05109
0.01	1.78543	0.08557	0.04792
0.009	1.52824	0.06683	0.04373
0.008	1.36645	0.0586	0.04289

Table 48. Small Grid at Far Position flow properties for Re_D 125,000.

Item	Value	Units
File Name	BGS2R2Y1	
Reynolds D	129570.2	
Temperature air	298.8134	K
Pressure in	98505.44	Pa,
Pressure Drop	61.85845	Pa,
Velocity	5.108343	m/s

Table 49. Small Grid at Far Position profile measurement for Re_D 125,000.

Y (inch)	U (m/s)	u' (m/s)	Tu
0.3	3.65469	0.11788	0.03225
0.27	3.68615	0.1208	0.03277
0.24	3.72274	0.11922	0.03202
0.21	3.78408	0.12417	0.03281
0.185	3.84221	0.12218	0.0318
0.165	3.89448	0.12373	0.03177
0.145	3.96127	0.12571	0.03174
0.13	4.00681	0.13238	0.03304
0.115	4.06388	0.13132	0.03231
0.1	4.12731	0.13704	0.0332
0.09	4.16911	0.13499	0.03238
0.08	4.21615	0.14548	0.0345
0.07	4.28195	0.15249	0.03561
0.065	4.29203	0.15701	0.03658
0.06	4.31823	0.16196	0.03751
0.055	4.33601	0.17245	0.03977
0.052	4.33092	0.17715	0.0409
0.049	4.32912	0.18471	0.04267
0.046	4.33416	0.19813	0.04571
0.043	4.32723	0.20151	0.04657
0.04	4.30795	0.21633	0.05022
0.039	4.29863	0.22102	0.05142
0.038	4.2968	0.22084	0.0514
0.037	4.28911	0.22604	0.0527
0.036	4.26004	0.23119	0.05427
0.035	4.24881	0.23412	0.0551
0.034	4.22155	0.23887	0.05658
0.033	4.20729	0.24417	0.05803
0.032	4.18838	0.24705	0.05898
0.031	4.15502	0.24919	0.05997
0.03	4.12076	0.26081	0.06329
0.029	4.08232	0.25485	0.06243
0.028	4.03533	0.26356	0.06531
0.027	3.98663	0.26257	0.06586
0.026	3.9293	0.263	0.06693
0.025	3.87576	0.2569	0.06628
0.024	3.80298	0.25902	0.06811
0.023	3.72664	0.25767	0.06914
0.022	3.63404	0.25515	0.07021

Table 49 Continued.

0.021	3.54022	0.25244	0.07131
0.02	3.4436	0.23927	0.06948
0.019	3.31197	0.23432	0.07075
0.018	3.1848	0.21902	0.06877
0.017	3.06798	0.20138	0.06564
0.016	2.90738	0.18872	0.06491
0.015	2.75214	0.17388	0.06318
0.014	2.57077	0.15782	0.06139
0.013	2.38942	0.13654	0.05714
0.012	2.2053	0.12408	0.05626
0.011	2.0046	0.10242	0.05109
0.01	1.78543	0.08557	0.04792
0.009	1.52824	0.06683	0.04373
0.008	1.36645	0.0586	0.04289

Table 50. Small Grid at Near Position flow properties for Re_D 250,000.

Item	Value	Units
File Name	BGS2R3Y1	
Reynolds D	252448.9	
Temperature air	298.8305	K
Pressure in	98505.44	Pa,
Pressure Drop	235.0018	Pa,
Velocity	9.95388	m/s

Table 51. Small Grid at Far Position profile measurement for Re_D 250,000.

Y (inch)	U (m/s)	u' (m/s)	Tu
0.3	7.78883	0.28332	0.03638
0.27	7.85351	0.28227	0.03594
0.24	7.97063	0.28948	0.03632
0.21	8.07169	0.28615	0.03545
0.185	8.19866	0.29221	0.03564
0.165	8.33922	0.29069	0.03486
0.145	8.45409	0.29642	0.03506
0.13	8.58054	0.29418	0.03428
0.115	8.71968	0.30092	0.03451
0.1	8.85569	0.30556	0.0345
0.09	8.9523	0.30693	0.03428

Table 51 Continued.

0.08	9.0511	0.30979	0.03423
0.07	9.17566	0.32369	0.03528
0.065	9.22722	0.32845	0.0356
0.06	9.25865	0.33547	0.03623
0.055	9.31938	0.34293	0.0368
0.052	9.35671	0.34699	0.03708
0.049	9.37751	0.36043	0.03844
0.046	9.41518	0.37382	0.0397
0.043	9.40925	0.39214	0.04168
0.04	9.41904	0.39615	0.04206
0.039	9.40897	0.40376	0.04291
0.038	9.42056	0.40144	0.04261
0.037	9.42832	0.4228	0.04484
0.036	9.41683	0.42701	0.04535
0.035	9.43237	0.4289	0.04547
0.034	9.41141	0.43199	0.0459
0.033	9.42576	0.43504	0.04615
0.032	9.3824	0.45561	0.04856
0.031	9.34886	0.47449	0.05075
0.03	9.32954	0.47458	0.05087
0.029	9.30752	0.49223	0.05289
0.028	9.24908	0.5064	0.05475
0.027	9.18806	0.51824	0.0564
0.026	9.13816	0.54013	0.05911
0.025	9.05056	0.54647	0.06038
0.024	8.95208	0.56194	0.06277
0.023	8.87093	0.56134	0.06328
0.022	8.7506	0.58066	0.06636
0.021	8.60439	0.59027	0.0686
0.02	8.46647	0.59658	0.07046
0.019	8.29652	0.5994	0.07225
0.018	8.05641	0.6009	0.07459
0.017	7.84302	0.58356	0.07441
0.016	7.57157	0.56244	0.07428
0.015	7.25138	0.54799	0.07557
0.014	6.92254	0.52522	0.07587
0.013	6.55561	0.48704	0.07429
0.012	6.1576	0.44296	0.07194
0.011	5.65706	0.38657	0.06833
0.01	5.13582	0.32253	0.0628

Table 51 Continued.

0.009	4.54753	0.26539	0.05836
0.008	3.94939	0.20795	0.05265
0.007	3.56925	0.18319	0.05132

Table 52. Small Grid at Far Position flow properties for Re_D 500,000.

Item	Value	Units
File Name	BGS2R4Y5	
Reynolds D	489151.3	
Temperature air	304.6336	K
Pressure in	98674.7	Pa,
Pressure Drop	927.1138	Pa,
Velocity	19.91984	m/s

Table 53. Small Grid at Far Position profile measurements for Re_D 500,000.

Y (inch)	U (m/s)	u' (m/s)	Tu
0.3	17.74102	0.56119	0.03163
0.27	17.85771	0.5759	0.03225
0.24	18.05225	0.57651	0.03194
0.21	18.26363	0.59687	0.03268
0.185	18.48979	0.59858	0.03237
0.165	18.73291	0.61168	0.03265
0.145	18.9351	0.60469	0.03193
0.13	19.17094	0.60691	0.03166
0.115	19.42974	0.62671	0.03226
0.1	19.69983	0.64083	0.03253
0.09	19.87957	0.63544	0.03196
0.08	20.01245	0.64931	0.03245
0.07	20.19597	0.66663	0.03301
0.065	20.31476	0.68046	0.0335
0.06	20.32851	0.68515	0.0337
0.055	20.42225	0.69608	0.03408
0.052	20.46458	0.71419	0.0349
0.049	20.48662	0.70872	0.03459
0.046	20.53032	0.72778	0.03545
0.043	20.52107	0.74201	0.03616
0.04	20.49144	0.75781	0.03698
0.039	20.53829	0.75076	0.03655

Table 53 Continued.

0.038	20.53661	0.79219	0.03857
0.037	20.53907	0.78698	0.03832
0.036	20.51811	0.80822	0.03939
0.035	20.52216	0.80114	0.03904
0.034	20.47377	0.79985	0.03907
0.033	20.4659	0.83284	0.04069
0.032	20.4651	0.82545	0.04033
0.031	20.43339	0.8378	0.041
0.03	20.41905	0.84778	0.04152
0.029	20.3784	0.87124	0.04275
0.028	20.34166	0.9048	0.04448
0.027	20.29119	0.92641	0.04566
0.026	20.22357	0.94913	0.04693
0.025	20.12279	0.96813	0.04811
0.024	20.00527	1.0005	0.05001
0.023	19.84598	1.06187	0.05351
0.022	19.70765	1.08968	0.05529
0.021	19.47957	1.12316	0.05766
0.02	19.19979	1.16343	0.0606
0.019	18.93651	1.18172	0.0624
0.018	18.5646	1.21865	0.06564
0.017	18.11816	1.26838	0.07001
0.016	17.55996	1.24894	0.07112
0.015	16.9115	1.25657	0.0743
0.014	16.10938	1.22764	0.07621
0.013	15.1523	1.17074	0.07726
0.012	14.08729	1.10277	0.07828
0.011	12.84527	0.97779	0.07612
0.01	11.48907	0.86708	0.07547
0.009	10.4341	0.73662	0.0706

Table 54. Large Grid flow properties for Re_D 62,500.

Item	Value	Units
File Name	BGR1R1Y3	
Reynolds D	63855.3	
Temperature air	301.5972	K
Pressure in	99351.71	Pa,
Pressure Drop	15.24813	Pa,
Velocity	2.537358	m/s

Table 55. Large Grid profile measurements for Re_D 62,500.

Y (inch)	U (m/s)	u' (m/s)	Tu
0.3	2.07287	0.13471	0.06499
0.27	2.08906	0.13703	0.06559
0.24	2.10462	0.13712	0.06515
0.21	2.11952	0.13748	0.06486
0.185	2.13925	0.13242	0.0619
0.165	2.16855	0.13754	0.06342
0.145	2.18417	0.13671	0.06259
0.13	2.20322	0.14122	0.0641
0.115	2.23278	0.14364	0.06433
0.1	2.25054	0.14592	0.06484
0.09	2.25679	0.15136	0.06707
0.08	2.27414	0.15618	0.06868
0.07	2.27933	0.16279	0.07142
0.065	2.28556	0.16906	0.07397
0.06	2.2843	0.16765	0.07339
0.055	2.28165	0.17675	0.07747
0.052	2.27121	0.17461	0.07688
0.049	2.26886	0.18291	0.08062
0.046	2.25927	0.18497	0.08187
0.043	2.24756	0.18704	0.08322
0.04	2.22875	0.19255	0.08639
0.039	2.22681	0.18943	0.08507
0.038	2.21932	0.19125	0.08617
0.037	2.22015	0.19318	0.08701
0.036	2.21374	0.19297	0.08717
0.035	2.20719	0.19696	0.08923
0.034	2.19478	0.19626	0.08942
0.033	2.18782	0.1956	0.08941

0.032	2.16613	0.19873	0.09175
0.031	2.1562	0.19966	0.0926
0.03	2.15278	0.19806	0.092
0.029	2.13149	0.19574	0.09183
0.028	2.11874	0.19854	0.09371
0.027	2.10345	0.20152	0.0958
0.026	2.08431	0.20437	0.09805
0.025	2.06335	0.20028	0.09707
0.024	2.0384	0.19962	0.09793
0.023	2.02758	0.19769	0.0975
0.022	1.99082	0.19704	0.09898
0.021	1.97068	0.19623	0.09957
0.02	1.94111	0.19845	0.10224
0.019	1.90006	0.19332	0.10174
0.018	1.87127	0.1861	0.09945
0.017	1.82111	0.18224	0.10007
0.016	1.77524	0.17767	0.10008
0.015	1.7348	0.17524	0.10101
0.014	1.67148	0.16546	0.09899
0.013	1.62189	0.16072	0.09909
0.012	1.5626	0.15198	0.09726
0.011	1.4993	0.14478	0.09656
0.01	1.43786	0.13643	0.09488
0.009	1.37036	0.13065	0.09534
0.008	1.30123	0.11656	0.08958
0.007	1.22907	0.1093	0.08893
0.006	1.14801	0.10283	0.08957
0.005	1.07102	0.09262	0.08648
0.004	0.99132	0.08367	0.0844
0.003	0.90804	0.07457	0.08212
0.002	0.82809	0.06472	0.07816
0.001	0.75049	0.05228	0.06966

Table 56. Large Grid flow properties for Re_D 125,000.

Item	Value	Units
File Name	BGR1R2Y3	
Reynolds D	127218.5	
Temperature air	300.916	K
Pressure in	99351.71	Pa,
Pressure Drop	60.18689	Pa,
Velocity	5.034986	m/s

Table 57. Large Grid property measurements for Re_D 125,000.

Y (inch)	U (m/s)	u' (m/s)	Tu
0.3	2.07287	0.13471	0.06499
0.27	2.08906	0.13703	0.06559
0.24	2.10462	0.13712	0.06515
0.21	2.11952	0.13748	0.06486
0.185	2.13925	0.13242	0.0619
0.165	2.16855	0.13754	0.06342
0.145	2.18417	0.13671	0.06259
0.13	2.20322	0.14122	0.0641
0.115	2.23278	0.14364	0.06433
0.1	2.25054	0.14592	0.06484
0.09	2.25679	0.15136	0.06707
0.08	2.27414	0.15618	0.06868
0.07	2.27933	0.16279	0.07142
0.065	2.28556	0.16906	0.07397
0.06	2.2843	0.16765	0.07339
0.055	2.28165	0.17675	0.07747
0.052	2.27121	0.17461	0.07688
0.049	2.26886	0.18291	0.08062
0.046	2.25927	0.18497	0.08187
0.043	2.24756	0.18704	0.08322
0.04	2.22875	0.19255	0.08639
0.039	2.22681	0.18943	0.08507
0.038	2.21932	0.19125	0.08617
0.037	2.22015	0.19318	0.08701
0.036	2.21374	0.19297	0.08717
0.035	2.20719	0.19696	0.08923
0.034	2.19478	0.19626	0.08942
0.033	2.18782	0.1956	0.08941

0.032	2.16613	0.19873	0.09175
0.031	2.1562	0.19966	0.0926
0.03	2.15278	0.19806	0.092
0.029	2.13149	0.19574	0.09183
0.028	2.11874	0.19854	0.09371
0.027	2.10345	0.20152	0.0958
0.026	2.08431	0.20437	0.09805
0.025	2.06335	0.20028	0.09707
0.024	2.0384	0.19962	0.09793
0.023	2.02758	0.19769	0.0975
0.022	1.99082	0.19704	0.09898
0.021	1.97068	0.19623	0.09957
0.02	1.94111	0.19845	0.10224
0.019	1.90006	0.19332	0.10174
0.018	1.87127	0.1861	0.09945
0.017	1.82111	0.18224	0.10007
0.016	1.77524	0.17767	0.10008
0.015	1.7348	0.17524	0.10101
0.014	1.67148	0.16546	0.09899
0.013	1.62189	0.16072	0.09909
0.012	1.5626	0.15198	0.09726
0.011	1.4993	0.14478	0.09656
0.01	1.43786	0.13643	0.09488
0.009	1.37036	0.13065	0.09534
0.008	1.30123	0.11656	0.08958
0.007	1.22907	0.1093	0.08893
0.006	1.14801	0.10283	0.08957
0.005	1.07102	0.09262	0.08648
0.004	0.99132	0.08367	0.0844
0.003	0.90804	0.07457	0.08212
0.002	0.82809	0.06472	0.07816
0.001	0.75049	0.05228	0.06966
0.0314452	2.60413	0.45652	0.17531
0.0289052	2.45584	0.42898	0.17468
0.0263652	2.29301	0.39245	0.17115
0.0238252	2.10504	0.34575	0.16425
0.0212852	1.92612	0.30522	0.15846
0.0187452	1.73831	0.26173	0.15056
0.0162052	1.52086	0.22114	0.14541
0.0136652	1.29627	0.17395	0.13419
0.012446	1.18432	0.14575	0.12306

Table 58. Large Grid flow properties for Re_D 250,000.

Item	Value	Units
File Name	BGR1R3Y3	
Reynolds D	251405.5	
Temperature air	302.8752	K
Pressure in	99351.71	Pa,
Pressure Drop	239.0989	Pa,
Velocity	10.06481	m/s

Table 59. Large Grid profile measurements for Re_D 250,000.

Y (inch)	U (m/s)	u' (m/s)	Tu
0.3	8.7191	0.67893	0.07787
0.27	8.78555	0.67921	0.07731
0.24	8.85363	0.68799	0.07771
0.21	8.95573	0.69183	0.07725
0.185	9.05416	0.68121	0.07524
0.165	9.15126	0.67644	0.07392
0.145	9.26321	0.69639	0.07518
0.13	9.34112	0.6865	0.07349
0.115	9.50731	0.70412	0.07406
0.1	9.63329	0.7105	0.07375
0.09	9.71232	0.71811	0.07394
0.08	9.76199	0.73087	0.07487
0.07	9.82608	0.73399	0.0747
0.065	9.88049	0.74482	0.07538
0.06	9.90715	0.75767	0.07648
0.055	9.90428	0.76019	0.07675
0.052	9.87298	0.77878	0.07888
0.049	9.86776	0.79285	0.08035
0.046	9.88326	0.79115	0.08005
0.043	9.86025	0.79946	0.08108
0.04	9.84362	0.82178	0.08348
0.039	9.82396	0.82872	0.08436
0.038	9.79933	0.82801	0.0845
0.037	9.79023	0.82396	0.08416
0.036	9.78586	0.84011	0.08585
0.035	9.74484	0.84688	0.08691
0.034	9.76019	0.84305	0.08638
0.033	9.74404	0.85689	0.08794

Table 59 Continued

0.032	9.6869	0.86542	0.08934
0.031	9.64332	0.85042	0.08819
0.03	9.58224	0.85395	0.08912
0.029	9.51243	0.85956	0.09036
0.028	9.46434	0.871	0.09203
0.027	9.48467	0.88644	0.09346
0.026	9.44839	0.88602	0.09377
0.025	9.39723	0.88798	0.09449
0.024	9.28887	0.91256	0.09824
0.023	9.17723	0.90724	0.09886
0.022	9.09695	0.91998	0.10113
0.021	8.93255	0.90807	0.10166
0.02	8.78514	0.92694	0.10551
0.019	8.57172	0.90622	0.10572
0.018	8.36618	0.90771	0.1085
0.017	8.14077	0.89186	0.10956
0.016	7.86935	0.86601	0.11005
0.015	7.51753	0.81852	0.10888
0.014	7.1655	0.79755	0.1113
0.013	6.72941	0.74148	0.11019
0.012	6.2693	0.69207	0.11039
0.011	5.7487	0.60951	0.10603
0.01	5.24279	0.51809	0.09882
0.009	4.64964	0.4335	0.09323
0.008	4.03151	0.34281	0.08503
0.007	3.61573	0.29589	0.08183

Table 60. Large Grid flow properties for Re_D 500,000.

Item	Value	Units
File Name	BGR1R4Y1	
Reynolds D	501578.6	
Temperature air	301.6854	K
Pressure in	99182.45	Pa,
Pressure Drop	946.267	Pa,
Velocity	19.97509	m/s

Table 61. Large Grid profile measurements for Re_D 500,000.

Y (inch)	U (m/s)	u' (m/s)	Tu
0.3	17.9087	1.57749	0.08808
0.27	18.06391	1.60684	0.08895
0.24	18.22157	1.60666	0.08817
0.21	18.4008	1.62326	0.08822
0.185	18.6427	1.65632	0.08885
0.165	18.82308	1.64378	0.08733
0.145	19.05765	1.62553	0.0853
0.13	19.25181	1.64817	0.08561
0.115	19.47627	1.68011	0.08626
0.1	19.72006	1.73528	0.088
0.09	19.88115	1.6967	0.08534
0.08	20.00581	1.69715	0.08483
0.07	20.16529	1.75309	0.08694
0.065	20.27207	1.77279	0.08745
0.06	20.38548	1.72754	0.08474
0.055	20.41502	1.77381	0.08689
0.052	20.48174	1.71929	0.08394
0.049	20.53672	1.75351	0.08538
0.046	20.58589	1.78444	0.08668
0.043	20.66185	1.77668	0.08599
0.04	20.67392	1.79016	0.08659
0.039	20.68912	1.78985	0.08651
0.038	20.76208	1.76196	0.08486
0.037	20.74575	1.80868	0.08718
0.036	20.8079	1.75181	0.08419
0.035	20.82321	1.72258	0.08272
0.034	20.85507	1.72277	0.08261
0.033	20.84404	1.70432	0.08177
0.032	20.8924	1.73988	0.08328
0.031	20.87027	1.72822	0.08281
0.03	20.92371	1.7345	0.0829
0.029	20.94686	1.7388	0.08301
0.028	20.94971	1.76899	0.08444
0.027	20.9804	1.73971	0.08292
0.026	21.03436	1.70842	0.08122
0.025	21.03505	1.75163	0.08327
0.024	21.04675	1.73048	0.08222
0.023	21.0705	1.74109	0.08263
0.022	21.06181	1.76521	0.08381

Table 61 Continued

0.021	21.11228	1.75308	0.08304
0.02	21.13774	1.76634	0.08356
0.019	21.13418	1.76502	0.08351
0.018	21.10661	1.78459	0.08455
0.017	21.08998	1.77559	0.08419
0.016	21.13118	1.76042	0.08331
0.015	21.13536	1.73194	0.08195
0.014	21.19328	1.7264	0.08146
0.013	21.17134	1.7307	0.08175
0.012	21.1818	1.72336	0.08136
0.011	21.25558	1.74849	0.08226
0.01	21.20042	1.74855	0.08248
0.009	21.30244	1.75772	0.08251
0.008	21.27474	1.74482	0.08201
0.007	21.24759	1.74409	0.08208
0.006	21.25064	1.76766	0.08318
0.005	21.26642	1.76531	0.08301
0.004	21.31491	1.76814	0.08295
0.003	21.27194	1.78343	0.08384
0.002	21.27417	1.78004	0.08367
0.001	21.23953	1.7945	0.08449
0	21.19399	1.78706	0.08432
-0.001	21.17479	1.77621	0.08388
-0.002	21.14097	1.81371	0.08579
-0.003	21.13441	1.8116	0.08572
-0.004	21.0435	1.8165	0.08632
-0.005	21.02759	1.79762	0.08549
-0.006	20.98913	1.82433	0.08692
-0.007	20.9497	1.86603	0.08907
-0.008	20.9225	1.84024	0.08795
-0.009	20.78116	1.85448	0.08924
-0.01	20.68644	1.87272	0.09053
-0.011	20.55921	1.90701	0.09276
-0.012	20.45374	1.90931	0.09335
-0.013	20.34001	1.93189	0.09498
-0.014	20.21652	1.92086	0.09501
-0.015	19.95595	1.92298	0.09636
-0.016	19.71767	1.93278	0.09802
-0.017	19.43238	1.94103	0.09989
-0.018	19.09277	1.93108	0.10114

Table 61 Continued.

-0.019	18.61831	1.91863	0.10305
-0.02	18.12131	1.85856	0.10256
-0.021	17.52095	1.8251	0.10417
-0.022	16.6915	1.75698	0.10526
-0.023	15.71097	1.69023	0.10758
-0.024	14.46181	1.54508	0.10684
-0.025	12.75485	1.33116	0.10437
-0.026	11.4477	1.15448	0.10085
-0.027	10.70533	1.06561	0.09954

REFERENCES

Ames, F. (1996). *Experimental Study of Vane Heat Transfer and Film Cooling*. Indianapolis: NASA.

Ames, F. E. (1996). *Experimental Study of Vane Heat Transfer and Film Cooling at Elevated Levels of Turbulence.* Allison Engine Company, NASA Lewis Research Center, Internal Fluid Mechanics Division. Indianapolis: National Aeronautics and Space Administration.

Ames, F. E., Kwon, O., & Moffat, J. R. (1999). "An Algebraic Model For High Intensity Large Scale Turbulence. *ASME TURBO EXPO 1999.* Indianapolis, Indiana, USA.

Bae, S., Lele, S. K., & Sung, H. J. (2000). Influence of Inflow Disturbances on Stagnation Region Heat Transfer. *Journal of Heat Transfer*, 258-265.

Billing, L. O., & Galle, K. R. (May 1970, pages 245-251). A Numerical Method for Calculating Fully Developed Laminar Velocity Profiles From Temperature Profiles. *Journal of Heat Transfer*.

Blair, M. F. (1982, October). Influence of Free-Stream Turbulence on Boundary Layer Transition in Favorable Pressure Gradients. *104*, 743-750.

Blair, M. F. (1983, February). Influence of Free-Stream Turbulence on Turbulent Boundary Layer Heat Transfer and Mean Profile Development, Part I-Experimantal Data. *Journal of Heat Transfer, 105*, 33-40.

Blair, M. F. (1983, February). Influence of Free-Stream Turbulence on Turbulent Boundary Layer Heat Transfer and Mean Profile Development, Part II- Analysis of Results. *Journal of Heat Transfer, 105*, 41-47.

Britter, Hunt, & Mumford. (1979). The Distortion of Turbulance By a Circular Cylinder. *Journal of fluid mechanics*, 269-301.

Chowdhury, M. N. (2012). *Mesurement and Analysis of Turbulence Responce Near the Stagnation Region of Large Diameter Cylindrical Leading Edges.* Grand Forks: University of North Dakota .

Chowdhury, N. H. (2012). *"Measurement and Analysis of Turbulence Responce Near The Stagnation of Large Diameter Cylindrical Leading Edges" Masters Thesis.* Grand Forks: University of North Dakota.

Dvorak, L. A. (2003). *"TURBULENT AUGMENTATION OF HEAT TRANSFER OFF PIN AND ENDWALL SURFACES IN A STAGGERED PIN FIN ARRAY " Masters Thesis.* Grand Forks: University of North Dakota.

Dynamics, D. (2015, May 26). *Probes for Hot-Wire Anemometry.* Retrieved from www.dantecdynamics.com: http://pdf.directindustry.com/pdf/dantec-dynamics-s/probes-hot-wire-anemometry/15753-405807.html

Erickson, E. L., Ames, F. E., & Bons, J. P. (2012). "Effects of a Realistically Rough Surface on a Vane Heat Transfer Including the Influence of Turbulence Condition and Reynolds Number". *Journal of Turbomachinery, 134*(March).

Figiola, R. S., & Beasley, D. E. (2006). *THEORY AND DESIGN FOR MECHANICAL MEASUREMENTS* (Fourth Edition ed.). Hoboken, New Jersey , USA: John Wiley and Sons, Inc,.

Fossen, J. O. (1985). The Influence of Jet-Grid Turbulence on Heat Transfer from the Stagnation Region of a Cylinder in Crossflow. *National Heat Transfer Conference. 1.* Denver, Colorado: Cleveland Ohio: National Aeronautical and Space Administration, Lewis Research Center.

Gandavarapu, P. (2011). *"The Influence of High Turbulence Intensity and Large Leading Edge Reynolds Numbers on Stagnation Heat Transfer" Masters Thesis.* Grand Forks: University of North Dakota.

Gandavarapu, P., & Ames, F. A. (2013). "The Influence of Leading Edge Diameter on Stagnation Region Heat Transfer Augmentation Including Effects of Turbulence Level, Scale, and Reynolds Number". *The Journal of Turbomachinery, 135*(January).

Gandavarapu, P., & Ames, F. E. (2013). The Influence of Leading Edge Diameter on Stagnation Region Augmentation Including Effects of Turbulence Level, Scale, and Renolds Number. *135*.

Hicks, R. A., & Cliff, S. E. (1991). *An Evaluation of Three Two-Dimensional Computational Fluid Dynamics Codes Including Low Reynolds Numbers and Transonic Mach Numbers.* Moffet Field : Ames Research Center .

Kingery, J. E., & Ames, F. E. (2015). Stagnation Region Heat Transfer Augmentation at Very High Turbulence Levels. *ASME Turbo Expo 2015.* Montreal: ASME.

Mayle, R. E. (1991). The Role of Laminer Turbulent Transition in Gas Turbine Engines.

Mayle, R., Schultz, A., & H.J., a. B. (2008). "Reynolds Stress Calculations for Pre-Transition Boundary Layers With Turbulent Free Streams". *ASME Turbo Expo 2008: Power for Land, Sea and Air.* Berlin, Germany: ASME.

Miyazaki, H., & Sparrow, E. M. (1977). Analysis of Effects of Free-Stream Turbulence on Heat Transfer and Skin Friction. *Journal of Heat Transfer* , 614 -619.

Moffat, R. J. (1988). "DESCRIBING THE UNCERTAINTIES IN EXPIERIMENTAL RESULTS". *Expierimental and Thermal Science*, 3-17.

Nix, A., & Diller, T. (2005). "Experiments On The Physical Mechanism of Heat Transfer Augmentation By Free Stream Turbulence At A Cylindrical Stagnation Point. *ASME Turbo Expo 2005.* Nevada: ASME.

Radomsky, R. W., & Thole, K. A. (1999). Flowfield Measurements for a Highly Turbulent Flow in a Stator Vane Passage. *122*(2).

Radomsky, R. W., & Thole, K. A. (2001). Detailed Boundary Layer Measurements on a Turbine Stator Vane at Elevated Freestream Levels. *2001-GT-0169*.

Radomsky, R., & Thole, K. A. (2000). High Freesteam Turbulence Effects on Endwall Heat Transfer for a Gas Stator Vane. *ASME Turbo Expo 2000. 2000-GT-0201*. Munich, Germany: ASME.

Volino, R. J., & Simon, T. W. (1997, A). "Boundary Layer Transition Under High Free-Stream Turbulence and Strong Acceleration Conditions: Part 1-Mean Flow Results. *119*(August), pp. 420-426.

Volino, R. J., & Simon, T. W. (1997, B). "Boundary Layer Transition Under High Free-Stream Turbulence and Strong Acceleration Conditions: Part 2-Mean Flow Results". *119*(August), pp. 420-426.

White, F. M. (1974). *"Viscous Fluid Flow"* . McGraw-Hill, Inc.

William Kays, M. C. (2005). *Convective Heat and Mass Transfer* (Vol. IV). New York: McGraw-Hill Companies.

Willmarth, W. W. (1970). "Wall-Pressure Fluctuations beneath Turbulent Boundary Layers on a Flat Plat and a Cylinder" . *41, Page 47-80*.

Wissinck, J. G., & Wolfgang, R. (2011). Direct Numerical Simulation Of Heat Transfer From The Stagnation Region Of A Heated Cylinder Affected By An Impinging Wake. *Journal of Fluid Mechanics*, 64-89.

Zukauskas, A., & Ziugzda, J. (1985). *Heat Transfer of a Cylinder in Cross Flow*. Hemisphere Publishing Corporation.